공학박사 학위논문

Development of Membrane-Based Coculture Platforms for Effective Stem Cell Therapy

효과적인 줄기세포 치료를 위한 막 기반 공배양 플랫폼 개발

2017 년 8 월

서울대학교 대학원

협동과정 바이오엔지니어링

유 승 미

Development of Membrane-Based Coculture Platforms for Effective Stem Cell Therapy

효과적인 줄기세포 치료를 위한 막 기반 공배양 플랫폼 개발

지도교수 김 병 수
이 논문을 공학박사 학위논문으로 제출함

2017 년 8 월

서울대학교 대학원
협동과정 바이오엔지니어링
유 승 미

유승미의 박사학위논문을 인준함
2017 년 8 월

위 원 장	황석연	(인)
부 위 원 장	김병수	(인)
위 원	한지숙	(인)
위 원	서상우	(인)
위 원	이수홍	(인)

Abstract

Development of Membrane-Based Coculture Platforms for Effective Stem Cell Therapy

Seungmi Ryu

Interdisciplinary Program for Bioengineering

The Graduate School

Seoul National University

There is an increasing demand for stem cell therapy to treat various degenerative diseases and impaired organs. Determining the fate of stem cells prior to transplantation has been reported as a strategy to improve the therapeutic outcomes of stem cell therapy. Stem cells are regulated *in vivo* through interactions with the surrounding microenvironments in three-dimensional (3D) manner. Coculture of stem cells with desired cell types, which recapitulates the complex *in vivo* cell-cell communications, has been reported as an effective method to direct stem cell

differentiation into a specific lineage. The porous membrane-based cocultured system has been widely used to support both cell-cell interactions through the membrane, and easy separation of the cells following coculture. The features of the membrane used for coculturing are crucial to achieve the best outcome. Not only should the membrane act as a physical barrier that prevents the mixing of the cocultured cell populations, it should also allow effective interactions between the cells. Unfortunately, conventional membranes used for coculture do not sufficiently meet these requirements. The micro-thick thickness and the low porosity of the membranes used in conventional coculture systems, facilitate a very limited interaction between cocultured cells, thereby resulting in low efficacy of stem cell differentiation. Furthermore, cell harvesting using proteolytic enzymes following coculture impairs cell viability and the extracellular matrix (ECM) produced by the cultured cells.

This dissertation presents the development of membrane-based coculture platforms for effective stem cell therapy. The major goals of this study are summarized as follows: 1) Fabrication of nanothin and highly porous membranes with thermoresponsive functionality to promote efficient stem cell differentiation and avoid enzymatic cell harvesting procedure. 2) Establishment of a coculture system with 3D cellular geometry through cellular layer-by-layer (cLbL) arrangement using biodegradable, nanothin, and highly porous membranes. Such a system mimics the *in vivo* 3D cell-cell interaction, and readily allows formation of implantable differentiated stem cells-membrane construct following coculture. 3) Demonstration of reversible cell layering platform, mediated by chitosan thin film to layer/delayer stem cells and differentiated cells in coculture, and the therapeutic application of these differentiated cells in tissue regeneration.

First, we developed nanothin and highly porous (NTHP) membranes, which are ~ 20-fold thinner and ~ 25-fold more porous than the conventional

coculture membranes. The tunable pore size of NTHP membranes at the nanoscale level was found crucial for the formation of direct gap junction-mediated contacts between the cocultured cells. Differentiation of the cocultured stem cells was dramatically enhanced with the pore size-customized NTHP membrane system compared to conventional coculture methods. This was likely due to effective physical contacts between the cocultured cells and the fast diffusion of bioactive molecules across the membrane. Also, the thermoresponsive functionality of the NTHP membranes enabled the efficient generation of homogeneous, ECM-preserved, highly viable, and transfer-printable sheets of cardiomyogenically differentiated cells.

Second, we developed a cellular layer-by-layer (cLbL) coculture platform using biodegradable, nanothin, highly porous (BNTHP) membranes. The cLbL coculture platform better mimicked the *in vivo* 3D microenvironments and facilitated higher extent of cellular cross-talks between cocultured cells, which occurred in nanoscale range, resulting in more efficient stem cell differentiation compared to the conventional bilayer coculture systems. Furthermore, the biodegradable, biocompatible and highly flexible features of BNTHP membranes enabled conversion of the cell-attached membranes into implantable 3D cell constructs, thus avoiding harmful enzymatic harvesting of the cells.

Finally, we developed a reversible cell layering platform in coculture mediated by chitosan thin film formed *in situ* between the cocultured cell layers. Anionic maleimide-chondroitin-sulfate was grafted onto the surface membrane of myogenic C2C12 cells and human mesenchymal stem cells (hMSCs) to modify surface charge of the cells without cytotoxicity. A highly porous chitosan thin film is formed *in situ* interspacing between the heterogeneous cell layers *via* ionic crosslinking of cationic chitosan and anionic functionalized-cells, forming compactly assembled double-layered cell constructs. The chitosan film enabled

layering of the cells, which allowed active direct interactions between the cell layers, and facile delayering of the cells by a simple treatment of mild shear stress. The developed platform promoted the myogenic commitment of hMSCs *via* direct contact with C2C12 cells. Delivery of the myogenic committed cells to muscle-injured animal models showed evident muscle regeneration.

Keywords : coculture • differentiation • membrane • mesenchymal stem cells • stem cell therapy

Student Number : 2012-23294

Table of Contents

List of figures

List of tables

Abbreviations

2D	Two-dimensional
3D	Three-dimensional
AFM	Atomic force microscopy
ASCs	Adult stem cells
BNTHP	Biodegradable, nanothin, highly porous
BSA	Bovine serum albumin
CA	Cellulose acetate
CCK-8	Cell counting kit-8 assay
CFD	Computational fluid dynamics
cLbL	Cellular layer-by-layer
CS	Chondroitin sulfate
CSA	Cross-sectional area
cTnT	Cardiac troponin T
DAPI	4,6-diamidino-2-phenylindole
DDR2	Discoidin domain receptor 2
DI	Deionized
DMA	Dynamic mechanical analyzer
DMEM	Dulbecco's modified Engle's Medium
DPPTE	1,2-dipalmitoyl-sn-glycero-3-phosphothioethanol
DSC	Differential scanning calorimetry
ECM	Extracellular matrix
EDC	N-(3-dimethylaminopropyl)-N-ethylcarbodiimide hydrochloride
ERK	Extracellular signal-regulated kinase
ESCs	Embryonic stem cells

FACS	Fluorescence-activated cell sorting
FBS	Fetal bovine serum
FT-IR	Fourier transform infrared spectroscopy
GPC	Gel permeation chromatography
H&E	Hematoxylin and eosin
hMSCs	Human mesenchymal stem cells
HNA	Human nuclear antigen
HS	Horse serum
iCVD	Initiated chemical vapor deposition
iPSCs	Pluripotent stem cells
JNK	c-jun N-terminal kinases
LCST	Lower critical solution temperature
MCS	Maleimide-conjugated chondroitin sulfate
Mn	Molecular weight
MSCs	Mesenchymal stem cells
NHS	N-hydroxysulfosuccinimide sodium salt
NTHP	Nanothin and highly porous
OCT	Optimal cutting temperature
p38	p-38 mitogen-activated protein kinases
PBS	Phosphate buffer saline
PCL	Polycaprolactone
PCNA	Proliferating cell nuclear antigen
PDDA	Poly(diallyldimethylammonium chloride
PFA	Paraformaldehyde solution
pGMA	Poly(Glycidyl Methacrylate)
PLGA	Poly(lactic-*co*-glycolic) acid
PNIPAAm	Poly(N-isopropylacrylamide)

PS	Penicillin-streptomycin
PSS	Poly(sodium styrene sulfonate
PUA	Poly(urethane acrylate)
qRT-PCR	Quantitative reverse transcriptase polymerase chain reaction
RH	Relative humidity
SA	Sarcomeric α-actinin
SEM	Scanning electron microscopy
Si	Silicon
TA	Tibialis anterior
TBPO	Tert-butyl peroxide
TCEP	Tris(2-chloroethyl) phosphate
TCPS	Tissue culture polystyrene
T_g	Transition temperature
TGF-β3	Transforming growth factor beta 3
THF	Tetrahydrofuran
VIPS	Vapor-induced phase separation

Chapter 1.

Research backgrounds and objectives

1.1. Stem cell therapy in tissue engineering and regenerative medicine

Stem cell therapy has great potential to treat various degenerative and age-related diseases, and damaged tissues.[1] In general, stem cells are classified into two categories namely, embryonic stem cells (ESCs) and adult stem cells (ASCs), which include mesenchymal stem cells (MSCs), hematopoietic stem cells (HSCs), and induced pluripotent stem cells (iPSCs).[2] Even though ESCs and iPSCs are pluripotent, their clinical application has been hindered by ethical and safety issues such as limited accessibility, low efficiency, risk of teratoma formation, and immune response.[2-4] Unlike ESCs, ASCs do not have ethical issues, have unlimited accessiblity and low risk of tumorigenicity.[4-5] Therefore, ASCs has been considered as the gold standard cell candidate for stem cell therapy.[6] Among various types of ASCs, MSCs have generated a great interest as a stem cell source due to their high expansion capability,[7-8] along with easy accessiblity from various tissue organs, such as the bone marrow, fat tissue, placenta, and the tooth.[9] Additionally, MSCs not only have the capacity to differentiate into a variety of cell lineages under defined environmental conditions,[10] they also exhibit immunosuppressive effects showing satisfying transplantation outcomes to an allogeneic graft.[11] As of 2012, there were 218 therapeutic clinical trials using MSCs internationally, which is attributed to the suitable characteristics of MSCs for therapeutic use.[12]

Despite the impressive virtues of MSCs as a potential source for stem cell therapy, they have two main limitations to succesful stem cell therapy. The primary limitation is the low survival rates and engraftment of MSCs in the transplanted site.[13-14] The transplanted MSCs undergo anoikis as the transplanted MSCs are in single-cells with lack of ECM.[13-14] Second, transplanted naïve MSCs show poor *in vivo* differentiation efficiency at the damaged transplanted sites, hampering

replacement of the damaged tissue cells by MSCs.[15] A number of previous studies reported that transplantation of naïve MSCs for myocardial infarction treatment showed low therapeutic efficacy because of the low differentiation rate of MSCs into cardiomyoytes *in vivo*.[16-19] The inharmonious physiological characteristics of naïve MSCs with the heart tissue not only hampers the therapeutic effect of MSCs, but could also impose the risk of arrhythmia.[16-19] In addition to its limitation in cardiac tissue repair, transplanted MSCs in the damaged cartilate often undergo cellular hypertrophy with dedifferentiated cartilage phenotype, thereby degenerating the cartilage regeneration process.[20-21]

Determining the fate of MSCs *ex vivo* prior to transplantation has been reported to show better tissue regenerative effects.[22-23] Han *et al.* demonstrated that cardiac priming of MSCs improved therapeutic efficacy of these cells in cardiac repair.[24] Also, delivery of pre-cultured, chondrogenic differentiated MSCs produced more stable neo-cartilage formation *in vivo*.[25] Myogenic promoted MSCs also reported to show better engraftment and differentiation in injured muscle compared to naïve MSCs.[26] Thus, establishing *in vitro* approaches to effectively promote the fate of MSCs prior to transplantation would greatly improve the outcomes of stem cell therapy.

1.2. Factors influencing the differentiation of native stem cell during *in vivo* tissue repair

Stem cells *in vivo* are widely distributed in various tissue organs and act as natural reparative agents in damaged tissue.[27] The damaged tissue recruits circulating or residing stem cells to the damaged site through the abundant inflammatory factors produced by immune cells during inflammation at lesion site.[28-29] Inflammatory factors, such as TNF-α, IL-8, IL-1β, and SDF-1α,[27] trigger chemotactic migration of stem cells to the damaged site.[29] The migrated stem cells repair the tissue through proliferation and differentiation into either stromal cells or the damaged cell types by interacting with heterogeneous cells within the microenvironment of the damaged tissue, such as host tissue cells, fibroblasts, immune cells, endothelial cells and epithelial cells.[27]

Concerted actions of various factors, such as direct cell-cell/cell-ECM contact and cytokines, in the microenvironment have been reported to play critical roles in modulating the fate of stem cells. Shapiro *et. al.* demonstrated functional repair of full-thickness defects of articular cartilage through differentiation of MSC from bone marrow. They conclusively indicated the replacement of the defected tissue through chondrogenic differentiation of the migrated MSCs within the cartilage microenvironments.[30] In particular, chondrogenic differentiation outcomes of MSCs, whether it become hypertrophic or functional hyaline cartilage, largely depends on the local cues presented in the immediate microenvironment.[31-32] In a specific region where hypertrophic chondrocytes are abundant, the migrated cells eventually produced type X collagen, a hypertrophic ECM marker.[32] On the other hand, cartilage-specific ECM molecules, including various proteoglycans, provide effective cue in suppressing such process.[33-34] Also, chondrocytes secrete cocktails of soluble factors, such as TGF-β1, BMP-2, IGF-1, and FGF-2, that promote

chondrogenic differentiation of MSCs.[35-40] Furthermore, the secreted soluble factors also abundantly exist in the ECM of the chondrocytes, leading to effective chondrogenic differentiation of MSCs through MSC-chondrocytes ECM contact.[35] A previous study has also reported the differentiation of MSCs into cardiomyocytes in the infarcted myocardium model is large depend on the proximity of the cells with the myocardial environment, indicating the importance of myocardial microenvironment in inducing cardiomyogenic differentiation of MSC.[41-42] MSCs surrounded by viable cardiomyoctyes showed direct cell-cell connection with host cardiomyocytes through formation of connexin 43 gap junction between the cells.[43] Such MCSs showed effective cardiomyocyte differentiation with well-organized cardiomyocyte structure. Myogenic differentiation outcome of MSCs for muscle repair is also large affected by presence of the host cells.[44] Myoblasts secretes m-calpain and myoferlin that are important for myoblast fusion by inducing cytoskeletal reorganization and membrane resealing of the cells.[45-46] ECM of the host tissues also acts as a critical factor in determining stem cell fate.[47] Solid tissues, such as brain, muscle, and bone, exhibit distinct and diverse matrix stiffness.[48] Stiffness of the matrix confers unique mechanical cues to stem cells through modulation of cytoskeleton and focal-adhesion structure of the attached stem cells.[47]

1.3. Differentiation of stem cell through coculture

As stem cell plasticity is mainly influenced by the surrounding microenvironment, called the stem cell niche,[49] the differentiation of stem cells *in vitro* can be controlled through proper regulation of this niche.[49] A common approach to induce *in vitro* differentiation of stem cells is through the addition of artificial factors, such as introducing bioactive molecules or biomimetic scaffolds that stimulate the differentiation of stem cells.[50-52] However, such artificial microenvironments may be insufficient in mimicking the complex cues of native *in vivo* microenvironments that regulate stem cell differentiation.[53] For instance, despite the great potential of MSCs in chondrogenesis, the commonly used approach to promote chondrogenic differentiation of MSCs with addition of growth factors, like the transforming growth factor beta 3 (TGF-β3), often resulted in elevated hypertrophic markers with unstable chondrogenic phenotypes.[20,54] Hypertrophy of chondrogenic differentiated MSCs causes apoptosis, vascular invasion, and ossification of the cells, which degenerate the cartilage regeneration process.[20]

As an alternative approach, coculture of stem cells with somatic cells has been reported as a method to promote the differentiation of stem cells.[55] Stem cells coexist with other neighboring heterogeneous cells in the body. The coculture method, in which stem cells are directly or indirectly cocultured with somatic cells, is aimed to recapitulate the complex intercellular interactions of stem cells with the surrounding cells in living tissue providing essential dynamic stimuli that affect the fate of stem cells.[55] Previous studies indicated that coculture of stem cells in direct contact with somatic cells, such as myoblasts,[56] osteoblasts,[57] chondrocytes,[58] and cardiomyocytes,[59] is effective in promoting stem cell commitment *in vitro*. In addition, the coculture strategy is often more cost-effective than dosing the culture medium with specific biomolecules, including growth factors.[60] Thus, coculture

strategy could be employed to effectively promote MSCs lineage prior to transplantation and benefit the therapeutic outcomes of stem cell therapy.

1.4 Cell-cell interactions in coculture

There are two main mechanisms of cell-cell interactions in coculture system that regulate the differentiation of a stem cell: indirect and direct interactions (Figure 1.1).[55] In indirect interaction, cell-to-cell crosstalk proceeds through diffusion of secreted paracrine factors.[61-62] In direct cell-cell interaction, the cell-cell interactions occurs based on direct contact between the somatic cells and the stem cells,[63-64] or the ECM of somatic cells and stem cells.[65-66] All of these interactions may occur simultaneously, indirectly and directly, or solely indirectly, depending on the employed coculture system.

1.4.1. Indirect interaction through paracrine soluble factors

In general, the widely used conventional method to induce differentiation of stem cells is by adding certain artificial growth factors or cytokines.[50-51] However, this artificial supplement is rather insufficient to simulate the complex cues of the native microenvironement that trigger the commitment of stem cells *in vivo*.[53] Paracrine soluble factors that affect the differentiation of stem cells in the body are not limited to one or two specific factors, but are composed of multiple factors that are directly secreted by the surrounding cells. In line with this, in the coculture system, cocktails of paracrine soluble factors are reported to be provided by the cocultured, differentiated cells that induce stem cell differentiation in a more effective way, rather than the addition of artifical growth factors.

A study conducted by Birmingham *et al.* reported that in comparison to culture of stem cells with osteocytes conditioned medium, indirect coculture of stem cells with osteocytes showed higher osteogenic differentiation efficiency.[67] Thus, the method by which the secreted soluble factors are provided to the stem cells is shown to affect the differentiation outcomes of stem cells. Compared to the conditioned medium, soluble factors directly secreted by the cocultured differentiated cells are promptly and continuously transmitted to the stem cells, better simulating the way in which paracrine cues reach the stem cells *in vivo*. Hwang *et al.* also reported that paracrine soluble factors of chondrocytes promote chondrogenic differentiation of stem cells.[68] Liu *et al.* reported that chondrocytes secrete soluble chondroinductive factors such as TGF-β1, IGF-1, and BMP-2 that effectively promote the chondrogenic differentiation of stem cells.[28-33]

1.4.2 Direct interaction through cell-cell or/and cell-matrix contact

Direct interaction between the cocultured cells is formed through either direct cell-cell and/or cell-ECM contact.[63-66] Directly contacting cells typically form cell-cell gap junctions. Through these junctions, directly contacting cells facilitate cellular communications through the spontaneous intercellular transfer of cellular components, including components of the plasma membrane and the cytosol.[69-70] Morever, the ECM of the cocultured differentiated cells provides physical and chemical cues that promote stem cell fate commitment.[71]

Although diffusion of secreted paracrine soluble factors by the differentiated cells can induce the differentiation of stem cells, numerous previous studies have reported that direct cell-cell/cell-ECM contact play a crucial role to efficiently promote the differentiation of stem cells into specific cell lineages, such as cartilage, heart, and muscle. Fukuhara *et al.* reported that coculture of MSCs and myocardial cells in direct contact effectively induces myocardial differentiation of stem cells.[59] In contrast, cells that were cocultured without forming direct cell-cell contact showed ineffective cardiac differentiation of stem cells. This indicates the importance of direct cell-cell contact in cardiac differentiation of stem cells through coculture.[59] Also, direct cell-to-cell contact was reported to be an important factor in chondrogenic differentiation of stem cells through coculture with chondrocytes. Acharya *et al.* reported that MSCs cocultured with chondrocytes in direct contact expressed more elevated chondrogenic markers such as glycosaminoglycan and collagen type II compared to MSCs cocultured witout direct contact.[58] The study also reported that MSCs differentiated through direct contact coculture with chondrocytes expressed suppressed hypertrophic marker.

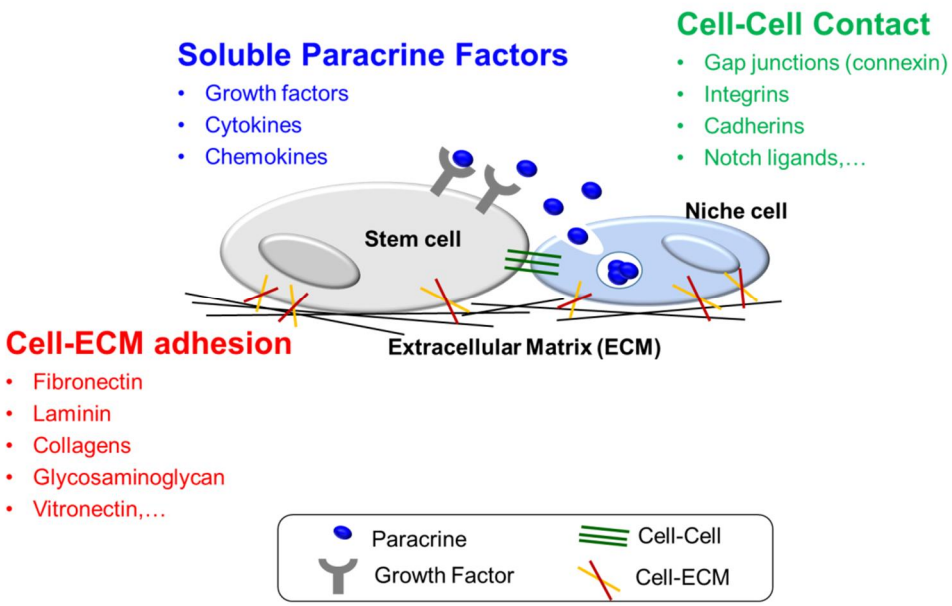

Figure 1.1. Various modes of cell-cell interactions in coculture.

1.5. Current coculture systems and their limitations

Coculture systems were developed in the 1980s to study cell-cell communication.[72] Adaptation of the coculture system to promote differentiation of stem cells was introduced for the first time by Scheven *et al.* in 1986.[73] Since then, various coculture systems have been established to allow proper cell-cell interactions between the cocultured cells. Generally, coculture systems are categorized into two groups; indirect and direct coculture (Figure 1.2).[55]

In indirect coculture system, the cells with different types are physically separated within the same culture batch. The cell interactions only occurs *via* diffusion of paracrine soluble factors with absence of direct cell-cell contact between the two cell populations. A porous membrane is often applied between the cells to separate the cell populations. In direct coculture system, cells are in close contact to form direct cell-cell contact. Cells are communicating in a more complex and dynamic manner *via* paracrine soluble factors, cell-cell, and cell-ECM interactions. Also, direct coculture can be done in either a two-dimensional (2D) or a three dimensional (3D) system. In 2D coculture, cells are typically mixed and cocultured in a monolayer on tissue culture plate dishes (TCPS). For 3D coculture, the cells can be mixed on 3D materials, such as alginate gels[55] or collagen sponge,[74] or aggregated as 3D cell pellet. Indirect coculture may also be performed in 3D wherein, each cell population is encapsulated in separate 3D materials and cocultured within the same batch environment.[75]

Subsequent homogeneous cell separation and collection of the differentiated stem cells following coculture is important for further analysis and clinical application.[68,76] For therapeutic applications, the homogeneity of the cells collected post-coculture should be strictly preserved as contamination of the collected cells with exogenous cells might result in serious complications, such as immune rejection after *in vivo* transplantation.[77] 'Transwell®' is a commercially

available porous membrane-based coculture system that is conventionally used for coculture. The membrane acts as a barrier between the cocultured cell populations. 'Transwell' system is also available for both indirect and direct coculture. For indirect coculture, the target differentiated cells are seeded on the porous membrane of the Transwell insert, while stem cells are seeded on the bottom chamber, allowing diffusion of the secreted paracrine factors through the porous membrane[68]. For direct coculture, the target differentiated cells are seeded on the porous membrane of the Transwell insert and stem cells are seeded on the opposite side of the porous membrane.[78] Both diffusion of the secreted paracrine factors and direct cell-cell contact through the porous Transwell membrane are allowed in this system.

The role of the membrane as a physical barrier between the two types of cell populations, in the membrane-based coculture system, is important to prevent cross contamination and preserve the homogeneity within the cocultured cell population. The features of the membrane used in coculture systems constitute the critical factors that affect the outcomes of stem cell differentiation.[79] However, due to the 'track-etched' fabrication method, the membrane in Transwell® system is more than 10 μm thick and has a low porosity.[80] Moreover, a previous study demonstrated that the physical properties of Transwell membranes hinder sufficient physical contact between cocultured cells, and also the diffusion of bioactive molecules, which are secreted by the cultured cells across the membrane.[81]

In addition, enzymatic harvesting of cells following coculture is a major drawback of conventional coculture systems, since such methods damage the ECM produced by the cultured cells and reduce their viability. This results in poor survival and low therapeutic efficacy of the implanted cells.[82-83] This poor survival also hampers the functional benefits of cell therapy.[84]

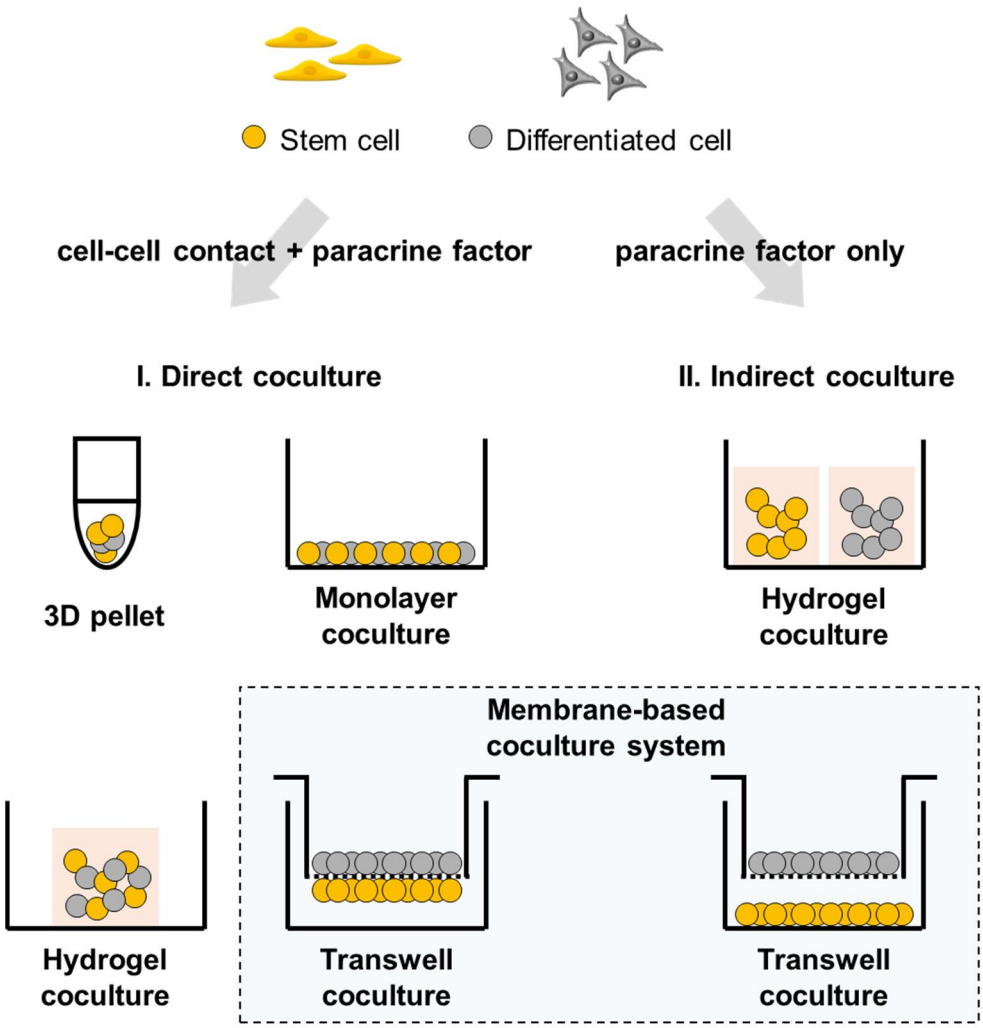

Figure 1.2. Various coculture systems. Depending on the design parameters of the coculture systems, the cocultured cells are interacting in different modes.

1.6. Research objectives of this dissertation

Stem cell therapy has evolved over the past decade with high expectancy to treat various diseases and replace injured organs. MSCs have attracted great interest as potential candidates for stem cell therapy. While a high number of pre-clinical and clinical studies have been conducted, there are still some limitations that need to be resolved to make advance in the clinical translation of stem cell therapy. These limitations include, low engraftment and differentiation efficiency of the delivered stem cells *in vivo*. Promoting the MSCs commitment prior to transplantation has been reported to improve their therapeutic efficacy as committed MSCs were reported to show higher engraftment and differentiation in the transplanted site. While introducing artificial factors to the stem cell niche are insufficient to induce the differentiation of MSCs, coculture of MSCs and target differentiated cells has been reported as an alternative strategy to promote efficient differentiation of MSCs. This is achieved by mimicking the complex heterogeneous cell-cell interactions, in coculture, that stem cells encounter *in vivo* within their native microenvironment during differentiation. Membrane-based coculture system has been widely employed for cell separation following coculture and is important for further analysis and application of the cells. However, currently available membrane-based coculture systems have major limitations of inefficient cell-cell interactions between the cocultured MSCs and differentiated cells, causing low differentiation efficacy of MSCs, and damaged ECM of the cells following coculture.

Therefore, in this dissertation, we proposed various novel membrane-based coculture platforms to effectively induce the differentiation of MSCs through coculture and potentiate the therapeutic application of differentiated MSCs. We developed a bilayer coculture platform using thermoresponsive, nanothin, and highly porous (NTHP) membranes to generate ECM-preserved, transfer-printable

sheets of cardiac differentiated MSCs by coculture. Next, we developed a cellular layer-by-layer (cLbL) coculture platform using biodegradable, nanothin, and highly porous (BNTHP) membranes to establish a coculture system with 3D coculture geometry, better mimicking the *in vivo* cell-cell interactions, and readily allow the formation of 3D chondrogenic differentiated MSCs-laden membrane constructs following coculture. We also developed a reversible cell layering platform mediated by chitosan thin film for asssembly of MSCs and myoblast cells in coculture. Ultimately, the therapeutic efficacy of the differentiated MSCs was evaluated in animal models.

Chapter 2.

Experimental procedures

2.1. Preparation of membranes/film for coculture

2.1.1. Fabrication of NTHP membranes

Cellulose acetate (CA) with an average molecular weight (Mn) of 30,000 g/mol (39.8wt% acetyl labeling extent) was prepared (Sigma-Aldrich Co., USA). CA was dissolved in a good solvent, THF, at 4 wt% for NTHP-380 membranes. For NTHP-860 membranes, 3 wt% CA was dissolved in THF, and acetone was used as a solvent for fabricating NTHP-100 membranes. NTHP membranes were deposited onto silicon (Si) wafers, which were previously cleaned by dipping in a piranha solution, a mixture of 70 vol% H_2SO_4 and 30 vol% H_2O_2, for 20 minutes at room-temperature, then rinsed with deionized (DI) water and dried with a nitrogen stream. To obtain the nanoporous structure of NTHP membranes, the spin-casting of CA solutions onto Si wafers was performed with a spinning rate of 3000 rpm (NTHP-100 and NTHP-380) or 1000 rpm (NTHP-860), for 25 seconds, using an automatic spin coater in a closed humid chamber with controlled relative humidity (RH). Since CA polymers are not soluble in water, the porous structure in NTHP membranes was developed using a vapor-induced phase separation (VIPS) mechanism, and the pore size was controlled by the RH in the closed chamber packed with different types of supersaturated salt solutions (KCl for RH 55-85%). For the NTHP membranes used in our experiment, we set up the RH to 65±5 % (NTHP-100 and NTHP-380), and 55±5 % (NTHP-860). The freestanding NTHP membranes were obtained by peeling off the membranes from the Si wafers in water after efficiently drying the samples. We modified the NTHP membranes using the method proposed by Ku *et al.*[85] to enhance cell adhesion. NTHP membranes were coated in a dopamine hydrochloride solution for up to 16 hours. Dopamine hydrochloride (Sigma-Aldrich Co.) was dissolved in 10 mM Tris buffer at 2 mg/ml, and the pH was adjusted to 8.5 using dilute NaOH solution. A PET film was used as a frame for easier handling of the NTHP membranes. The PET-frame

was fixed with UV-curable poly(urethane acrylate) (PUA, 311-RM, Minuta Tech, Korea), which acts as a glue. The PUA was irradiated with UV (λ=365 nm) for 3 hours.

GMA monomer (97%) and the tert-butyl peroxide (TBPO) initiator (98%) were purchased from Sigma-Aldrich and used without further purification. Polymerized GMA films were deposited onto the NTHP membranes in an initiated chemical vapor deposition (iCVD) reactor (Daeki Hi-Tech Co., Korea). The GMA monomer was heated to 35 °C and the vaporized GMA was fed into the reactor at a flow rate of 1.9 sccm for coating the poly(Glycidyl Methacrylate) (pGMA) film on the NTHP membrane. The vaporized TBPO initiator was fed into the reactor *via* metering valves at a flow rate of 0.8 sccm at room-temperature. In order to keep the NTHP membrane at 25 °C during the pGMA coating process, the membranes were placed on a stage cooled by a recirculating chiller. The filament temperature was maintained at 180 °C. The growth rate of film deposition was monitored *in situ* using a He-Ne laser (JDS Uniphase, Milpitas, USA). Amine-terminated poly(N-isopropylacrylamide) (PNIPAAm, Mn = 2500, Sigma-Aldrich Co.) was dissolved in DI water at a concentration of 1 g/30 mL. The PNIPAAm solution was reacted with the pGMA deposited NTHP membrane through epoxy-amine addition reaction in a shaker at 50 °C for 12 h at 55 rpm. Next, it was washed several times with DI water. Prior to cell seeding, membranes were sterilized with 70% (v/v) ethanol and UV treated for 1h on a clean bench.

2.1.2. Fabrication of BNTHP membranes

poly(lactic-*co*-glycolic) acid (PLGA, LA/GA molar ratio 75:25) with weight-average molecular weight (Mw) of 66,000-107,000 g/mol (Sigma, USA) was dissolved in a good solvent, tetrahydrofuran (THF), at 4 wt% and BNTHP membranes were prepared by VIPS technique. The polymer solution was prepared by filtering through a 0.4 μm polytetrafluoroethylene filter prior to use. While the phase separation is occurring, polymer solution-casted Si substrate was spin-coated with 1000 rpm spinning rate for 25 seconds. The spin-coating process was conducted in the closed chamber in order to control the RH with various types of supersaturated salt solution as proposed in previous studies.[86-87] Water vapor was used as a non-solvent in ternary phase system, and the solvent, THF, was all evaporated and the polymer was precipitated during spin-coating process. Si substrates were cleaned by dipping substrates in piranha solution (a mixture of 70 vol% H_2SO_4 and 30 vol% H_2O_2) for 20 minutes at room-temperature before casting the solution onto substrates. The self-standing BNTHP membranes were obtained by peeling off the membrane from Si substrates in aqueous environment. The edges of the spin-coated BNTHP membranes on Si substrate were scratched to expose the hydrophilic Si substrate to water,[88] leading to spontaneous detachment of the BNTHP membranes in water without sacrificial layer. Subsequently, the freely floating BNTHP membrane in water was collected and framed with the PET frame for easy handling of the membrane. The external and internal diameters of PET frame were 2.1 cm and 1.5 cm, respectively, and its thickness was 310 μm. BNTHP membrane spontaneously wrapped up the PET frame when brought to air atmosphere. Once dried, it remained adsorbed to the frame ever since.

2.1.3. Formation of chitosan thin films on cell surface membrane

MCS was synthesized by dissolving 500 mg of chondroitin sulfate sodium salt (CS; Tokyo Chemical Industry, Japan) in 24 mL of phosphate-buffered saline solution (PBS; Sigma Aldrich Co., USA). After fully dissolving CS by magnetic stirring, 23 mg of N-(3-Dimethylaminopropyl)-N′-ethylcarbodiimide hydrochloride (EDC; Sigma-Aldrich Co.) and 27 mg of N-Hydroxysulfosuccinimide sodium salt (NHS; Sigma-Aldrich Co.) were added and stirred for 20 min. Then, 62 mg of *N*-(2-Aminoethyl)maleimide trifluoroacetate salt (Maleimide; Sigma-Aldrich Co.) was dissolved 1 mL of PBS and added. 5 hr of reaction time was given in room temperature. Next, solution was dialyzed by dialysis membrane (SnakeSkin™ Dialysis Tubing, Mw cutoff 1kDa, Thermo, USA) against distilled water for 48 hr (distilled water was renewed every 12 hr) and freeze-dried for 48 hr. Synthesis was determined by ^{1}H-NMR, proton peak at 6.663 ppm was examined (maleimide proton). ^{1}H-NMR spectra were recorded in base of D2O.

hMSCs were plated at a density of $2.5x10^{3}$ cells/cm^{2} in a 12-well cell culture plate. When hMSCs reached its confluency, the cells were coated with MCS by treatment of mixed 1 mM TCEP and 500 μl of 10 mM MCS solution for 30 min in 37 ^{o}C incubator. After 30 min, the solution was removed. 334 μl of DMEM media was added followed by addition of 166 μl of 1.5 mg/mL chitosan in 1% acetic acid solution. After a brief shake, sample was incubated for 2 hr in 37 ^{o}C incubator. Chitosan film was formed through electrostatic complexation within 2 hr.

For synthesis of chitosan-FITC, 1.5 mg/mL chitosan polymer solution (Chitosan; low molecular weight, Sigma-Aldrich Co.) was prepared in 1% acetic acid solution (10 μl/mL). Next, 4 mL of the chitosan polymer solution was added with excess amount of FITC (dissolved in 4 mL of anhydrous ethanol, purged with N^{2} gas, Sigma-Aldrich Co.). Under magnetic stirring condition, the reaction was

performed in dark for 3 hr. About 6 mL of 0.1 M NaOH was added to the reaction mixture to precipitate the FITC labeled chitosan polymer. The precipitated chitosan-FITC was centrifuged and washed repeatedly with 70% ethanol solution till the washings showed free of FITC. Finally, the FITC labeled chitosan polymer was dissolved in 1% acetic acid and dialyzed against distilled water for 48 hr (distilled water was renewed every 12 hr).

2.2. Characterization of the developed membranes/films

2.2.1. Characterization of NTHP membranes

The surface morphologies of NTHP membranes were characterized by scanning electron microscopy (SEM, JSM-6701F, JEOL, Japan) and atomic force microscopy (AFM, JPK, Nanowizard 3, Germany & diInnova, Veeco, USA). The thicknesses of the NTHP membranes were measured using a step height measurement (AlphaStep IQ (Rev. A1-1), KLA-Tencor, USA). Based on previous studies, both SEM and AFM images were used to determine the average pore sizes of the NTHP membranes.[89-90] Pore size represents the average value of the shortest and the longest axes of each pore. The porosity of each membrane was analyzed using an image processing software, Image J (National Institutes of Mental Health, USA). AFM images were adjusted to black/white binary phase, and then the proportion of white area to the total area was considered as the porosity of the membrane. Fourier transform infrared spectroscopy (FT-IR, IFS 66VS, BRUKER, Billerica, USA) spectra were obtained in normal absorbance mode and averaged over 64 scans in order to confirm PNIPAAm functionalization. Water contact angle measurements were made using a contact angle meter (Phoenix 150, SEO, Korea) with a 2.5 μl DI water droplet. The contact angle meter was equipped with an environment chamber to control the temperature range from 25 °C to 250 °C.

2.2.2. Characterization of BNTHP membranes

The surface morphologies of BNTHP membranes both in air and water were characterized by AFM (JPK, Nanowizard 3, Germany & diInnova, Veeco, USA). The morphological structures of initial and degraded BNTHP membranes were also characterized by SEM (JSM-6701F, JEOL, Japan) following Pt coating using a sputter coater. The pore size and porosity of each membrane was analyzed using an image processing software, Image J (National Institutes of Mental Health, USA). AFM images were adjusted to black/white binary phase, and the portion of black area to the total area was considered as the porosity of membrane. We assumed the pores in the membrane were in circular shape, thus the pore diameters were calculated from the value of the area of each circle.

To measure the transition temperature (T_g), differential scanning calorimetry (DSC, DSC 4000, PerkinElmer, USA) equipped with a low-temperature environmental chamber was used. DSC thermograms were obtained by heating 5-7 mg samples in aluminum pans from 15 to 100°C with 10°C/min heating rate in a nitrogen atmosphere (flow rate 20 mL/min). DSC thermograms were obtained during the second heating cycle for pristine and partially degraded BNTHP membranes.

The weight loss of BNTHP membranes were detected by quartz crystal microbalance with dissipation (QCM-D) (Q-Sense D 300, Q-Sense, Sweden) and calculated with Sauerbrey's equation as previous studies.[91-93] The QCM-D measurements were performed to monitor the changes in frequency of Au sensor crystal (QSX301) which is spin-coated with PLGA adopting the same condition to fabricate BNTHP membranes. The changes of resonance frequency of a crystal quartz reflect the mass changes in a layer deposited on the quartz sensor. QCM-D simultaneously measures the absolute resonant frequency of the crystal for all four overtones (n=1, 3, 5 and 7, *i,e.,* 5, 15, 25, and 35 MHz), however, Δf_1 was

typically noisy due to insufficient energy trapping. Thus, frequency changes in the third overtone $\Delta f_3/3$ were chosen based on reports from previous studies.[91,94-95] PBS was injected into QCM-D chamber where the PLGA-coated Au sensor crystal was mounted. After the balance was established in 0.1M PBS as a baseline, the measurement of degradation was initiated. The released mass was calculated using Sauerbrey's equation:

$$\Delta \mathrm{m} = -\mathrm{C}\frac{\Delta f_n}{n} \; (\mathrm{C} = 17.7 \text{ ng} \cdot cm^{-2} \cdot Hz^{-1} \; at \; f = 5MHz)$$

showing the relationship between frequency shift and mass change is linear. The initial weight of BNTHP membrane was calculated to be 0.06 mg and the remaining mass was obtained by addition of the mass change. The thickness of the BNTHP membranes was measured by a step height measurement (AlphaStep IQ (Rev. A1-1), KLA-Tencor, USA) as previous studies.[96-97]

The tensile strength and elongation of BNTHP membranes were measured by dynamic mechanical analyzer (DMA, DMA Q800, TA Instruments, USA). Prior to the measurement of the mechanical properties of initial BNTHP membranes, the membranes were completely dried, and degraded BNTHP membrane samples were placed into pH 7.4 PBS at 37°C for 2 weeks and then dried. The isothermal strain-stress curve was obtained with approximately 10 mm of the sample between the tension film clamps of the DMA at RT with a 0.001 N preload force, and 0.5 N/min ramp rate.

The average molecular weights and molecular weight distributions of the initial and degraded BNTHP membranes were determined by the gel permeation chromatography (GPC, YL9100, Young Lin Instruments, Korea). The samples were dissolved in THF with a 2 mg/mL polymer concentration and before the GPC measurements, a calibration curve was prepared with poly(styrene) standards.

2.2.3. Characterization of chitosan thin films

The z-stacked, 3D morphology of the chitosan thin film-based coculture was imaged by a confocal microscope (SP8 X STED, super-resolution confocal microscope, Leica, Germany). Pore size, porosity, and height of the chitosan thin film were measured by processing the obtained z-stacked images of the chitosan thin film using image processing software, Image J (National Institutes of Mental Health, USA).

To measure the deposition of chitosan thin film, quartz crystal microbalance analysis was performed. Prior to analysis, base layer of positively charged polyelectrolyte poly(diallyldimethylammonium chloride (PDDA; Sigma-Aldrich Co.) and negatively charged poly(sodium styrene sulfonate) (PSS; Sigma-Aldrich Co.) were deposited on a gold electrode to mimic the lipid bilayer of cell surface membrane. Concentrations of both PDDA and PSS were 1 mg/mL and the salt concentration was 0.1M. Then, combination of two types of lipid, 1,2-dipalmitoyl-sn-glycero-3-phosphatidylcholine (Avanti Polar Lipids, USA) and 1,2-Dipalmitoyl-sn-Glycero-3-Phosphothioethanol (DPPTE; Avanti Polar Lipids) were deposited in 4:1 ratio. DPPTE was used to resemble the free thiol groups on the cell surface. Formation of lipid bilayer allowed MCS to bind on the substrate by dipping in 10 mM MCS solution for 30 min. Finally, substrate was dipped in 1.5 mg/mL chitosan solution for 2 hr. Every examination was held after washing two times with PBS.

2.3. Cell culture

2.3.1. Cell preparation

Human bone marrow-derived mesenchymal stem cells were purchased from a commercial source (Lonza, USA). H9C2 cells, a rat cardiac myoblast cell line, were purchased from Korean Cell Line Bank (Korea). Articular cartilage tissue slices from knee joints of 2-3 months New Zealand white rabbits (Hallim Experimental Animals Ltd., Korea) were treated with 0.2% collagenase D (Sigma, USA) in a high-glucose DMEM (Gibco BRL, USA) overnight at 37°C in humid air with 5% CO_2 in our laboratory. After treated for 16 hours overnight, the chondrocytes were enzymatically released. The cell yield was $5x10^5$ cells/knee joint. The released cells were plated on TCPS (Corning, USA) at density $1x10^4$ cells/cm^2 for assessment of the chondrogenic phenotypes at various passage numbers. Mouse skeletal myoblast cell line C2C12 cells were purchased from Korean Cell Line Bank (Korea). Prior to coculture, all of the cells were cultured in growth medium consisting of high-glucose Dulbecco's modified Engle's Medium (DMEM; Gibco BRL, USA) containing 10% (v/v) fetal bovine serum (FBS; Gibco-BRL) and 1% (v/v) penicillin-streptomycin (PS; Gibco-BRL) at 37 °C in humid air with 5% CO_2.

2.3.2. Coculture of MSCs and H9C2 cells with NTHP membranes

For the coculture of MSCs and H9C2 cells using NTHP membranes, H9C2 cells were plated at a density of $2x10^3$ cells/cm^2 on TCPS dishes, and MSCs were plated at a density of $3x10^3$ cells/cm^2 on NTHP membranes. The following day, the MSC-seeded NTHP membrane was layered on top of the H9C2-seeded TCPS dish. To prevent the layered membrane from moving, a square stainless steel ring was placed on top of the NTHP membrane. Two coculture methods using the Transwell system, *i.e.* indirect and direct coculture, were used for comparison. In indirect coculture, H9C2 cells were seeded on a Transwell insert and MSCs were seeded on the lower six-well plate compartment. In direct coculture, MSCs were seeded on the bottom side of the Transwell membrane. The following day, H9C2 cells were seeded on the other (top) side of the Transwell membrane. For non-cocultured control groups, MSCs were cultured on TCPS dishes or NTHP membranes. Cells were cultured in growth medium consisting of low-glucose DMEM (Gibco BRL, USA) containing 10% (v/v) FBS (Gibco-BRL) and 1% (v/v) PS (Gibco-BRL) at 37 °C in humid air with 5% CO_2. The medium was changed every 2 days.

2.3.3. Coculture of MSCs and chondrocytes with BNTHP membranes

Five groups were compared to elucidate the effects of cLbL culture system on chondrogenic differentiation of the MSCs; non-cocultured MSCs cultured on BNTHP membranes, non-cocultured MSCs in pellet without BNTHP membranes, cocultured MSCs with BNTHP-based indirect system, cocultured MSCs with BNTHP-based direct system membranes, and cocultured MSCs with BNTHP-based cLbL system. For non-cocultured groups, MSCs were monocultured either on BNTHP membrane or in pellet form. For pellet formation, $1x10^5$ MSCs in 15 mL polypropylene tube (Corning, USA) were centrifuged at 150g for 5 minutes according to a previous study.[98] For coculture group, chondrocytes at passage 1 were plated at a density of $2.5x10^3$ cells/cm^2 on either TCPS or BNTHP membrane. MSCs at passage 5 were plated at a density of $7.5x10^3$ cells/cm^2 on BNTHP membrane. 24 hours after cell seeding, MSCs and chondrocytes were stacked for coculture. In BNTHP-based indirect coculture, the MSCs-attached BNTHP membrane was layered on top of the chondrocytes-attached TCPS. A round, 1-mm high stainless steel ring was placed between MSCs-attached BNTHP membrane and chondrocytes-attached TCPS to eliminate cell-cell contact. In BNTHP-based direct coculture, the MSCs-attached BNTHP membrane was directly layered on top of the chondrocytes-attached TCPS. In BNTHP-based cLbL coculture, the MSCs-attached BNTHP membrane was directly layered between chondrocytes-attached BNTHP membrane (top) and chondrocytes-attached TCPS (bottom). To prevent the layered membranes from moving, a round stainless steel ring was placed on top of the cells-attached BNTHP membranes. A chondrogenic medium consisting of serum-free high-glucose DMEM (Gibco BRL, USA), 50 mg/mL ascorbic acid (Sigma, USA), 100 nM dexamethasone (Sigma, USA), 1% (v/v) ITS (Gibco-BRL,

USA) and 1% (v/v) penicillin-streptomycin (PS; Gibco-BRL,USA) supplemented with 10 ng/mL TGF-β3 (PeproTech, USA) was changed every 2 days.

2.3.4. Coculture hMSCs and C2C12 cells with chitosan thin films

C2C12s were collected in 1.7 mL tube and coated with 10 mM MCS and 1 mM TCEP solution. Then, MCS-grafted C2C12s were seeded on top of the chitosan film-deposited hMSCs layer for coculture at cell number ratio of hMSC:C2C12 = 1:2. The cells were cocultured in DMEM (Gibco-BRL, USA) containing 5% (v/v) horse serum (HS; Gibco-BRL) and 1% (v/v) PS (Gibco-BRL). For analyses that required visualization of the coculture system under fluorescence microscope, hMSCs were labelled with red fluorescent DiI dye (6.25 μg/mL; Sigma-Aldrich Co.), C2C12s with blue fluorescent CellTracker Blue CMAC Dye (25 μM, Life Technologies, USA), and chitosan with FITC prior to coculture. Z-stack images of chitosan thin film-based coculture of hMSCs and C2C12s were captured 48 hr after coculture using a confocal microscope (Carl Zeiss; LSM 780). As a comparative group, direct coculture of hMSCs and C2C12s using commercial Transwell system (8 μm pore, polyester membrane; Corning, USA) was also performed. hMSCs were seeded on the bottom side of the Transwell membrane. The following day, C2C12s were seeded on the other (top) side of the Transwell membrane. Cell number ratio of hMSCs and C2C12s was cultured at the same cell number ratio with the chitosan thin film-based coculture group. The cells were cocultured in 5% HS growth medium (a high-glucose DMEM with 1% (v/v) PS (Gibco-BRL) and 5% (v/v) HS (Gibco-BRL)). For non-cocultured control groups, hMSCs were monocultured in either 10% FBS growth medium (a high-glucose DMEM with 1% (v/v) PS (Gibco-BRL) and 10% (v/v) FBS (Gibco-BRL)), 5% HS growth medium, or myogenic-induction medium ((a high-glucose DMEM with 1% (v/v) PS (Gibco-BRL) and 5% (v/v) HS (Gibco-BRL) supplemented with 100 nM dexamethasone (Sigma Aldrich Co.) and 50 μm hydrocortisone (Sigma Aldrich Co.)). Monoculture

of hMSCs with chitosan thin in 10% FBS growth medium was also set as a comparative group. The medium was changed every 2 days.

2.4. Experimental procedures *in vitro*

2.4.1. Cytotoxicity studies

2.4.1.1. Cell viability and proliferation on NTHP membranes

MSCs were seeded at a density of $3x10^3$ cells/cm^2 on TCPS dishes, Transwell membranes (pore size 400 nm), and NTHP membranes (pore size 380 nm). Transwell culture inserts for six-well plates (0.4 μm pore, polyester membrane) were purchased from a commercial source (Corning, USA). The viable cell number was determined using cell counting kit-8 assay (CCK-8, Sigma-Aldrich Co.) (n=3 per groups). The gene expression levels of BAX and Bcl-2 in MSCs were determined by qRT-PCR to assess the expression of apoptotic and anti-apoptotic genes, respectively (n=3 per group). The proliferating cells were evaluated by immunocytochemistry using antibodies against PCNA. The samples were mounted in 4,6-diamidino-2-phenylindole (DAPI, Vector Laboratories, USA) for nuclear staining. Each image was photographed using a fluorescence microscope (IX71 inverted microscope, Olympus, Japan). The numbers of PCNA-positive cells were digitally quantified (n=10 images per group) using Image Pro Plus software (Media Cybernetics, UK).

2.4.1.2. Cell viability and proliferation on BNTHP membranes

MSCs and chondrocytes were seeded at a density of $3x10^3$ cells/cm^2 on either TCPS or BNTHP membrane. The adhesion of MSCs and chondrocytes on BNTHP membranes at day 3 were captured with a light microscope (IX71 inverted microscope, Olympus, Japan). The gene expression levels of *BAX*, *BCL2*, and caspase 3 in MSCs were determined by qRT-PCR (n=3 per group). The number of viable MSCs was determined using CCK-8 assay (Sigma, USA) (n=3 per groups). Live and dead cells were assessed using a two-colour fluorescence live/dead assay kit (Molecular Probes, USA). Each image was photographed using a fluorescence microscope (IX71 inverted microscope, Olympus, Japan). The number of live cells were digitally quantified (n=12 images per group) using Image Pro Plus software (Media Cybernetics, UK).

2.4.1.3. Cell viability and proliferation upon TCEP reductant treatment and MCS engraftment

Cell viability was imaged by Live/Dead® viability/cytotoxicity kit (Live/Dead; Thermo) that contains calcein-AM and ethidium homodimer solution. After treatment of TCEP for 10 min on both cell types, Live/Dead assay were used to indicate live cells and dead cells. To examine the cellular proliferation rate, Click-iT® EDU Alexa Fluor® 488 Imaging kit (EDU; Thermo) was used and analyzed by fluorescence-activated cell sorting (FACS, FACS Aria II, BD Biosciences, USA). Prior to EDU assay, both cells were cultured overnight in serum free media for the synchronization of cell growth. After synchronization, cells were treated with reductant and EDU assay kit was then applied to indicate cells in S phase. For the determination of daily cell number, CCK-8 (Sigma-Aldrich Co.) was treated and measured by the absorbance at 450 nm using a microplate reader(Infinite® 200 PRO, Tecan, Swiss). The cytotoxity effect of MCS grafting was evaluated with the same procedure. Cells were grafting with 10 mM MCS solution. Cell apoptosis markers were also measured by qRT-PCR analysis.

2.4.2. Analyses of cell-cell interactions in various coculture systems

2.4.2.1. Cell-cell interactions in coculture using NTHP membranes

The proximities between MSCs and H9C2 cells cocultured on the two sides of the NTHP membranes with different pore sizes and the Transwell membranes were observed by pre-labelling the MSCs with DiO (6.25 μg/ml; Sigma-Aldrich Co., USA) and H9C2 with DiI (6.25 μg/ml; Sigma-Aldrich Co.), prior to coculture. Images were captured using a confocal microscope (SP8 X STED, super-resolution confocal microscope, Leica, Germany) after 48 hours of coculture.

For the dye transfer assay, MSCs were dual-labelled with DiI (Sigma-Aldrich Co.) and calcein-AM (Sigma-Aldrich Co.). MSCs on TCPS were incubated in DiI working solution (6.25 μg/ml) for 2 hours at 37 ℃ and then rinsed with culture medium three times to wash off excess DiI. Next, the MSCs were incubated in serum-free culture medium containing calcein-AM (10 μmol/L, a cell-permeable ester form of calcein) for 30 minutes at 37 ℃, and rinsed with PBS three times to wash off the extracellular calcein-AM. Subsequently, the dual-labelled MSCs were trypsinized and plated on NTHP membrane. The MSC-seeded NTHP membrane was layered on top of H9C2-seeded glass-bottom culture dishes (Corning). Images were captured after 48 hours of coculture using a confocal microscope (SP8 X STED, super-resolution confocal microscope, Leica) to investigate dye transfer from MSCs to H9C2. The dye transfer assay was performed based on previous studies.[24,99-100]

To determine the rate of protein diffusion through the NTHP and Transwell membranes, a protein diffusion chamber was designed. A Transwell or NTHP membrane was used to partition the protein diffusion chamber into two secluded compartments filled with 10 mL of 10 μg/mL bovine serum albumin

(BSA, Sigma-Aldrich Co.) solution on one side and phosphate buffer saline (PBS, Sigma-Aldrich Co.), of equal volume, on the other side. Samples were collected from the PBS chamber at various time points, and the concentrations of BSA in the samples were quantified using the Bradford protein assay (n=3 per group) (Sigma-Aldrich Co.).

2.4.2.2. Cell-cell interaction in coculture using BNTHP membranes

MSCs and chondrocytes were pre-labelled with DiI (6.25 μg/mL; Sigma, USA) and DiO (6.25 μg/mL; Sigma, USA), respectively and cocultured *via* BNTHP-based direct and cLbL coculture systems. After 48 hours of coculture, images for colocalizations of MSCs and chondrocytes were captured using a confocal microscope (SP8 X STED, super-resolution confocal microscope, Leica, Germany) and visualized with LAS AF software (Leica, Germany).

For the dye transfer assay, either MSCs or chondrocytes on TCPS were incubated in DiI working solution (6.25 μg/mL; Sigma, USA) for 2 hours at 37 ℃ and then rinsed with culture medium three times to wash off excess DiI. Next, the cells were incubated in serum-free culture medium containing calcein-AM (10 μmol/L; Sigma, USA) for 30 minutes at 37 ℃, and rinsed with PBS three times to wash off the extracellular calcein-AM. Subsequently, the dual-labelled cells were trypsinized and plated on BNTHP membranes. Meanwhile, chondrocytes on TCPS were incubated in DAPI working solution (0.1 μg/mL; Sigma, USA) for 30 minutes, rinsed with culture medium three times, and re-plated onto new dishes at 37 ℃. For the BNTHP-based direct coculture, dual-labelled MSCs-seeded BNTHP membrane was layered on culture dish seeded with DAPI-labelled chondrocytes. For the BNTHP-based cLbL coculture, additional BNTHP membrane seeded with un-labelled MSCs was prepared. Then, dual-labelled chondrocytes-seeded BNTHP membrane was sequentially layered with un-labelled MSCs-seeded BNTHP membrane followed by dual-labelled chondrocytes-seeded BNTHP membrane. Images were captured after 48 hours of coculture using a confocal microscope (SP8 X STED, super-resolution confocal microscope, Leica) to investigate the calcein dye transfer. The dye transfer assay was performed based on previous studies.[101-102]

In separate experiments with identical coculture system of unlabeled MSCs and chondrocytes, western blot analyses for integrin β1, DDR2, and

connexin 43 expressed by MSCs collected from either BNTHP-based direct bilayer or cLbL coculture system were performed to analyze the cell-ECM interactions between the cocultured cells (n=3 per group). In addition, western blot analyses on ERK, JNK, p38 and their phosphorylation forms expressed by the MSCs collected from either BNTHP-based direct or cLbL coculture system were performed to analyze the extent of interactions between MSCs and chondroinductive paracrine factors secreted by chondrocytes, such as TGF-β1,[35,37] BMP-2,[38] IGF-1,[39] and FGF-2 based on previous reports (n=3 per group).[40]

2.4.2.3. Cell-cell interaction in coculture using chitosan thin films

C2C12s were pre-labelled with DiI (6.25 μg/mL; Sigma, USA) for 2 hr at 37 ℃ and washed with PBS three times to wash off excess DiI. DiI-labelled C2C12s were were incubated in serum-free culture medium containing calcein-AM (10 μM; Sigma-Aldrich Co.) for 30 min at 37 ^{o}C, and washed with PBS three times to wash off the extracellular calcein-AM. The dual-labelled C2C12s were trypsinized and layered on top of chitosan thin film-deposited, non-labelled hMSCs. Calcein dye transfer was evaluated after 48 hr of coculture using a confocal microscope (SP8 X STED, super-resolution confocal microscope, Leica).

2.4.3. Homogeneity assessment of the collected MSCs post-coculture

Prior to coculture, MSCs were pre-labelled with DiO (6.25 μg/ml; Sigma-Aldrich Co.). H9C2 and chondrocytes were pre-labelled with DiI (6.25 μg/ml; Sigma-Aldrich Co.). In coculture with C2C12s, hMSCs were non-labelled, while C2C12s were pre-labelled with blue fluorescent CellTracker Blue CMAC Dye (25 μM, Life Technologies).

After coculturing for 1 week, images of the cocultured MSCs and H9C2 cells were captured using a fluorescence microscope (IX71 inverted microscope, Olympus). Images of the MSCs harvested from the transfer of MSC-seeded NTHP membranes (380 nm pore size) onto new culture dishes after coculturing for 1 week, were photographed using a fluorescence microscope (IX71 inverted microscope, Olympus). Also, after coculturing for 2week, Images of the MSCs harvested from the transfer of MSC-seeded BNTHP membranes onto new culture dishes were photographed using a fluorescence microscope (IX71 inverted microscope, Olympus) and quantified (n=12 images per group).

To assess the purity of the collected cells following coculture, cells adhered to the transferred NTHP membranes or BNTHP membranes were trypsinized and evaluated by fluorescence-activated cell sorting (FACS Aria II BD Biosciences, USA) installed at the National Center for Interuniversity Research Facilities at Seoul National University and fluorescence microscopy (IX71 inverted microscope, Olympus) (n=10 images per group). MSCs from the Transwell direct coculture group were collected *via* trypsinization. Also, one week after coculture, the population of non-fluorescence labeled hMSCs was quantified in non-cocultured hMSCs, C2C12s-layered hMSCs, and C2C12s-delayered hMSCs. The cells were trypsinized and the population was evaluated by FACS (FACS Aria II BD Biosciences).

2.4.4. Generation of transfer-printable cell sheets

Cell sheet printing was achieved by transferring an MSC-seeded, thermoresponsive NTHP membrane onto a new culture dish and changing the temperature. The MSC-seeded membrane was turned upside down and incubated for 4 hour at 37 °C, allowing the cell sheet to adhere to the new culture dish. Printing was then induced by incubating the membrane for 30 minutes at 20 °C. Cell sheet printing was observed under a light microscope (IX71 inverted microscope, Olympus). For histological analysis, the printed cell sheet was embedded in Optimal Cutting Temperature (OCT) compound (Sakura Finetek, USA), frozen, and cut (10 μm in thickness) using a cryostat cryocut microtome (Leica, CM3050S, Germany). After hematoxylin and eosin (H & E) staining, the stained cross-sections of the cell sheet were examined by light microscopy (IX71 inverted microscope, Olympus). The viability of the cells harvested *via* transfer-printing was compared to that of trypsinized cells by assessing the nmber of live and dead cells using calcein-AM and ethidium homodimer, respectively. A two-colour fluorescence live/dead assay kit (Molecular Probes, USA) (n=10 images per group) was used for analysis. To analyze the extracellular matrices of the transfer-printed cell sheet, immunocytochemical staining and western blot analyses (n=3) were performed. For examination of bilayered cell sheets, prior to transfer-printing, each cell sheet was pre-labelled with DiI (6.25 μg/ml; Sigma-Aldrich Co.) or DiO (6.25 μg/ml; Sigma-Aldrich Co.). Subsequently, transfer-printing was performed and the DiI-labelled cell sheet was stacked on the DiO-labelled cell sheet. The z-stack 3D confocal images of the bilayered cell sheets were obtained using a confocal microscope (SP8 X STED, super-resolution confocal microscope, Leica).

2.4.5. Quantitative reverse transcriptase polymerase chain reaction (qRT-PCR)

The gene expressions of cells were evaluated using qRT-PCR. RNA was extracted and reverse-transcribed into cDNA. mRNA expressions were evaluated using StepOnePlus real-time PCR system (Applied Biosystems, USA) with FAST SYBR Green PCR master mix (Applied Biosystems). Each gene expression was normalized to *GAPDH* expression. The PCR consisted of 45 cycles of denaturing (95 ^{o}C, 10 seconds), annealing (60 ^{o}C, 15 seconds), and elongation (72 ^{o}C, 15 seconds) (n=3 per group). All of the data were analyzed using the $2^{-\Delta\Delta Ct}$ method.

2.4.6. Cell double-labelling with mal-alexa fluor 488 and PKH26

PKH26 Red Fluorescent Cell Linker Kit (PKH26; Sigma-Aldrich Co.) was used to label each cell types, hMSCs or C2C12s, according to the manufacturer's protocol. For hMSCs, PKH26 labeled cells were cultured at a glass bottom dish for confocal imaging. Prior to cell coating with Alexa Fluor® 488 C_5 Maleimide (Mal-Alexa Fluor 488; 1 mg/mL, Thermo), cells were washed twice with PBS (Sigma Aldrich Co.). Then, cells were reduced by 1 mM TCEP (Sigma-Aldrich Co.) reductant solution for 5 min. Next, after eliminating the reductant solution, Mal-Alexa Fluor 488, dissolved in PBS solution (final concentration of 3 μg/mL) was added to the cells and incubated for 20 min in 37 ^{o}C incubator. Double-labeled hMSCs were washed with PBS twice and fixed with 4% paraformaldehyde (PFA) solution (Sigma-Aldrich Co.) for 10 min. For C2C12s, $2x10^{6}$ PKH26 labeled cells were collected in 1.7 mL-tubes by centrifugation and washed two times with PBS. Washed cells were suspended by 1 mL of PBS containing 1 mM of TCEP. After reduction, 1 mL of 3 μg/mL Mal-Alexa Fluor 488 solution was treated for surface coating. Samples were incubated for 20 min in 37 ^{o}C. After incubation, cells were washed with PBS twice and also fixed with 4% PFA solution for 10 min. Confocal images were obtained by Carl Zeiss LSM 780 confocal microscope (Germany).

2.4.7. ζ-potential Analysis

MCS-grafted cells were collected to 1.7mL tubes ($2x10^6$ cell/tube). 750 μl of DMEM media and 250 μl of chitosan solution (1.5 mg/ml) were added to the tube. Sample tube was incubated in 37 ^oC incubator for an hour followed by washing two times with PBS. Non-treated, MCS-grafted, and chitosan-deposited cells ($2x10^6$ cell/group) were prepared. All groups were loaded to Nanozs (Malvern, Germany) for ζ-potential measurement.

2.4.8. Delayering of C2C12 cells following coculture with chitosan thin film

In situ fluorescence microscopic observation (IX71 inverted microscope, Olympus, Japan) of the chitosan thin film detachment was carried out using a custom made flow cell with a height of 2.5 mm, a width of 11.5 mm and a length of 50.7 mm. The flow cell was consisted of two transparent slide glasses as the bottom and upper walls of the flow channel. On the bottom wall, hMSCs and C2C12s were cocultured with chitosan-FITC thin film. A peristaltic pump (Masterflex, USA) was used to generate a constant flow rate within the flow cell. PBS, with density of $1.0x10^3$ kg/m^3 and viscosity of 1.0x10 Pa·s, was used as the feed solution. Shear force generated by the pressure-driven flow at certain flow rate induced detachment of the chitosan thin film and delayering of C2C12s. This experiment was repeated three times to obtain the critical flow rate that induced the detachment of the chitosan thin film. From the measurement of the critical flow rate, the critical wall shear stress was calculated with computational fluid dynamics (CFD) using a commercial CFD software. To delayer C2C12s from a chitosan thin film-based heterogeneous coculture system built on tissue culture plate, a 1 mL-micropipette was used to generate a PBS flow and initiate detachment of the chitosan thin film.

2.4.9. Elimination of MCS along with Removal of the Chitosan Thin Film

FITC-conjugated MCS was used in chitosan thin film-based coculture system to observe the elimination of MCS. The presence/elimination of MCS was observed with a fluorescence microscope (IX71 inverted microscope, Olympus) after deposition/delayering of the chitosan thin film.

2.4.10. Analysis of Paracrine Secretion Profiles

Paracrine secretion by hMSCs was analysed using proteome profiler human angiogenesis array (R&D systems, USA) according to the manufacturer's instruction. After 1 week of coculture, C2C12s were delayered from hMSCs with chitosan thin film. hMSCs from all groups were trypsinized and plated at a density of $8000x10^3$ cells/cm^2 in a 6-well cell culture plate. 48 hr later, conditioned medium was collected for analysis. Quantitative analysis was performed with densitometry using Image J (National Institutes of Mental Health).

2.5. Experimental procedures *in vivo*

2.5.1. Generation and subcutaneous implantation of cells-laden BNTHP membrane 3D constructs into athymic mice

After 2 weeks of coculture/monoculture in a chondrogenic medium consisting of serum-free high-glucose DMEM (Gibco BRL, USA), 50 mg/mL ascorbic acid (Sigma, USA), 100 nM dexamethasone (Sigma, USA), 1% (v/v) ITS (Gibco-BRL, USA) and 1% (v/v) PS (Gibco-BRL,USA) supplemented with 10 ng/mL TGF-β3 (PeproTech, USA), chondrogenic differentiated cells-attached BNTHP membranes were collected, washed with PBS to remove the excessive chondrogenic culture media, separated from the PET frame, and formed into 3D constructs through centrifugation at 500 g for 5 minutes. Each 3D construct consisted of three layers of chondrogenic differentiated cells-laden BNTHP membrane. The 3D constructs were subcutaneously implanted into six-week-old female BALB/c athymic mice (Orient Bio, Korea). Nice mice were tested in each group. Each mouse was implanted with samples from four different sample groups (non-cocultured, indirect, direct, and cLbL group) in separate subcutaneous pocket region to eliminate bias between individuals. The mice were anesthetized using ketamine (100 mg/kg) and xylazine (10 mg/kg). Previous studies examined the formation of cartilage tissue at 4-week time point after subcutaneous implantation of chondrogenic differentiated cells in athymic mice.[25,35,103] Thus, after 4 weeks of implantation, the animals were euthanized by CO_2 asphyxiation, and the implanted constructs were harvested for gross observation, immunohistochemical analyses, and Western blot analyses. The animal study was approved by the Institutional Animal Care and Use Committee of Seoul National University (SNU-160720-12).

2.5.2. Induction of cardiotoxin-induced skeletal muscle injury model and implantation of differentiated cells

Six-week-old female BALB/c athymic mice (Orient Bio, Korea) were anesthetized using ketamine (100 mg/kg) and xylazine (10 mg/kg). 50 μl of 10 μM cardiotoxin (Latoxan, France) in PBS was injected into right tibialis anterior muscles. 24 hr after cardiotoxin treatment, the mice were anesthetized as described above and $5x10^5$ cells of hMSCs cultured for 1 week in various culture conditons (cultured in 10% FBS medium, myogenic medium or C2C12-cocultured with chitosan thin film) were delivered *in vivo* by intra-muscular injection into the injured muscle. 10 days after cell injection, the animals were euthanized by CO_2 asphyxiation and the tibialis anterior muscles were harvested tendon-to-tendon for histological observation, immunohistochemical analysis, and western blot analysis. The animal study was approved by the Institutional Animal Care and Use Committee of Seoul National University (SNU-160720-12).

2.6. Western blot analyses

Cell and tissue lysates were prepared with cell lysis buffer (Cell Signaling, USA). The total concentration of the protein was quantified with the Bradford protein assay (Sigma, USA) prior to samples loading on a 10% (w/v) SDS-polyacrylamide gel. Proteins were transferred to Immobilon-P membrane (Millipore Corp., USA), blocked with 5% skimmed milk solution for 1 hour at RT, and incubated with antibodies overnight at 4 ^{o}C. The membrane was incubated with horseradish peroxidase-conjugated secondary antibody (Santa Cruz Biotechnology, USA) for 1 hour at RT. The blots were developed using a chemiluminescence detection system (Amersham Bioscience). All antibodies were purchased from Abcam (USA).

2.7. Histochemical and immunohistochemical staining

Cells were fixed in 4% paraformaldehyde solution, permeabilized with 0.1% Triton X-100, and then blocked with 1% BSA for 1 hour for actin filament staining. The actin filaments of the cells were stained by tetramethylrhodamine isothiocyanate-conjugated phalloidin (1:40; Molecular Probes, USA). The cell nuclei were counterstained DAPI (Vector Laboratories, USA). The number of multinucleated hMSCs following 1 week of culture in various conditions was observed *via* fluorescence microscope (IX71 inverted microscope, Olympus) based on images of cellular actin filaments stained by tetramethylrhodamine isothiocyanate-conjugated phallodin (n = 200 cells per group).

For immunocytochemical staining, cells were fixed in 4% paraformaldehyde solution, permeabilized with 0.6% Triton X-100 and then blocked with 10% donkey serum (Jackson ImmunoResearch Laboratories, USA). Prior to permeation, cells from the *in vitro* pellet group were embedded in O.C.T. compound (Scigen, USA) and sectioned at a thickness of 10 μm. The samples were then reacted with antibody and detected with either tetramethylrhodamine isothiocyanate-conjugated secondary antibodies (Jackson ImmunoResearch Laboratories) or fluorescein isothiocyanate-conjugated secondary antibodies (Jackson ImmunoResearch Laboratories). The samples were mounted in 4,6-diamidino-2-phenylindole (DAPI, Vector Laboratories, USA) for nuclear staining. Fluorescence images were captured using a fluorescence microscope (IX71 inverted microscope, Olympus, Japan).

The subcutaneously implanted 3D constructs were explanted and fixed in 4% PFA (Sigma, USA), dehydrated in a graded alcohol series, and embedded in paraffin. The constructs were sectioned at a thickness of 4 μm, stained with antibody, and detected with either tetramethylrhodamine isothiocyanate-conjugated secondary antibodies (Jackson ImmunoResearch Laboratories) or fluorescein

isothiocyanate-conjugated secondary antibodies (Jackson ImmunoResearch Laboratories). The cell nuclei were counterstained DAPI (Vector Laboratories, USA). Fluorescence images were captured using a fluorescence microscope (IX71 inverted microscope, Olympus, Japan).

To examine degradability of the BNTHP membranes inside the constructs, constructs of cLbL coculture group were retrieved at 1, 2, 3, and 4 weeks following implantation. The constructs were fixed, dehydrated, embedded, and sectioned as stated above. The cross-sectioned constructs were stained with H&E staining.

The harvested muscle tissues were immersed in 4% PFA solution (Sigma Aldrich Co.), embedded in O.C.T. compound (Scigen, USA) and sectioned at a thickness of 10 μm. The sections were stained with Hematoxylin & Eosin staining method and observed under light microscope ((IX71 inverted microscope, Olympus). Based on the obtained images, the number of myofibre and the cross-sectional area of myofibre were determined using Image J (National Institutes of Mental Health). n = 6 images per group. The sections were immunohistologically stained with antibodies. The immunostaining signal was detected either tetramethylrhodamine isothiocyanate-conjugated secondary antibodies (Jackson ImmunoResearch Laboratories) or fluorescein isothiocyanate-conjugated secondary antibodies (Jackson ImmunoResearch Laboratories). The nuclei were counterstained with DAPI (Vector Laboratories).

2.8. Statistical analysis

The quantitative data are expressed as the means ± standard deviations. The statistical analyses were performed through one-way analysis of variance (ANOVA) with Tukey's significant difference post hoc test using the SPSS software (SPSS Inc., USA). A value of $p<0.05$ was considered to denote statistical significance.

Chapter 3.

Development of nanothin coculture membranes with tunable pore architecture and thermoresponsive functionality for generation of transfer-printable stem cell-derived cardiac sheets

3.1. Introduction

Stem cell therapy has been spotlighted as a promising approach for various types of disease treatments and tissue regeneration. However, despite their multipotency, transplantations of naïve stem cells have shown low differentiation efficiency *in vivo*.[15] Such outcomes are the result of the incompatible physicochemical characteristics of stem cells with the surrounding *in vivo* environment,[15,104] discouraging the creation of an optimal milieu for tissue repair. Thus, inducing stem cell differentiation into the desirable cell type, prior to implantation, has been proposed to improve their therapeutic results.[15,17,104] The differentiation of stem cells can be regulated by the surrounding microenvironment, the so-called stem cell niche.[64] Several approaches, such as introducing bioactive molecules or scaffolds that provide the biomimetic microenvironments, have been reported to promote the differentiation of stem cells.[50-52] However, such artificial microenvironments may be insufficient in mimicking the complex nature of native microenvironments to regulate the differentiation of stem cells.[53] Instead, coculturing stem cells with the desired type of differentiated cells is highly effective in controlling their fate.[59,105-106] The coculture strategy induces stem cell differentiation by providing the naturally occurring cell-to-cell cross-talk, either through soluble paracrine factors or direct cell-cell contact, mimicking the native tissue microenvironment.[107] Several studies using coculture have reported effective stem cell differentiation into osteoblast,[105] cardiomyocyte,[59] neuronal and glial cells.[106]

The features of the membrane used in coculture systems are critical to stem cell differentiation outcomes. The membrane should allow effective cell-to-cell cross-talk and at the same time prevent mixing of the cells.[78,80] ‘Transwell®’ is a commercially available porous membrane that is conventionally used for coculture. However, due to the ‘track-etched' fabrication method, the membrane showed poor membrane parameter as an ideal coculture membrane, with 10 μm

thick thickness and low porosity.[80] Thus, developing an ultra-thin, highly porous membrane that allows effective direct cocultured cellular contacts and paracrine factor diffusion across the membrane, is required for efficient stem cell differentiation. In addition, implanting multilayered cell sheets was reported to result in better therapeutic outcomes than single-layered cell sheets, as more cell-cell junctions and ECM resulted in better reparative effects of the cells.[108-110]

Here, we report the development of NTHP membranes with a thermoresponsive property for generating transfer-printable sheets of cells differentiated from stem cells through coculture. The nanothin and highly nanoporous architecture of the NHTP membrane was realized by a VIPS mechanism using a spin-coating process. By using this process, the pore size of NTHP membranes was finely tuned at the nanoscale level by changing the process parameters and conditions. The NTHP membranes are ~ 20-fold thinner and ~ 25-fold more porous than conventional 'Transwell' membranes. Also, the iCVD process was employed to graft a thermoresponsive layer conformally onto the NTHP membranes without altering their porous structure. We hypothesized that such features of the NTHP membrane would induce effective differentiation of stem cells into the desired cell type through coculture. The NTHP membrane would allow active cell-to-cell communication between the heterogeneous cocultured cells, as it significantly shortens the distance between the cells to the nanoscale level, creating a more *in vivo*-like environment. At the same time, the NTHP membrane would function as an effective physical barrier preventing cell cross-contamination. Another expected benefit of the free-standing, thermoresponsive NTHP membrane is that it can generate a transfer-printable cell sheet in response to temperature change. The NTHP membrane would allow easy harvesting of the differentiated cell sheets after coculture due to its free-standing, transferable property. In addition, it could be used to print the differentiated cell sheets to form

multilayered cell sheets or tissue for implantation. The ECM of the cell sheets are preserved with this technique, which would enhance the therapeutic efficacy of the cells following implantation. In short, the NTHP membrane developed in this study can be used as an effective coculture tool for engineering multilayered sheets of differentiated cells originating from stem cells, and serve as a promising modality for cell therapy.

3.2. Results and discussion

3.2.1. Fabrication and characterization of NTHP membrane

Figure 3.1A illustrates the procedure for the fabrication of the thermoresponsive NTHP membrane. When a non-solvent in the liquid phase comes in contact with a polymer solution, mass exchange between the polymer solution and non-solvent occurs rapidly, forming macrovoids in the membrane.[111] To induce the nanoscale pore architecture, the mass exchange rate was slowed down by using the vapor phase of the non-solvent (*i.e.*, water), with controlled RH, during the spin-coating process. RH has a decisive effect on the number and size of pores as it results in different composition paths as shown in the ternary phase diagram (Figure 3.1B).[112] Among the various process parameters in designing VIPS-based membranes,[113] in this study, the pore size of the NTHP membrane was tuned by controlling the RH, spin-rate and different types of solvent in polymer solution. NTHP membranes with distinctively different sizes of well-defined pores (*i.e.*, an average of 100 nm, 380 nm, and 860 nm pore size, respectively, with similar thickness) can be generated by changing the process parameters (Figure 3.1C)

The surface morphologies of commercial Transwell and our NTHP membranes (with comparable pore size of 400 nm and 380 nm, respectively) were examined and compared by SEM and AFM (Figure 3.1D). While the thickness and porosity of the Transwell membrane were 10 μm and 2%, respectively, those of the NTHP membrane were 380 nm and 54%, respectively (Figure 3.1E). This highlights the nanothin and highly porous architecture of the developed NTHP membrane.

To harvest transfer-printable cell sheets from NTHP membranes, the surface of the membrane was grafted with a thermoresponsive polymer, PNIPAAm.[114] Previous studies reported that changes in hydration of PNIPAAm

polymer in response to temperature can alter the cellular adhesiveness/non-adhesiveness of PNIPAAm-grafted surface.[114-117] Above the lower critical solution temperature (LCST) in aqueous solution of 32 °C, PNIPAAm-grafted polymer become mildly hydrophobic since the conformation of the PNIPAAm polymer chains collapses. The collapsed state of PNIPAAm polymer chains promotes adsorption of cell-adhesive proteins (*e.g.,* fibronectin) on the PNIPAAm-surface and allows subsequent cellular adhesion. Below the LCST, the PNIPAAm-grafted polymer rapidly swells and becomes highly hydrophilic. The entropic repulsion of the protein adsorption initiates the detachment of the cells.[118] To conformally graft a PNIPAAm layer onto NTHP membranes, while preserving the porous structure of the membranes, the iCVD method was adopted. iCVD is an effective method of coating various types of functional polymer thin films uniformly onto complex surfaces, including nano-patterned substrates and nanoporous membranes without altering the substrate structure and properties.[119] The NTHP membranes were initially coated with an epoxy-containing linker layer composed of pGMA,[120] followed by a grafting reaction with amine-terminated PNIPAAm using an epoxy-amine addition reaction (Figure 3.1F). This method successfully preserved the highly porous architecture of the NTHP membrane even after PNIPAAm engraftment (Figure 3.1G).

The chemical compositions of deposited polymer films were examined by FT-IR (Figure 3.1H). In the FT-IR spectrum of the pGMA-coated membrane, the characteristic epoxy pendant peaks at 760, 847, and 908 cm^{-1}, were clearly identified (yellow box in Figure 3.1H), indicating that the GMA monomers were successfully polymerized by the iCVD process without degradation of the epoxy functionality of the GMA monomer. The FT-IR spectrum of the PNIPAAm-immobilized surface clearly showed the increase of the secondary amides N-H stretching vibrations (3370-3270 cm^{-1}), compared to the pristine pGMA deposited

surfaces, confirming the PNIPAAm functionalization onto the NTHP membranes (gray box of inset spectra). Furthermore, in comparison with PNIPAAm powder, the decreased primary amine peak intensity of the PNIPAAm-immobilized surface clearly illustrated that the primary amine functionality in the amine-terminated PNIPAAm was consumed by the epoxy-amine addition reaction with the surface pGMA linker layer (blue box). A sharp, reversible phase transition of PNIPAAm-grafted surface was monitored by measuring the water contact angle change with repeated temperature variation (Figure 3.1I), demonstrating the thermoresponsive property of the PNIPAAm-grafted NTHP membranes.

Both SEM and AFM images were used to determine the average pore sizes of the NTHP membranes (Figure 3.2). Pore size represents the average value of the shortest and the longest axes of each pore. The average thickness, pore-size and porosity of commercial Transwell membrane and NTHP membranes with various pore sizes are presented in Table 3.1.

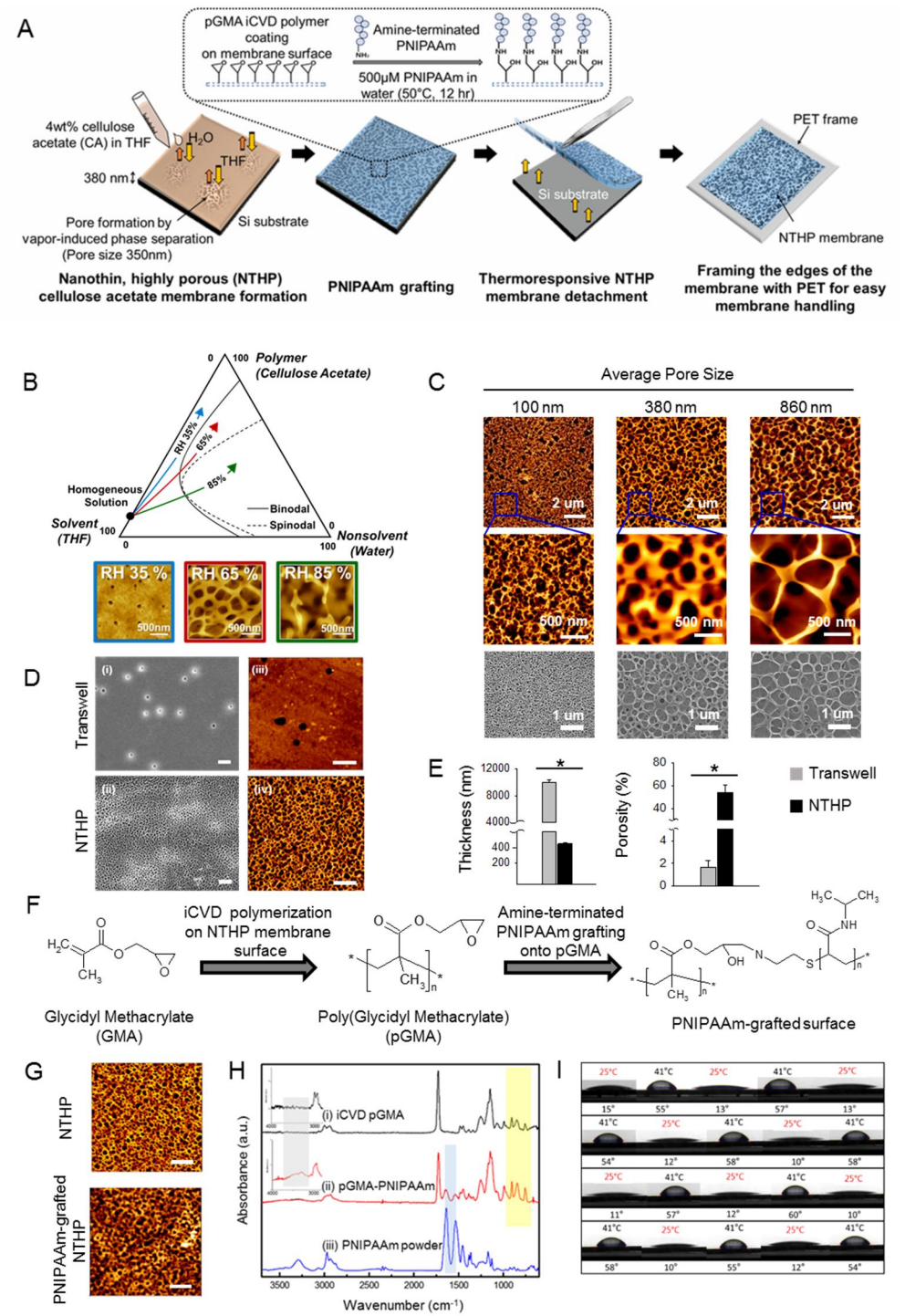

Figure 3.1. Fabrication and characterization of NTHP membranes with tunable pore architecture. (A) A schematic diagram showing the fabrication of

thermoresponsive NTHP membranes. (B) VIPS composition paths of NTHP membranes in a ternary phase diagram and the corresponding AFM images obtained at different RH. Bars, 500 nm. (C) Morphologies of NTHP membranes with different pore sizes. (D) SEM and AFM images of (i, ii) a Transwell membrane and (iii, iv) an NTHP membrane. Bars, 2 μm. (E) Thickness and porosity of a Transwell membrane and an NTHP membrane (with comparable pore size of 400 nm and 380 nm, respectively). $*p < 0.05$. (F) Schematic of the chemical reactions for the iCVD polymerization of GMA monomers and the grafting of PNIPAAm onto the pGMA-coated NTHP surface. (G) AFM images of NTHP membranes before and after the grafting of PNIPAAm. Bars, 2 μm. (H) FT-IR spectra of (i) iCVD pGMA polymer, (ii) PNIPAAm-grafted surface, and (iii) PNIPAAm powder. (I) Water contact angle measurements of the PNIPAAm-grafted surfaces at different temperatures.

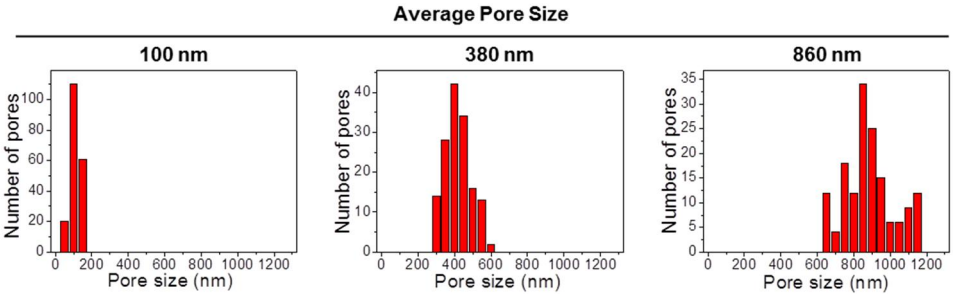

Figure 3.2. Pore size distributions of the NTHP membranes.

Table 3.1. The average thickness, pore-size and porosity of commercial Transwell membrane and NTHP membranes with various pore sizes (i.e., average pore size of 100 nm, 380 nm, and 860 nm pore-size of NTHP membranes), respectively. *p < 0.05 compared to the other groups.

	Transwell	**NTHP**		
		100 nm	**380 nm**	**860 nm**
Membrane Thickness (nm)	10,000	400 ± 12*	380 ± 7*	340 ± 6*
Pore Size (nm)	400	100 ±30*	380 ± 10*	860 ± 30*
Porosity (%)	2	45 ± 4*	54 ± 2*	59 ± 6*

3.2.2 Biocompatibility of NTHP membrane as cell culture substrate

To investigate the biocompatibility of NTHP membrane, MSCs were cultured on TCPS dishes (TCPS), Transwell membranes (Transwell), and NTHP membranes (NTHP). The viability, apoptotic activity, and proliferative activity of MSCs on each surface were measured for comparison. The numbers of live cells were obtained at various time points using a Cell Counting Kit-8 assay. The assay revealed no significant differences in the number of live cells among the groups (Figure 3.3A). In addition, we examined the expressions of a pro-apoptotic regulatory gene, BAX, and an anti-apoptotic regulatory gene, Bcl-2, on day 3 of the MSC culture. The data showed that MSCs on TCPS, Transwell, and NTHP membranes expressed comparable levels of apoptosis-regulatory genes (Figure 3.3B). Proliferating cell nuclear antigen (PCNA) staining on day 3 and day 7 also indicated comparable proliferation of MSCs between the groups (Figure 3.3C). Collectively, the data indicate that the NTHP membrane is a biocompatible cell culture substrate.

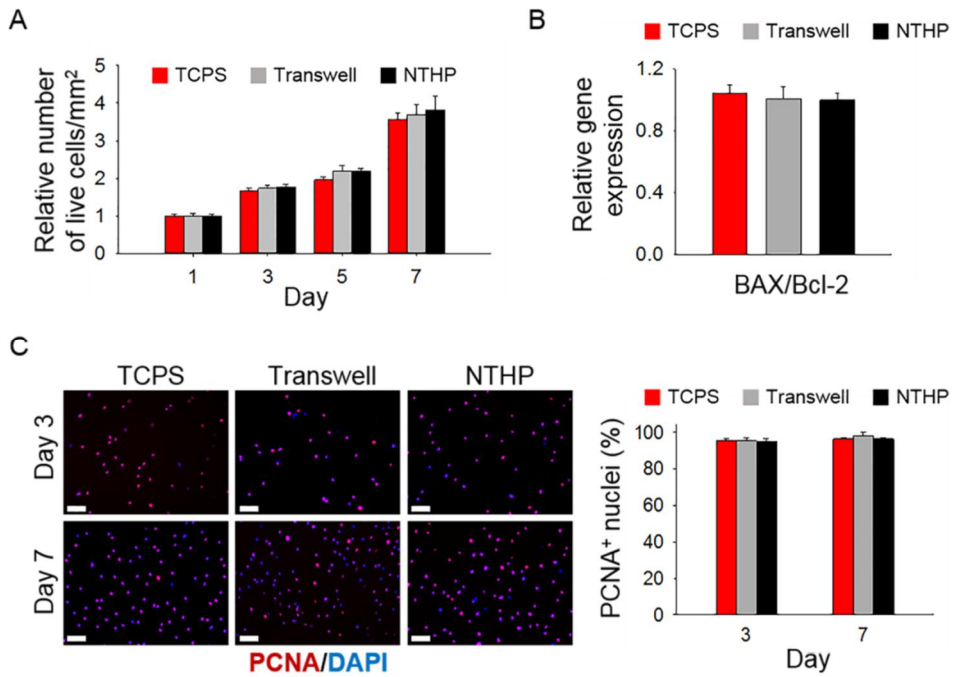

Figure 3.3. Biocompatibility of NTHP membranes evaluated in terms of live cell number, proliferation, and apoptotic activity of MSCs on the membranes. (A) The number of live cells expressed relative to the number of live cells on TCPS dish at day 1. The data were obtained using the CCK-8 assay. (B) Changes in expressions of apoptosis regulatory genes, a pro-apoptotic marker BAX and an anti-apoptotic marker Bcl-2, in MSCs cultured on various surfaces for 3 days evaluated by qRT-PCR. (C) Images and quantification of proliferating cells evaluated by PCNA immunocytostaining. $PCNA^+$ (red) cells are proliferating cells. DAPI (blue) stains nuclei. Bars, 100 μm.

3.2.3. Coculture with thermoresponsive NTHP membrane for the generation of transfer-printable cell sheet

Figure 3.4 illustrates the NTHP-based coculture system for generating transfer-printable differentiated cell sheets originating from cocultured stem cells. MSCs were seeded on the PNIPAAm-grafted surface of NTHP membranes at 37 °C. H9C2 cells (H9C2), a cardiomyoblast cell line, were seeded on culture dishes. Following this, the MSC-seeded NTHP membrane was layered on top of the H9C2-seeded culture dish for coculture. To secure the membrane stacking on H9C2 and prevent membrane displacement during coculture, a square stainless steel ring was placed on top of the membrane. MSCs were cocultured with H9C2 to induce the cardiac differentiation of MSCs by simulating the niche of MSCs with paracrine factors secreted from H9C2 and direct MSCs-H9C2 contact across the NTHP membrane.[24] After 1 week of coculture, the NTHP membrane, originally seeded with MSCs, was transferred from the H9C2-cultured dish onto a new culture dish. At a lower temperature of 20 °C, a sheet of cardiac-differentiated cells was printed on to the new dish.

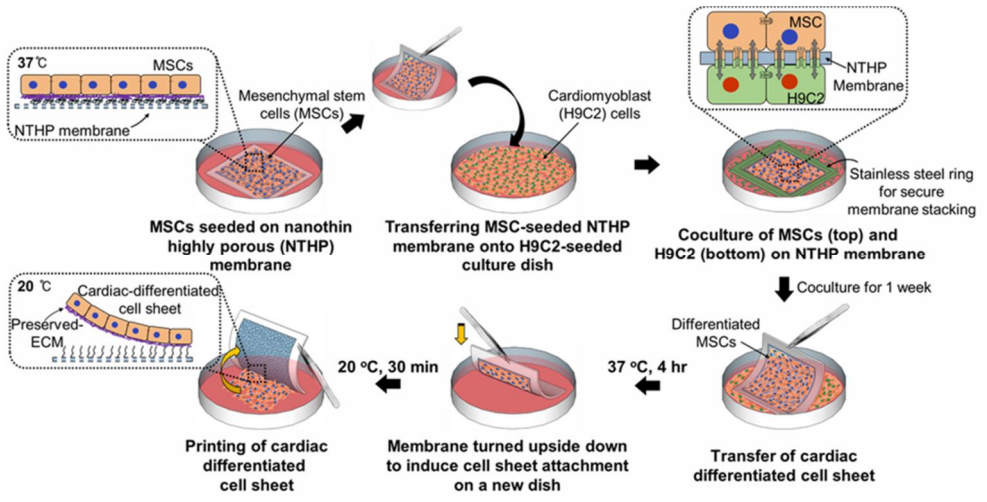

Figure 3.4. Schematic illustrations of the NTHP membrane-based generation of transfer-printable sheets of differentiated cells through coculture.

3.2.4 Varying extents of cellular interactions between cocultured cells depending on the different pore sizes of NTHP membranes

To determine the ideal pore size of NTHP membranes that would support maximum cell-to-cell communication (*i.e*, diffusion of paracrine soluble factors and cell junctions-mediated direct contacts), the extents of cellular interactions between the cocultured MSCs and H9C2 were examined. Cellular proximity along with protein diffusion across the NTHP membranes with varying pore sizes, were evaluated and compared to Transwell membranes. We also analyzed whether the pore dimensions of the membranes affect the functional gap-junction-mediated direct cell-to-cell cross-talk between MSCs and H9C2 using the calcein-AM dye transfer assay.

To observe the cell-to-cell proximity between MSCs and H9C2, each cell type was labelled with different colored dyes: MSCs with green and H9C2 with red (Figure 3.5A). The side view of the cocultured MSCs and H9C2, separated by a Transwell membrane, showed that the distance between the cocultured cells was as far as 10 μm, which corresponds to the thickness of the Transwell membrane (Figure 3.5Aii). In contrast, the cocultured MSCs and H9C2 in the NTHP membrane systems were in close contact (Figure 3.5Aiv, 3.5Avi, and 3.5Aviii). However, the distances between the cells using NTHP membranes with 380 nm and 860 nm pore sizes (NTHP-380 and NTHP-860, respectively) were in closer proximity (within the 200 nm resolution of super-resolution confocal microscopy) compared to cells cultured on 100 nm pore size membrane (NTHP-100), as some parts of the cells were observed in yellow due to the co-localized pixels of green and red fluorescence (arrows in Figure 3.5A v and 3.5Avii).

Next, to compare the rate of protein diffusion through the NTHP membrane *versus* the Transwell membrane, mathematical modeling and empirical studies on protein diffusion, were conducted. To evaluate the effects of thickness and porosity of the membrane on the interphase transfer of protein molecules, we employed a simplified one-dimensional mathematical model that was established in a previous study.[121]

$$\frac{\partial C}{\partial t} = D_{eff}\frac{\partial^2 C}{\partial x^2} \quad (D_{eff} = D_0 f(C_0, C_s) h[\varepsilon, \zeta, L(X)]) \qquad \text{(A)}$$

where C is the concentration of proteins, D_0 the diffusion coefficient in water, D_{eff} the effective diffusion coefficient of proteins which is influenced by the physical properties of the solute, $f(C_0, C_s)$, and the microstructural properties of the membrane, $h[\varepsilon, \zeta, L(X)]$. In addition, a hindrance factor of the diffusion coefficient,[122] which accounts for the decrease in the rate of diffusion in less porous material, was proposed as

$$\frac{D_{eff}}{D_0} \cong \frac{2\theta}{3-\theta} \qquad \text{(B)}$$

Equation (A) combined with equation (B) was solved numerically under proper boundary conditions. The results indicated that protein diffusion occurred faster when the membrane thickness is reduced and the membrane porosity is increased .

Subsequently, a chamber was designed to empirically compare the rate of protein diffusion through the NTHP and Transwell membranes. Each membrane was set to partition the protein diffusion chamber into two secluded compartments.

One compartment was filled with 10 mL of 10 μg/mL BSA solution, while the other with PBS of equal volume. Thus, BSA was allowed to diffuse into the PBS chamber only through the separating porous membrane (Figure 3.5B). The result showed that the BSA diffusion rate was not affected by the pore sizes of NTHP membranes (Figure 3.5Bi), which was likely due to the comparable porosity and thickness among the membranes (Table 3.1). However, the BSA diffusion rate was significantly higher in the NTHP membrane system compared to the Transwell membrane system (Figure 3.5Bii), which can be attributed to the reduced thickness and higher porosity of the NTHP membranes (Figure 3.1E).[121-122]

To investigate whether the cocultured MSCs and H9C2 were undergoing active direct cell-to-cell crosstalk *via* gap junctions, a calcein-AM dye transfer assay was performed (Figure 3.5C). MSCs, on the top side of each membrane, were dual-labelled with DiI (red) and calcein-AM (green). DiI is a dye that labels cell membrane and cannot be transferred through direct cell-cell contact. Calcein–AM is non-fluorescent outside cells. However, once calcein-AM penetrates cells, it is cleaved to fluorescent calcein by esterase within the cells.[99] The fluorescent calcein is cell membrane-impermeant and can pass only through direct cell-to-cell gap junction channels.[100] Thus, without direct cell-to-cell connections, calcein cannot diffuse from MSCs into the underlying H9C2 cells during the dye transfer assay. The results showed that calcein-AM was not transferred to H9C2 (green color only) in the Transwell system (Figure 3.5Ci). The side view of the cocultured cells clearly showed that none of the H9C2 (arrow heads in Figure 3.5Cii) on the bottom side of the Transwell membrane (indicated by yellow dashed line) exhibited green fluorescence, indicating that there was no calcein-AM transfer across the Transwell membrane (Figure 3.5Cii). This is due to the large thickness and low porosity of the Transwell membrane, which fails to permit effective cell-cell contact between the cocultured MSCs and H9C2 layers. In addition, calcein-AM

was not transferred to H9C2 across the NTHP-100 membrane system (arrowheads in Figure 3.5Civ), indicating that despite close proximity the cells were not forming direct cell-cell contacts. In contrast, calcein-AM transferred H9C2 were observed in the NTHP-380 and NTHP-860 systems. (Figure 3.5Cv and Figure 3.5Cvii). The side view also revealed extensive calcein-AM transfer across the NTHP membrane from the top MSC layer to the bottom H9C2 layer (arrows in Figure 3.5Cvi and 3.5Cviii). These data clearly indicate that while the ultra-thin thickness and high porosity of the NTHP membrane allows dynamic and direct MSCs-H9C2 contact *via* gap junctions, the nanoscale pore sizes of the membranes also play a crucial role in the formation of gap junctions between the cocultured cells. Finally, we found that NTHP membranes with pore size below 100 nm were not ideal for direct cell-cell gap junction-mediated interactions between the cocultured cells.

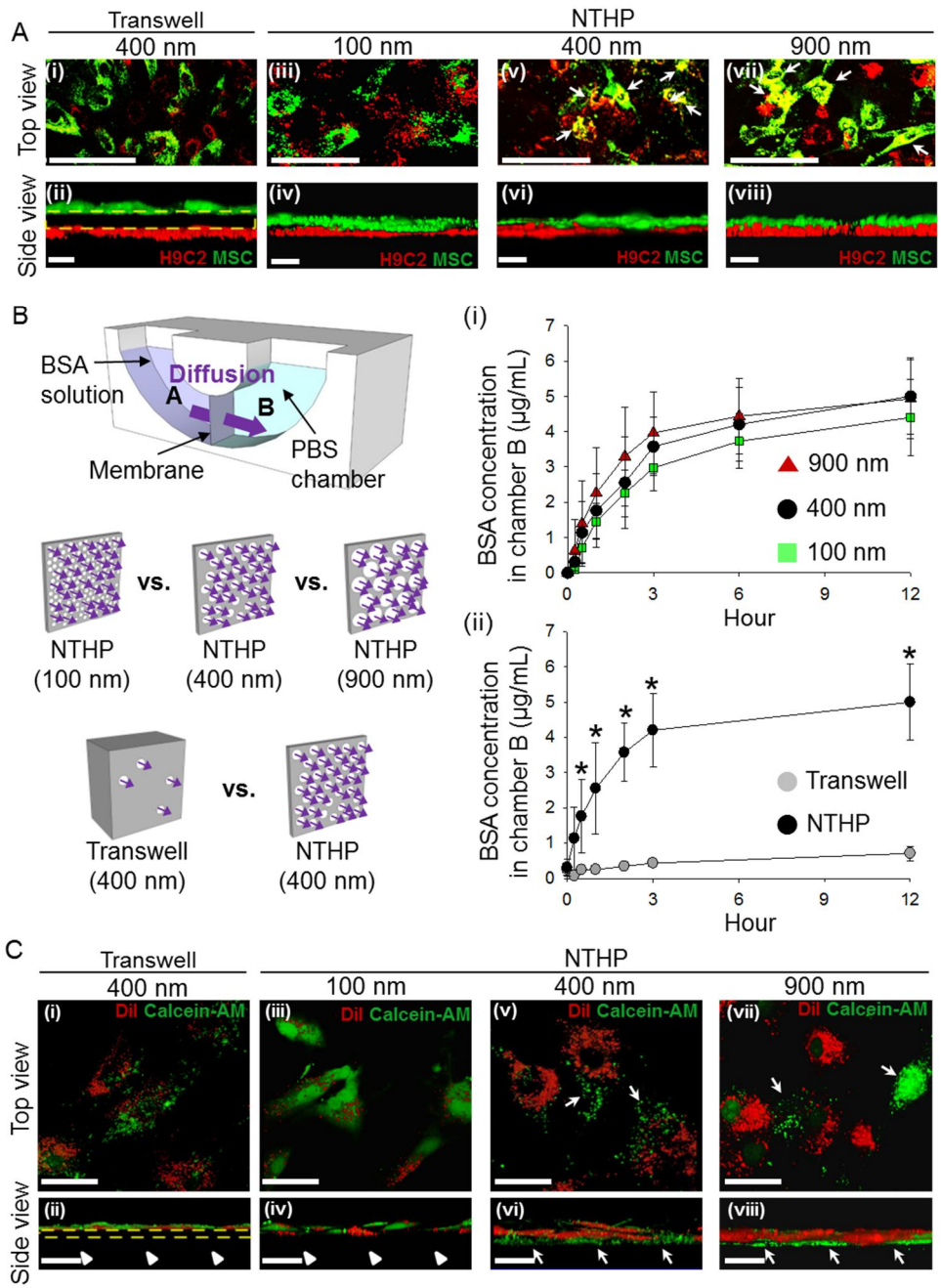

Figure 3.5. Assessments of direct intercellular interactions in the coculture systems

and the rates of protein diffusion through the NTHP membranes. (A) Confocal images of cocultured MSCs (green) and H9C2 cells (red). Bars, 20 μm. The Transwell membrane is marked with yellow dashed lines. (B) Illustration of protein diffusion chamber experiment and quantitative analysis of the rate of BSA molecule diffusion through NTHP membranes compared to Transwell membranes. *$p < 0.05$ (C) Confocal images of calcein-AM (green) dye transfer between cocultured MSCs and H9C2 cells *via* gap junctions. The Transwell membrane is marked with yellow dashed lines. Bars, 50 μm.

3.2.5. Facile, homogeneous collection of MSCs post-coculture

For cardiac differentiation of stem cells through coculture, the use of allogeneic cardiac cells or cell lines is inevitable due to limited access to human primary cardiac cells.[123] Thus, the role of the membrane as a physical barrier between the two types of cell populations is important to prevent the cross contamination and preserve the homogeneity of the cells.

A remarkable feature of the NTHP membrane system is facile harvesting of MSCs from the cocultured cell populations. Due to its free-standing capability, the NTHP membrane is readily transferable, facilitating the fast and easy collection of cultured MSCs (Figure 3.6A). Green fluorescence dye (DiO)-labelled MSCs, which have been cocultured with red fluorescence dye (DiI)-labelled H9C2, were exclusively isolated from the cocultured cell populations by NTHP membrane transfer after one week of coculture, demonstrating the fast and simple harvesting of MSCs with NTHP membranes (Figure 3.6B).

To determine whether NTHP membranes effectively prevent cellular cross-contamination across the membranes, the homogeneity of the collected MSCs after one week of coculture was assessed using FACS (Figure 3.6C) and fluorescence microscopy (Figure 3.6D). The quantitative analysis by FACS and qualitative observation through fluorescence microscopy revealed that the homogeneity of the collected MSCs from the NTHP-380 membrane was high and comparable to that from commercial Transwell membrane. This demonstrated the robust function of the NTHP-380 membrane as a competent physical barrier between the cocultured cells. In addition, the data indicated that adhesion of H9C2 on to the culture dish was strong enough to prevent their detachment upon transfer of the NTHP membrane, contributing to the high purity of the collected MSCs (Figure 3.6D). However, the impurity of the collected MSCs from the NTHP-860 membrane system was much higher compared to both MSCs collected from

Transwell and NTHP-380 systems (Figure 3.6C and Figure 3.6D). These data were consistent with a previous study that indicated cellular cross-migrations in cocultured populations separated by membranes with pore sizes around 1 μm.[124] Collectively, we deduced that the ideal pore size for the NTHP membrane system that allows dynamic interactions between the cocultured cells and at the same time acts as a robust physical barrier between them is 380 nm.

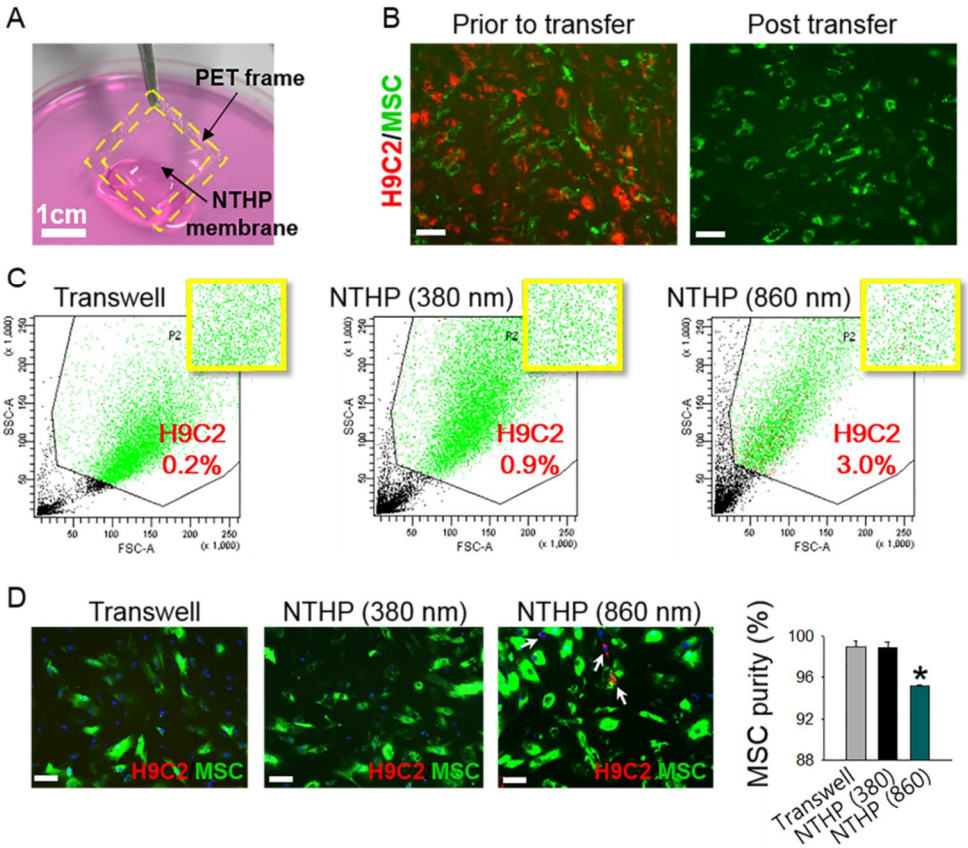

Figure 3.6. Facile collection and purity of MSCs following coculture with H9C2 cells using the transferable NTHP membrane. (A) Photograph showing the transfer of MSCs cultured on PET-framed NTHP membrane following coculture with H9C2 cells. The PET frame is marked using yellow dashed lines. (B) Fluorescent images of MSCs (green) and H9C2 cells (red) cocultured on the NTHP membrane and the MSCs collected following transfer of the NTHP membrane (pore size of 380 nm) onto a new dish. Bars, 100 μm. (C) Homogeneity of the collected MSCs analyzed by FACS analysis. MSCs are expressed in green and H9C2 cells in red. (D) Fluorescent images and quantification of the MSCs collected and re-plated on a new culture dish to analyze their purity. Bars, 100 μm. *$p < 0.05$ *vs.* other groups.

3.2.6. Enhanced differentiation of MSCs by NTHP coculture system

Previous studies have reported that naïve MSC transplantation for myocardial infarction treatment, is insufficient to achieve the best therapeutic outcome because transplanted MSCs rarely differentiate into cardiomyocytes *in vivo,* and the physiological characteristics of naïve MSCs is inharmonious with the heart tissue, imposing the risk of arrhythmia.[16-19] The transplantation of MSCs that express cardiac biomarkers was reported to have better reparative effects.[22-23] Thus, cardiac differentiation of MSCs *ex vivo* prior to transplantation is a high-priority requirement for improved therapeutic efficacy of MSCs for cardiac repair. As coculturing with cardiomyoblasts was shown to promote cardiac-lineage differentiation,[125] we investigated whether the cardiac differentiation of MSCs could be achieved through coculture with H9C2 on NTHP membranes.

Figure 3.7 briefly illustrates the advantages of the NTHP membrane system as a new-coculture system over the conventional 'Transwell' system. In general, there are two coculture methods in the 'Transwell' system: indirect coculture and direct coculture. In the indirect coculture method, H9C2, which provide important cues for the cardiac differentiation of MSCs, are seeded on the porous membrane of the Transwell insert, while the MSCs are seeded on the bottom chamber. This coculture system induces stem cell differentiation only *via* indirect intercellular communication, which is the diffusion of cytokines secreted by H9C2 across the porous membrane. Direct cell-cell contact is absent in this system. The other method is the direct coculture method, in which H9C2 are seeded on the porous membrane of the Transwell insert and MSCs are seeded on the opposite side of the porous membrane. This system is expected to allow both the diffusion of cytokines secreted by H9C2 and direct cell-cell contact through the micro-thin, porous Transwell membrane. In contrast, our NTHP membrane system

benefits from a nanothin, highly porous membrane, which enables dynamic crosstalk between H9C2 and MSCs through faster cytokine diffusion and more effective cell-cell contact compared to the Transwell system.

The expressions of cardiac-associated genes and proteins were assessed after one week of culturing MSCs in various conditions: non-cocultured, cocultured with H9C2 using the Transwell indirect coculture system (Transwell (Indirect)), cocultured with H9C2 using the Transwell direct coculture system (Transwell (Direct)), and cocultured with H9C2 using the NTHP coculture system (NTHP). Gene expressions of a cardiac transcription factor (MEF2C), a cardiac structural marker (MLC2v), a gap junction marker (connexin 43), and cardiac ion channel markers (CACNA1D, HCN2) were significantly higher in the NTHP group (Figure 3.8A). Western blot analysis (Figure 3.8B) and immunocytostaining (Figure 3.8C) of non-cocultured MSCs showed no expression of the cardiac structural proteins, sarcomeric α-actinin (SA) and cardiac troponin T (cTnT). The same results were observed in Transwell (Indirect). Meanwhile, Transwell (Direct) showed slightly increased expression of SA protein. In contrast, NTHP demonstrated significantly higher expressions of both SA and cTnT proteins compared to other groups. Also, NTHP showed a higher expression of connexin-43 compared to the other groups. Statistically, the percentages of MSCs that were positive for cardiac-specific markers were significantly higher in the NTHP group than the other groups (Figure 3.8C). Additionally, we cultured MSCs on their own on NTHP membranes and confirmed that the membrane itself does not affect their differentiation (Figure 3.9). These results showed that NTHP membranes improve the cardiac differentiation efficiency of MSCs compared to other coculture systems, which is likely due to the dynamic cell-to-cell interactions between the cell populations in this membrane system. While a number of previous studies attempted to induce terminal cardiac differentiation of MSCs, functional cardiac

behaviors such as contractility have not been observed in the differentiated cells.[22-23,59,126-130] Also, previous studies indicated that H9C2 cardiomyoblast cell line lacks many ion currents typical of the mature heart and shows no voltage-dependent current.[131-132] Hence, based on the aforementioned reports, the present study did not address the contractility of the differentiated cell sheets.

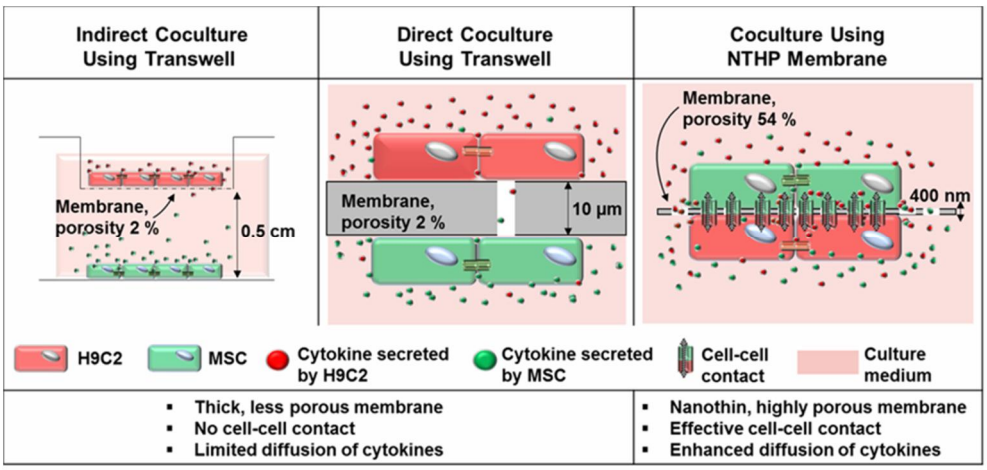

Figure 3.7. Comparison of the NTHP membrane-based coculture system with the conventional Transwell coculture systems.

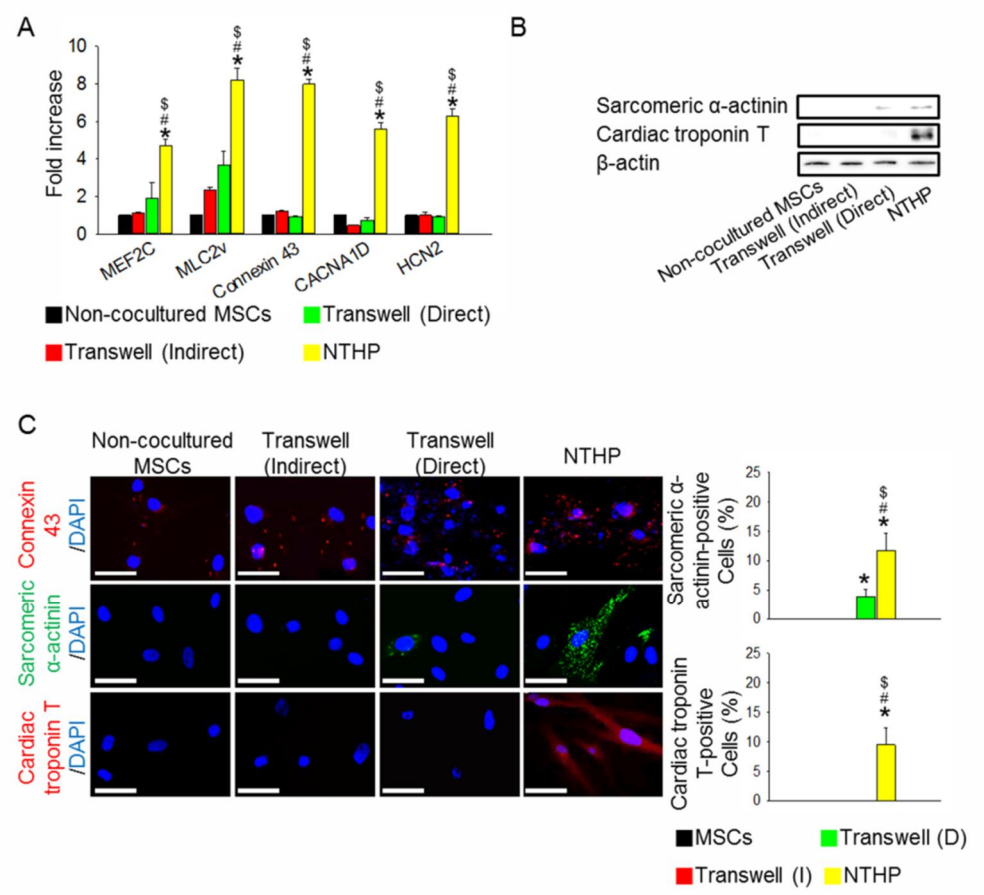

Figure 3.8. Enhanced cardiac differentiation of MSCs in the NTHP membrane system following 1 week of coculture with H9C2. (A) mRNA expression levels of cardiac-specific markers in MSCs after coculture. Gene expression levels were normalized to those of non-cocultured MSCs. (B) Western blot analysis for cardiac structural proteins of MSCs after coculture. (C) Immunocytochemistry of cardiac protein markers and quantification for the cardiac specific marker-positive MSCs after coculture. Bars, 50 μm. *$p < 0.05$ *versus* non-cocultured MSCs. $^{\#}p < 0.05$ *versus* Transwell (indirect). $^{\$}p < 0.05$ *versus* Transwell (direct).

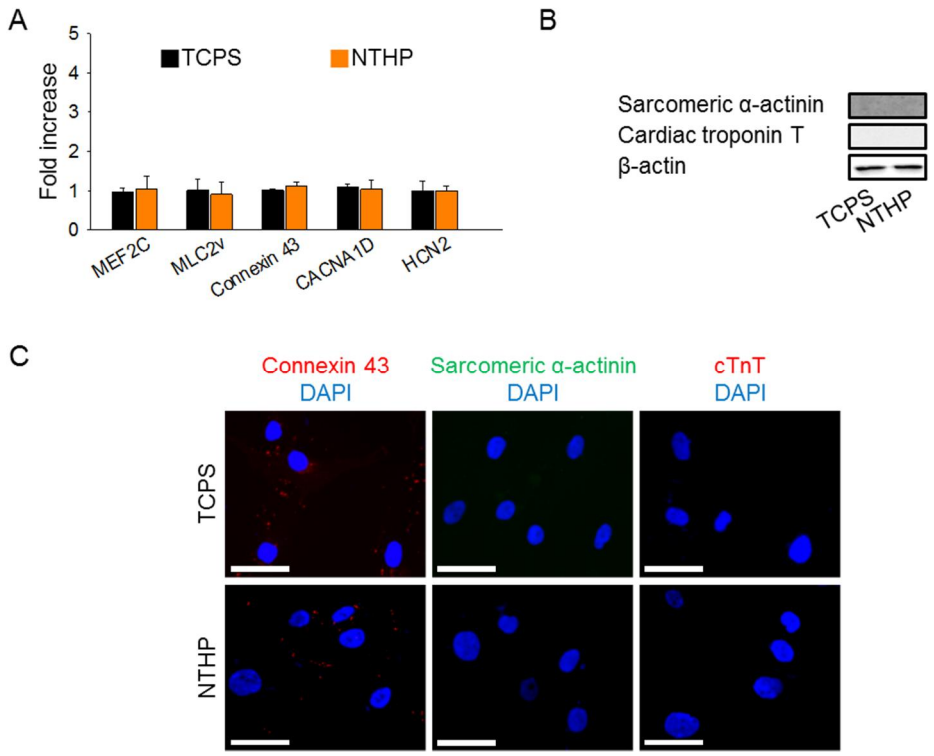

Figure 3.9. Effects of NTHP membrane on cardiac differentiation of MSCs without coculture. (A) mRNA expression levels of cardiac-specific markers in MSCs after one week culture on a TCPS dish or a NTHP membrane without coculture. Gene expression levels were normalized to the levels of MSCs cultured on TCPS. (B) Western blot analyses for cardiac structural proteins of MSCs after culture for 1 week. (C) Immunocytochemistry for cardiac protein markers of MSCs after culture for 1 week. Bars, 50 μm.

3.2.7. Generation of transfer-printable, multilayered sheets of differentiated cells

The transferable and thermoresponsive features of NTHP membranes allow the generation of transfer-printable, multilayered sheets of differentiated cells after coculture. Cell sheet printing can be achieved by turning the thermoresponsive NTHP membrane upside down, allowing the cell sheet to adhere to a new culture dish at 37 °C for 4 hours, and printing the cell sheet onto the culture dish from the membrane at 20 °C for 30 minutes. Repeating the transfer-printing of a new cell sheet layer on top of the first transfer-printed cell sheet layer can be used to fabricate multilayered sheets of differentiated cells (Figure 3.10A). Light microscopy images capturing the transfer printing process are shown in Figure 3.10B. A transferred NTHP membrane showed MSCs firmly adhered to the membrane (Figure 3.10Bi). Gradually, the cells started to detach from the NTHP membrane at 20 °C within 20 minutes, starting from the edge of the membrane (Figure 3.10Bii), followed by extensive detachment of the cell sheet within 30 minutes (Figure 3.10Biii). A cross-sectional view of the detached cell sheet stained by H&E displayed an intact monolayer cell sheet (Figure 3.10Biv). In addition, we demonstrated that it was possible to print the transferred and detached cell sheet onto a new culture dish (Figure 3.10Bv).

Next, to determine whether the transfer-printing technique with the thermoresponsive NTHP membrane can be used to fabricate multilayered cell sheets, consecutive cell sheets transfer-printing was performed. Prior to transfer-printing, each cell sheet was pre-labelled using red (DiI) or green (DiO) fluorescence dyes, respectively. The transfer-printing technique with the thermoresponsive NTHP membrane was performed by stacking a red fluorescent-labelled cell sheet onto a green fluorescent-labelled cell sheet, resulting in the fabrication of a bilayered cell sheet (Figure 3.10C). The z-stack 3D confocal

images of the bilayered cell sheets showed intact incorporation between the layers (Figure 3.10C).

Detachment of the cell sheet from a thermoresponsive substrate is reported to be an advanced approach to harvesting adherent cultured cells compared to the conventional method using trypsin.[133-134] Trypsin, a proteolytic enzyme that degrades ECM proteins, is known to have harmful effects on the viability of the trypsinized cells, since these proteins are crucial components of the cellular microenvironment for cell survival.[135-136] To examine the cell viability of the transfer-printed cell-sheet generated with thermoresponsive NTHP membranes, a live (green)/dead (red) cell staining assay was performed and compared with cells harvested by trypsinization. The data showed that cells recovered using trypsin treatment showed only 75% cell viability, while transfer-printed cell sheets by NTHP membranes showed higher cell viability, up to 96% (Figure 3.10D).

In addition, whilst actin cytoskeleton staining of the trypsinized cells showed dissociated single cells after cell harvesting, the transfer-printed cell sheet was intact (Figure 3.10E). Immunocytostaining and western blot analysis of ECM molecules of the transfer-printed cell sheets were also examined and compared with cells harvested by trypsinization. Notably, ECM proteins, such as fibronectin and laminin, were better preserved in the NTHP membrane-generated cell sheet compared to trypsinized cells (Figure 3.10E and Figure 3.10F). The data confirmed that transfer-printed cell sheets generated using thermoresponsive NTHP membranes had a higher survival rate and better preserved ECM proteins compared to the conventional cell-harvesting method.

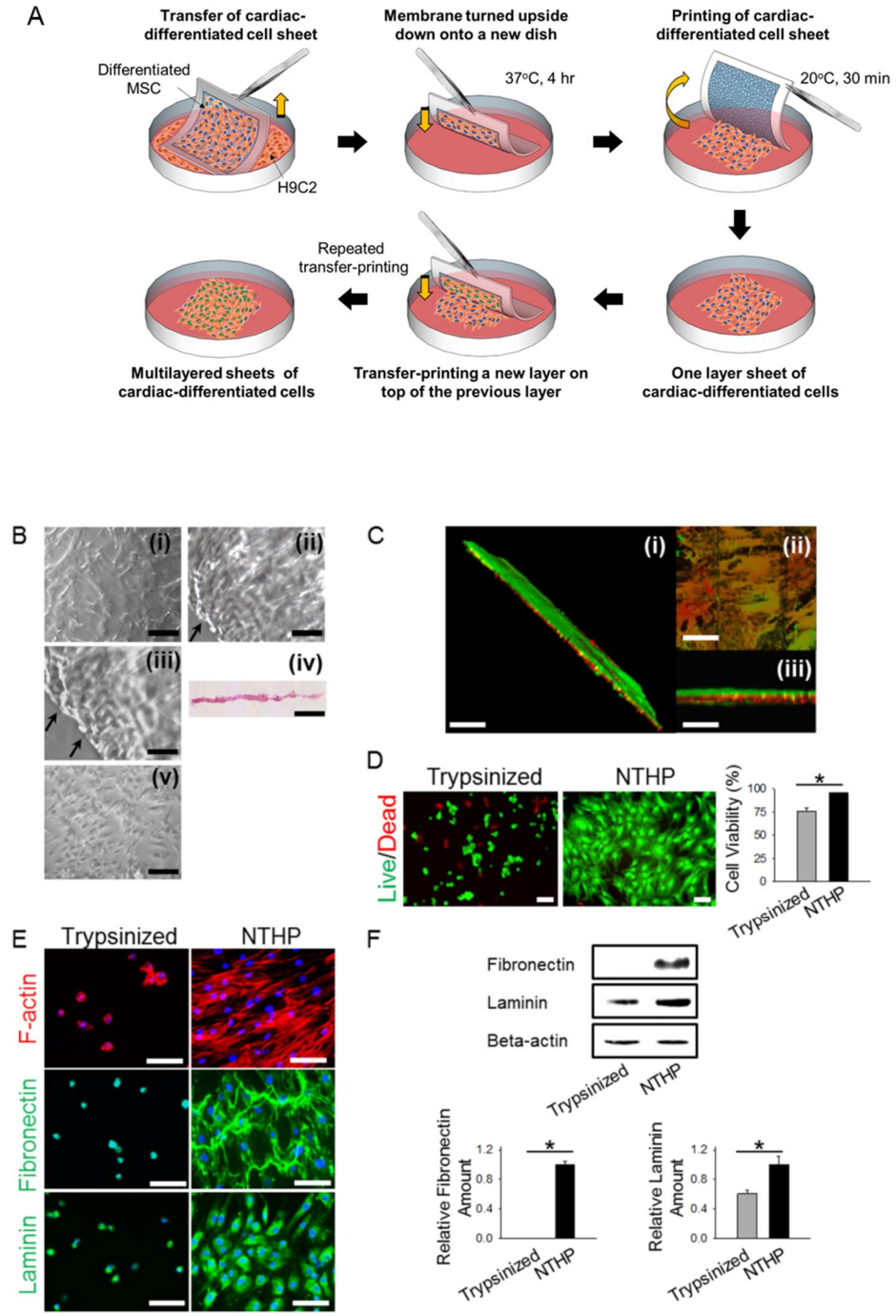

Figure 3.10. Generation of bilayered cells sheets by the transfer-printing technique using a thermoresponsive NTHP membrane, and characterization of the cells sheets. (A) Schematic diagram of the generation of multilayered cell sheets with the

transfer-printing technique using NTHP membranes. (B) Light microscopic images of (i) a cell sheet adhering on NTHP membrane at 37 °C, (ii) a cell sheet gradually detaching from NTHP membrane after 20 minutes at 20 °C and (iii) after 30 minutes at 20 °C, (iv) cross-sectional view of the detached membrane, (iv) H&E stained cell sheet, and (v) transfer-printed cell sheet on a new culture dish. Cell sheet detachment is marked with arrows. Bars, 100 μm. (C) Z-stack confocal images of bilayered cell sheets generated by the transfer-printing technique using NTHP membranes viewed from (i) 3D tilt angle, (ii) top and (iii) side. Bars, 100 μm. (D) Cell viability assessment and quantification after trypsinization or transfer-printing, as evaluated by live (green)/dead (red) assay. Bars, 100μm. *p<0.05 (E) Immunofluorescent images of actin cytoskeleton (F-actin) and ECM (fibronectin and laminin) proteins expressed in trypsinized (dissociated) single cells and a transfer-printed cell sheet. DAPI stained nuclei. Bars, 100μm. (F) Western blot analyses of ECM proteins in trypsinized single cells and transfer-printed cell sheet. *p<0.05

Chapter 4.

Development of a cellular layer-by-layer coculture platform using biodegradable, nanoarchitectured membranes for generation of implantable 3D differentiated cell constructs

4.1. Introduction

Stem cell differentiation in our body is regulated by interactions with the surrounding 3D microenvironment through direct cell-cell contact,[63-64] cell-matrix interactions,[65-66] and soluble paracrine factors secreted by neighboring cells.[61-62] Common artificial *in vitro* approaches to promote stem cell differentiation, such as the use of bioactive molecules or chemical cues, have been reported to be inefficient as they do not sufficiently convey the complexity of *in vivo* microenvironment.[20,54,127,130] As an alternative strategy, coculture of stem cells with desired differentiated cells has been reported to be effective in inducing stem cell differentiation to chondrocytes,[7-8,58,68,137] osteoblasts[57] and cardiomyocytes.[24,102] Coculture systems are designed to mimic complex cellular interactions which stem cells encounter within *in vivo* native microenvironments.[55]

Polymer-based porous membranes are generally used in coculture systems to physically separate the cocultured cell populations because subsequent cell separation from these cocultures is easy and important for further clinical application.[68,76] Ideally, membrane-based coculture system should allow for effective cell-cell communication between the cocultured, while preventing heterogeneous cell populations from mixing.[102] Despite the highly advantageous strategy of membrane-based coculture system, there are some major drawbacks of current membrane-based coculture systems for application in stem cell-based therapy. The membranes of current coculture systems, which have micro-scale thickness and low porosity, do not support active interactions between the cocultured cells, resulting in relatively low efficiency of stem cell differentiation.[80-81,102] Also, the 2D bilayer geometry of conventional coculture systems is inadequate to support chondrogenic differentiation.[60] Moreover, non-biodegradability of conventional coculture membrane necessitates proteolytic enzymatic treatment to detach and collect cells for *in vivo* implantation.[102] Enzymatic harvesting severely

damages the ECM produced by the differentiated cells and cellular viability, impairing cellular function following *in vivo* delivery of these cells.[82-83,102,138-139]

Here, we introduce a cLbL coculture platform using BNTHP membranes developed for stem cell differentiation and implantation. In BNTHP-based cLbL coculture system, MSC-seeded BNTHP membrane was sandwiched between top and bottom layers of chondrocyte-seeded BNTHP membrane. We hypothesize that cLbL coculture platform using ultra-thin, nanoarchitectured BNTHP membranes would provide 3D coculture geometry that better enhances cellular interaction occurring in nano-scale between the heterogeneous cell populations. The augmented cellular interactions between cocultured cells in cLbL coculture would improve stem cell differentiation efficiency compared to bilayer cocultures. Despite its nanoscale thickness, strong mechanical property of the BNTHP membranes as a cell substrate facilitates easy manipulation of each cell layer, thus allowing cellular layer-by-layer sandwich coordination and collection of the MSC layer following coculture. Furthermore, the biodegradable and biocompatible properties of the PLGA-based BNTHP membranes allow avoidance of the problematic enzymatic harvest of cells following coculture and the generation of readily implantable cell-laden scaffolds. High flexibility of the BNTHP membranes allows *in situ* folding of the 2D membranes into 3D construct of the differentiated cells along with the membranes prior to *in vivo* implantation.

We applied cLbL coculture technique for MSC chondrogenesis. Cartilage regeneration is in great need of stem cell therapy since cartilage has limited self-repair ability after excessive wear or aging.[140-141] For decades, MSCs have been in focus as a promising cell source for cartilage repair since MSCs are available *via* a minimally invasive method and have great potential for proliferation and chondrogenic differentiation.[142-143] Here, we compared cLbL coculture technique

with conventional bilayer coculture methods and pellet culture method[98,142], the widely accepted *in vitro* approaches to MSC chondrogenic differentiation.

4.2. Results and discussion

4.2.1. Fabrication and application of BNTHP membranes in cLbL coculture of stem cells and differentiated cells

Figure 4.1 illustrates the fabrication procedure of the BNTHP membranes and BNTHP-based cLbL coculture for generating chondrogenic-differentiated 3D constructs derived from stem cells. The BNTHP membranes were made from PLGA, a FDA-approved, biocompatible, and biodegradable material, suitable for biomedical applications.[52,144] Human bone marrow-derived MSCs were utilized in this study to evaluate the efficacy of the cLbL coculture platform for potential clinical tissue engineering applications using patients-derived MSCs. As human primary chondrocytes are hardly available for research, numerous previous studies have demonstrated successful chondrogenic differentiation of MSCs and cartilage tissue engineered through coculture of MSCs with xenogeneic chondrocytes,[58,68,137,145-151] and in this study, rabbit chondrocytes were cocultured with human MSCs. The cLbL coculture of MSCs between upper and lower layers of chondrocytes exhibited enhanced dual-sided direct cell-cell and cell-matrix contact along with more paracrine factor diffusion across the BNTHP membrane, better mimicking the complex 3D cell-cell crosstalk of the *in vivo* environment. After 2 weeks in coculture, the BNTHP membranes with chondrogenic differentiated cells that originated from stem cells were collected and separated from the PET frame, and converted into a 3D construct through centrifugation. Subsequently, the 3D constructs of the chondrogenic differentiated cells and BNTHP scaffolds were implanted into athymic mice. The developed membranes should be durable enough during 2-week *in vitro* coculture time period and yet to be promptly degraded following *in vivo* implantation. PLGA is known for its high biodegradability compared to other biodegradable materials, such as

polycaprolactone (PCL).[152-153] Also, previous study reported that greater amounts of ECM proteins in serum-containing media, such as fibronectin and vitronectin, adsorb onto PLGA than PCL. Such ECM proteins promote better cellular adhesion onto the substrate. In this respect, we chose PLGA to develop BNTHP membranes.[153]

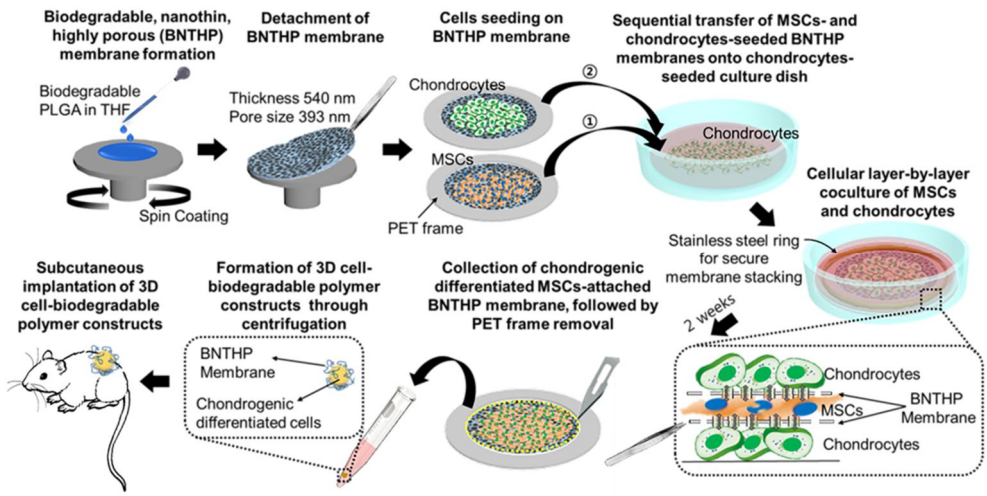

Figure 4.1. Schematic illustration of the fabrication of BNTHP membranes, and its application in cLbL coculture platform for chondrogenic differentiation of MSCs and generation of *in vivo*-implantable 3D constructs of chondrogenic differentiated cells and BNTHP membranes.

4.2.2 Physiochemical properties and biodegradation of BNTHP membranes

Previous studies have shown that micro- and nano-sized pores can be formed by VIPS in thin films.[112,154] This principle was applied to produce the BNTHP membranes in our study. Various process parameters (*i.e.*, solvent volatility, initial polymer concentration, relative humidity, *etc.*) have been used to control the morphology of polymer membranes that were obtained through VIPS process.[113] Among them, we controlled the relative humidity to alter the pore size of BNTHP membrane in Figure 4.2A. Since water vapor was employed as a non-solvent, the nanoporous architecture of the membranes was created by controlling the mass exchange rate by regulating the relative humidity. In addition, the spin-coating process was adopted to achieve nanothin thickness of membranes under closed environmental conditions that maintained constant RH.[79] We selected a RH of around 45% as this allowed formation of well-defined pores with an optimum pore size for cell coculture membranes based on our previous work.[102]

The suitability of BNTHP membranes for cell coculture was evaluated by AFM and DSC (Figure 4.2B). The AFM images of these BNTHP membranes in liquid state (water) showed that the nanoporous architecture of these membranes was preserved in the aqueous environment emphasizing their capacity as stable coculture membranes. The thermal properties of the BNTHP membranes were measured by DSC. The glass T_g of BNTHP membranes was above 37°C, which is consistent with results obtained in previous studies on PLGA-based thin films.[152] The DSC data also indicated that the BNTHP membranes are in the glassy state in a cell culture condition at 37°C, demonstrating the retention of their nanoporous architecture at this temperature due to fairly frozen chain structure of polymers under T_g.[144] In addition, an optical image of a PET-framed BNTHP membrane in

Figure 4.2B displayed notable optical transparency as well as the free-standing feature of the prepared BNTHP membranes.

Next, we investigated the degradation of BNTHP membranes *in vitro* in PBS solution, pH 7.4, at 37°C for 2 weeks. Several studies have reported *in vitro* degradation of porous PLGA foams or microthin films.[155-156] However, to the best of our knowledge, we believe that this is the first study to quantitatively characterize the physicochemical degradation profiles of nanothin membranes with nanoarchitecture. The degradation rate of biodegradable polymer scaffolds is influenced by various factors, including the type of polymer, environmental parameters, and surface area to volume ratio. Therefore, the systematic characterization of the degradation of newly developed BNHTP membranes is essential for bioengineering applications of BNTHP membranes. The weight loss of the BNTHP membrane was monitored by QCM-D and calculated from Sauerbrey's equation (Figure 4.2C). The blue curves are the changes in QCM-D frequency which represent the changes in mass of BNTHP membrane in PBS. The black curves represent the calculated values of real-time remaining mass of BNTHP membrane. The weight of a BNTHP membrane first significantly decreased upon exposure to PBS, followed by gradual weight loss over the next 2-week period. The BNTHP membranes showed significant decrease in film thickness after the 2-week-time period when compared with the initial thickness (Figure 4.2D).

The changes in average molecular weight and molecular weight distribution of the BNTHP membranes before and after degradation were measured by GPC (Figure 4.2E and Table 4.1). The molecular weight of the PLGA-based BNTHP membrane decreased after 2 weeks of incubation and the polydispersity index was also slightly increased, verifying the degradability of the BNTHP membrane after 2 weeks of incubation in PBS at 37°C.[156]

Mechanical properties, including Young's modulus and elongation-at-break, of the BNTHP membranes are shown in Figure 4.2F. The Young's modulus of the BNTHP membrane did not show any significant change over the 2-week-time period compared to the initial modulus. However, the level of elongation-at-break of the BNTHP membrane after 2 weeks of incubation was significantly lower than the initial elongation-at-break value. Although the BNTHP membrane showed a notably decreased elongation degree after the 2-week incubation period, such a change did not impose any significant influence during coculture since the PET-framed BNTHP membranes were rarely deformed, far away from the threshold of the attainable elongation degree, *i.e.* 4%. Together, the data on the physicochemical changes of the BNTHP membranes after 2 weeks of incubation in the PBS aqueous environment at 37°C confirmed the degradability of these membranes.

However, despite the degradation features of the BNTHP membranes, in reality, the BNTHP membranes used for the coculture retained their robust and transferable features after 2 weeks of incubation compared to the initial state (Figure 4.2G). Also, the porous structure of the BNTHP membranes after 2 weeks at 37°C was well preserved, as confirmed with AFM and SEM (Figure 4.2H and Figure 4.3). The physicochemical properties, including average molecular weight, polydispersity index, film thickness, pore size, and porosity for the initial- and 2-week-incubation of BNTHP membranes treated at 37°C in PBS aqueous environment are shown in Table 4.1. The data revealed that the biodegradable BNTHP membranes were initially 540 nm thick with 27% porosity and an average pore size of 393 nm. After 2 weeks of treatment under aqueous solution, biodegradation of the BNTHP membrane was observed with changes in thickness, pore size, and porosity.

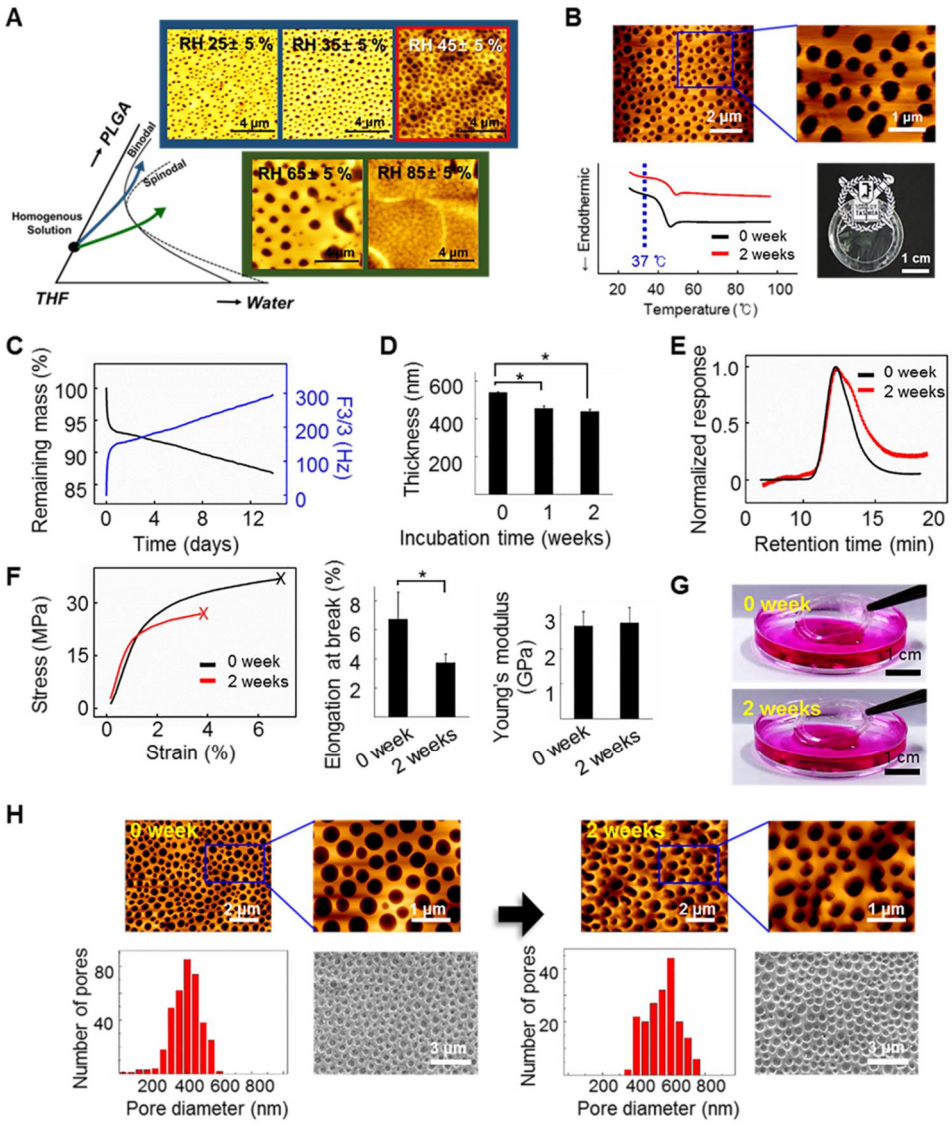

Figure 4.2. Physicochemical characterization and biodegradation of BNTHP membranes incubated at 37°C in aqueous environment. (A) Different VIPS composition paths of BNTHP membranes at ternary phase diagram and the corresponding AFM images with different RH. (B) AFM images of BNTHP membranes in aqueous state. DSC graph showed thermal stability of BNTHP membranes at 37°C and the photograph showed transparency of BNTHP membranes. (C) Real-time weight loss of the BNTHP membranes measured by

QCM-D. (D) Thickness decrease of BNTHP membranes after 1 and 2 weeks. *p < 0.05 between two groups, n=6 per group. (E) Gel permeation chromatograms of BNTHP membranes showed alteration in the molecular weight distribution 2 weeks after the membranes cultured in 37°C aqueous solution. (F) Changes in mechanical property of BNTHP membranes at different time points. *p < 0.05 between two groups, n=6 per group. (G) Photographs of robust and transferable features of BNTHP membranes at initial time point and 2 weeks after culture at 37°C aqueous environment. (H) Changes in pore size distribution and porosity of BNTHP membranes 2 weeks after membrane cultured in 37°C aqueous solution as evaluated by AFM and SEM images.

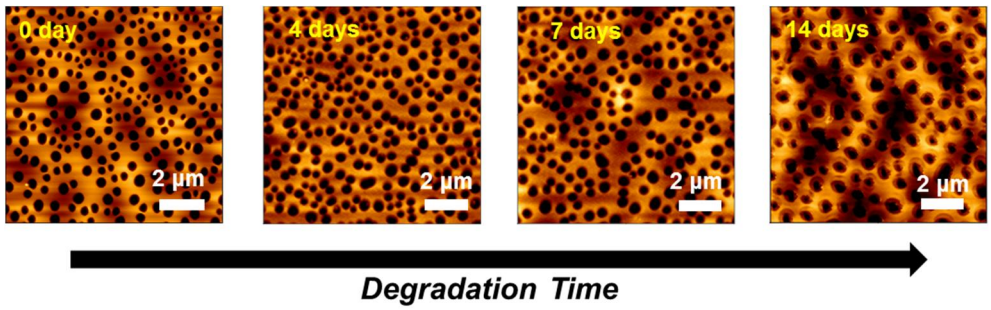

Figure 4.3. Changes in pore size and pore distribution with 2 weeks of degradation time. AFM images show that pore size of BNTHP membranes was increased as the degradation proceeding.

Table 4.1. Quantification of physiochemical properties of BNTHP membranes at different time points. *$p < 0.05$ compared to another group.

Time	Mn (Da)	Mw (Da)	PI	Thickness (nm)	Average pore size (nm)	Porosity (%)
0 week	44,100	79,500	1.8	540± 4*	393 ± 5*	27 ± 3*
2 week	30,800	61,100	2.0	438± 10*	528 ± 9*	34 ± 5*

4.2.3. Biocompatibility of BNTHP membranes as cell culture membranes

To investigate the biocompatibility of BNTHP membranes, MSCs and chondrocytes were cultured on either TCPS dishes or BNTHP membranes. The biocompatibility of BNTHP membrane was evaluated in terms of apoptotic activity, proliferation, and viability of the cells. Both MSCs and chondrocytes cultured on BNTHP membranes exhibited normal cell-adhesion morphology on the membranes (Figure 4.4A). Three days after MSC seeding on TCPS dishes and BNTHP membranes, the mRNA expression of a pro-apoptotic regulatory gene, *BAX*,[157] an anti-apoptotic regulatory gene, *BCL2*,[158] and an apoptotic marker, caspase 3,[159] were evaluated. Results showed that cells cultured on BNTHP membranes showed no difference in apoptotic activity compared with cells cultured on the conventional TCPS dishes (Figure 4.4B). Next, cell growth on TCPS dishes and BNTHP membranes was compared by determining the number of live cells at various time points with the CCK-8 assay (Figure 4.4C). No significant differences in cell growth were observed between the TCPS dish group and the BNTHP membrane group, indicating that MSCs proliferated normally on BNTHP membranes. Also, the live/dead cell assay confirmed that MSCs cultured on BNTHP membranes showed high cellular viability, similar to the MSCs cultured on TCPS (Figure 4.4D). Collectively, these data clearly indicate that BNTHP membrane is biocompatible and suitable as a cell culture substrate.

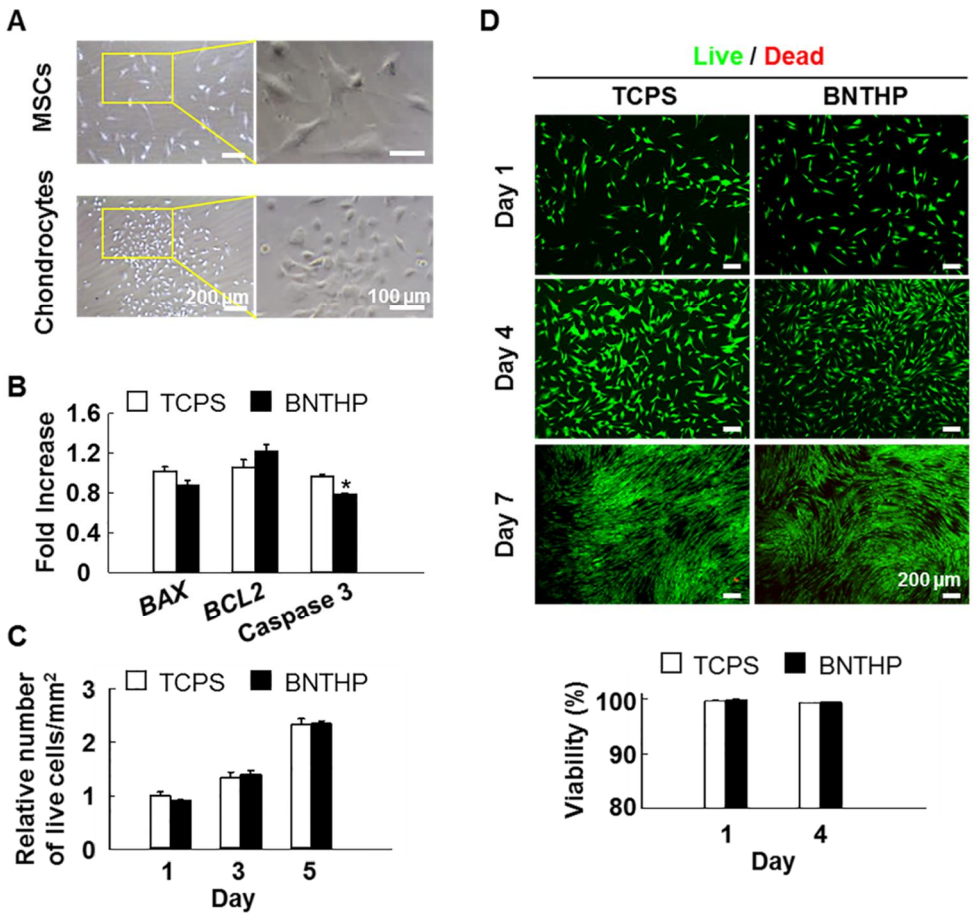

Figure 4.4. Biocompatibility and cytotoxicity of BNTHP membranes. (A) Bright field images of MSC and chondrocyte adhesion on transparent BNTHP membranes 3 days after seeding. (B) Changes in gene expressions of a pro-apoptotic regulatory gene, *BAX*, an anti-apoptotic regulatory gene, *BCL2*, and an apoptotic marker, caspase 3, in MSCs cultured on tissue culture polystyrene dishes (TCPS) or BNTHP membranes (BNTHP) at day 3. *$p < 0.05$, n=3. (C) The number of live MSCs cultured on BNTHP membranes relative to the number of live MSCs on TCPS at day 1, as determined by CCK-8 assay. (D) Fluorescent images and quantification of live & dead assay of MSCs cultured on TCPS or BNTHP membranes at various time points. Live cells are visualized as green and the dead

cells as red. The quantification of cell viability at day 7 was excluded since the cells at day 7 were too confluent for quantification of the viable cells.

4.2.4 Homogeneous collection of MSCs aided by BNTHP membranes following coculture with chondrocytes

Figure 4.5A briefly illustrates the various BNTHP-based coculture systems and other control groups compared in this study showing the extent of cellular interaction of the MSC and chondrocytes in coculture. The experimental culture system consists of five groups; the non-coculture groups, *i.e.* MSCs culture on BNTHP membranes (non-cocultured) or MSCs in pellet culture (pellet), and the coculture groups using different BNTHP membranes dispositions, *i.e.* indirect coculture (indirect), direct coculture (direct), and cLbL coculture (cLbL). Non-cocultured MSCs served as the negative control. Non-cocultured MSCs in pellet culture, a widely used method to induce chondrogenic differentiation,[98,142] served as a positive control. Even though coculture of MSCs with chondrocytes in pellet has been reported to show immense potential for chondrogenesis in some studies,[58,101] separation of MSCs from the pellet of MSCs-chondrocytes is challenging.[58,101] Thus, coculture of MSCs with chondrocytes in pellets was excluded from the experimental groups. In indirect coculture using BNTHP membrane, a stainless steel ring was placed between MSCs-seeded BNTHP membrane and chondrocytes-seeded TCPS dish to prevent direct cell-cell contact between the cocultured cells. Thus, cellular communication in indirect coculture system occured solely through diffusion of soluble paracrine factors between MSCs and chondrocytes. In direct coculture using BNTHP membrane, the MSC-seeded BNTHP membrane was placed directly on top of the chondrocyte-seeded TCPS dish, forming direct cell-cell contact and diffusion of the soluble factors between the cocultured cells. In the cLbL coculture system, the MSC-laden BNTHP membrane was stacked between the chondrocyte-seeded BNTHP membrane and the chondrocyte-seeded TCPS dish. We hypothesized that the cLbL configuration coculture system provides enhanced

dual-sided direct cell-cell contact and paracrine factor diffusion between the cocultured cells, mimicking more *in vivo*-like 3D cellular interactions.

Prior to evaluation of chondrogenic differentiation of MSCs cocultured in the various culture systems, we determined whether the coculture systems allow homogeneous collection of MSCs post-coculture. Green fluorescence-labeled MSCs were monocultured or cocultured with red fluorescence-labeled chondrocytes. After 2 weeks of coculture, MSCs from the BNTHP-based coculture system were retrieved from the heterogeneous cocultured cell populations *via* a simple transfer of the MSCs-attached BNTHP membranes. The remarkable features of freestanding and readily transferable BNTHP membranes in the coculture systems enabled easy collection of the MSCs from the heterogeneous cocultured cell populations. The quantitative and qualitative analyses *via* FACS (Figure 4.5B) and fluorescent microscopy (Figure 4.5C) revealed that MSCs collected from the all BNTHP-based coculture system exhibited high homogeneity (>99%). These data also clearly demonstrated that BNTHP membranes acted as robust physical barrier between the cocultured cells and enabled homogenous collection of the cells from the heterogeneous cell population following coculture.

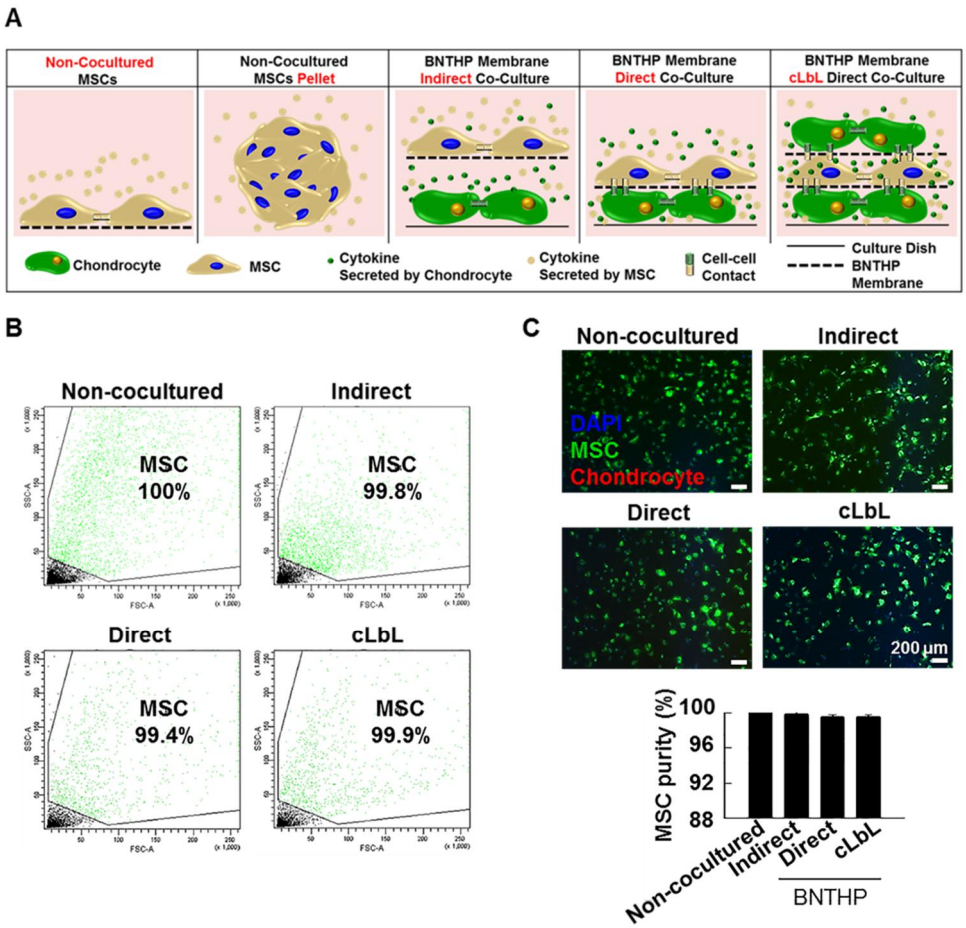

Figure 4.5. Schematic illustration of culture methods for chondrogenic differentiation of MSCs, and homogeneity of MSCs collected following various BNTHP membrane-based cocultures. (A) Illustrations of the various BNTHP membrane-based coculture systems and other comparative control groups evaluated in this study. (B) Homogeneity of MSCs collected after 2 weeks of coculture with chondrocytes, as evaluated by FACS analyses. MSCs and chondrocytes are in green and red, respectively. (C) Fluorescent images and quantification of the MSCs (green)-attached BNTHP membranes collected after 2 weeks of coculture with chondrocytes (red). Cell nuclei were counterstained with DAPI.

4.2.5. Higher intercellular interactions in the cLbL coculture compared to direct bilayer coculture

Next, we examined the proximity and intercellular interactions between the cocultured cells in the cLbL system compared to the direct bilayer system. MSCs and chondrocytes were labelled with red fluorescent DiI and green fluorescent DiO, respectively (Figure 4.6Ai and 4.6Aiv). The side view of both direct (Figure 4.6Aiii) and cLbL coculture (Figure 4.6Avi) obtained by confocal microscopy showed that MSCs and chondrocytes were in close contact despite the presence of BNTHP membranes and PET-frames among the cellular layers. The flexible, nanothin, and highly porous properties of BNTHP membranes enabled the close contact of two types of cell populations. Importantly, colocalization of the contacting MSCs and chondrocytes were analyzed with confocal microscopy and expressed in yellow pixels, showing significantly greater contact area of the cells in the cLbL coculture (Figure 4.6Av) compared to the direct bilayer coculture (Figure 4.6Aii).

To investigate further whether close proximity between MSCs and chondrocytes allowed formation of functional gap junctions between the cocultured cells through the BNTHP membranes and transfer of biomolecules *via* the gap junctions, the calcein-AM dye transfer assay was performed (Figure 4.6B). Cells plated on the top layer of each coculture system (MSCs for the direct bilayer coculture and chondrocytes for the cLbL coculture) were dual-labeled with DiI (red) and calcein-AM (green). Meanwhile, chondrocytes plated on the bottom-most TCPS were labeled with DAPI (blue) (illustrated in Figure 4.6B). DiI is a cell membrane-labelling fluorescence dye and cannot be transferred to the adjacent cells through direct cell-cell contact.[102] Calcein-AM, on the other hand, is a non-fluorescent molecule present outside the cells and becomes fluorescent calcein once it penetrates the cells.[100] Of note, the fluorescent calcein molecule is cell

membrane-impermeant and can be transferred to the adjacent cells only through gap junction channels formed by the directly contacting cells.[100-101] Thus, without direct cell-cell contact between top and underlying cell layers, calcein-AM in the top cellular layer would not transfer to the bottom cellular layer. Surprisingly, 48 hours after coculture, the bottom-most DAPI-labeled chondrocyte layers in both direct and cLbL system exhibited DAPI/calcein colocalization (arrows in Figure 4.6Bi and 4.6Biv). In the cLbL coculture, MSCs between two chondrocyte-layers (arrowheads in Figure 4.6Biv) also showed green fluorescence. These data collectively indicate that the cell layers in both direct bilayer and cLbL cocultures allowed direct cell-cell contact between adjacent cell-layers, formation of functional gap junctions, and transfer of intracellular molecules between adjacent cell-layers through the BNTHP membranes.

Next, we compared the extent of direct cell-cell and cell-ECM interactions between MSCs and chondrocytes in the cLbL coculture and the direct bilayer coculture by Western blot analysis. The expression of a gap junction channel, connexin 43,[101] and receptors to ECM of chondrocytes, integrin β1[160] and discoidin domain receptor 2 (DDR2)[161], were significantly higher in MSCs of the cLbL coculture compared to MSCs of the direct bilayer coculture (Figure 4.6C). These data indicate that MSCs in the cLbL coculture formed more extensive cell-cell and cell-ECM interactions with chondrocytes compared to MSCs in the direct bilayer coculture.

To compare the MSC interactions with chondroinductive paracrine factors secreted by cocultured chondrocytes in the cLbL coculture to those in the direct bilayer coculture, we investigated cellular signaling in the MSCs, which were induced by chondroinductive soluble factors secreted by the cocultured chondrocytes (Figure 4.6D). Soluble factors, such as TGF-β1,[35,37] BMP-2,[38] IGF-1,[39] and FGF-2,[40] have been reported as effective chondroinductive factors secreted

by chondrocytes,[35-36] inducing chondrogenic differentiation of MSCs. These factors trigger the activation of extracellular signal-regulated kinase (ERK), c-Jun N-terminal kinases (JNK), and p-38 mitogen-activated protein kinases (p38),[37,162] which subsequently promote chondrogenic differentiation (illustration in Figure 4.6D).[37,40,163] Conforming to reports from previous studies, MSCs in the cLbL coculture showed upregulated phosphorylation of ERK, JNK, and p38 compared to those in the direct bilayer coculture (Figure 4.6D). These data show that interaction of MSCs with chondroinductive paracrine factors secreted by the cocultured chondrocytes in the cLbL coculture were much more extensive than those in the direct bilayer coculture. Collectively, the data indicated partial infiltrations of the ECM and cell through the highly porous BNTHP membrane, thus allowing MSC-chondrocyte interactions through the cell-ECM and direct cell-cell contact between the two cell layers. The 393-nm pore size of the BNTHP membrane was adequate enough to support formation of the gap junction channel in the regions of the directly contacting cells across the pores of BNTHP membrane as the width of the gap junction channels channel reported to be 9~10 nm.[164] Also, the cLbL coculture supported greater cell-cell, cell-ECM, and cell-paracrine factor interactions between the cocultured MSCs and chondrocytes compared to direct bilayer coculture.

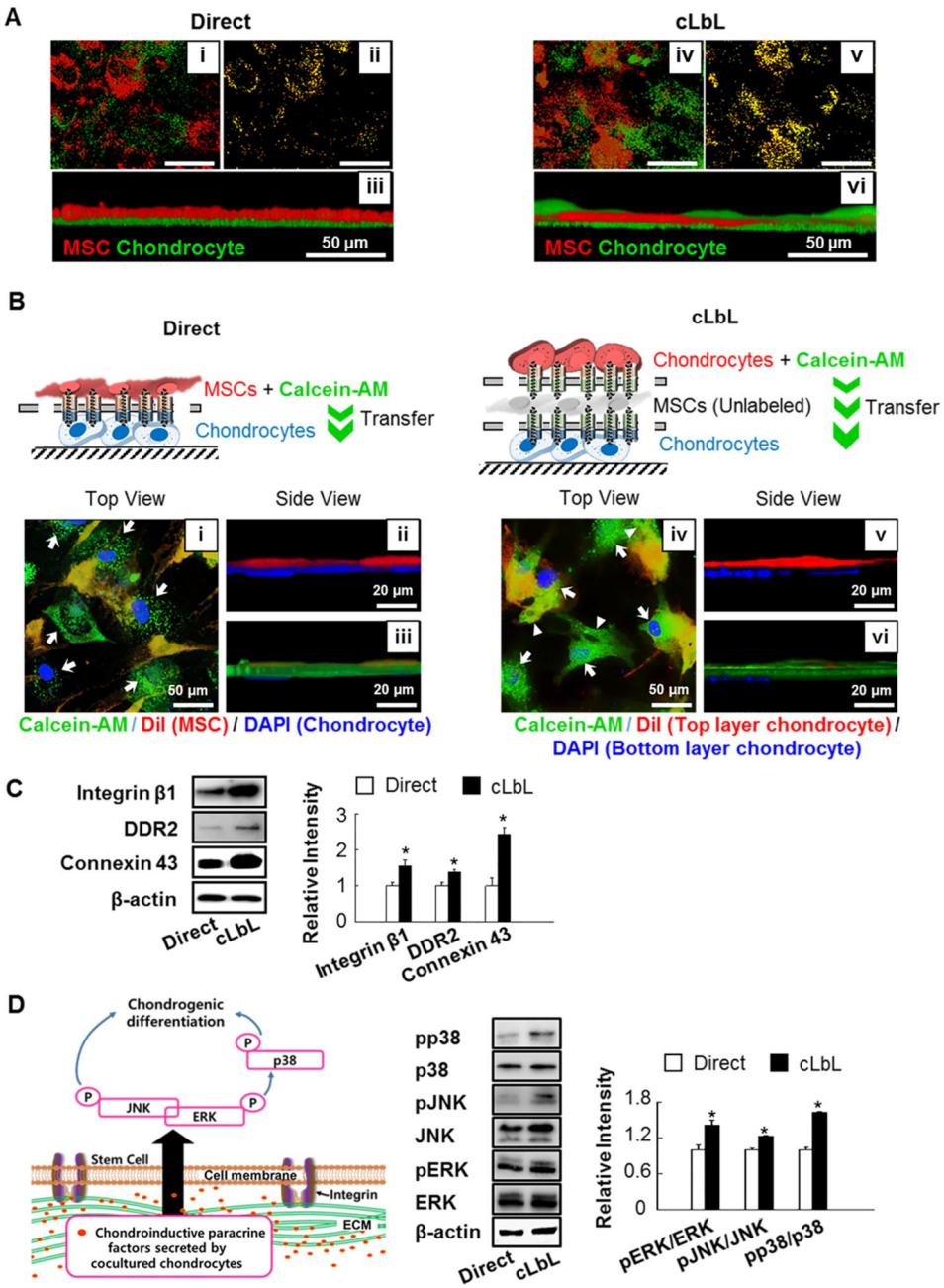

Figure 4.6. Evaluation of direct cell-cell, cell-ECM, and cell-paracrine factor interactions between MSCs and chondrocytes in the cLbL BNTHP coculture compared to the direct bilayer BNTHP coculture. (A) Z-stacked confocal images showing direct contact of MSCs (red) and chondrocytes (green) in the BNTHP-

based direct and cLbL cocultures. Yellow signals (ii and v) denote the direct contact of MSCs and chondrocytes in the z-stacked confocal images obtained from the top views. (B) Illustrations and confocal images of calcein-AM dye transfer between MSCs and chondrocytes through cellular gap junction in direct cell-cell contacts in the BNTHP-based direct or cLbL cocultures. Top views (i and iv), side views without calcein-AM (ii and v), and side views with calcein-AM (iii and vi). (C) Western blot analyses of MSCs 3 days post-coculture for evaluation of direct cell-cell and cell-ECM interactions. Connexin 43 is a gap junction channel, which can directly link MSCs to chondrocytes. Integrin β1 and DDR2 of MSCs are receptors for ECM of chondrocytes. $*p < 0.05$ between two groups, n=3 per group. (D) Schematic diagram of cellular signaling involved in chondrogenic differentiation of MSCs induced by chondroinductive paracrine factors secreted by cocultured chondrocytes, and Western blot analyses of MSCs 3 days post-coculture for evaluation of the signaling molecule expression. $*p < 0.05$ between two groups, n=3 per group.

4.2.6. Superior chondrogenic differentiation of MSCs through cLbL coculture

Since chondrogenic phenotypes of the chondrocytes play vital roles in promoting chondrogenic differentiation of MSCs in coculture of MSCs and chondrocytes,[165] we assessed the chondrogenic phenotypes of the chondrocytes at various passage numbers. The results showed that both passage 1 and passage 2 chondrocytes showed high collagen II (chondrogenic ECM)[166] protein expressions. However, while passage 0 and passage 1 chondrocytes showed comparable gene expressions of aggrecan (cartilage-specific proteoglycan core protein)[167], the aggrecan gene expression decreased with passage (Figure 4.7). Hence, passage 1 chondrocytes were exclusively used for coculture study. Also, we confirmed that chondrocytes cocultured using the BNTHP membranes maintained aggrecan and collagen II expressions during 2-week coculture period (Figure 4.8). Retained chondrogenic phenotypes of the chondrocytes would provide effective chondroinductive cues that promote chondrogenesis of MSCs.

Chondrogenic differentiation of the MSCs was evaluated by analyzing the expression of chondrogenic biomarkers after 2 weeks in coculture with chondrocytes. To comprehensively compare and elucidate the effects of cLbL culture system on chondrogenic differentiation of the MSCs, MSCs from the cLbL coculture (cLbL) were compared with MSCs cultured alone on BNTHP membranes (non-cocultured), MSCs cultured in pellets (pellet), MSCs from the indirect coculture using BNTHP membranes (indirect), and MSCs from the direct bilayer coculture using BNTHP membranes (direct). The cLbL group showed extensive upregulations in chondrogenic transcription factor (SOX9)[168] and collagen II at the gene and protein levels compared to the other groups, even compared to the pellet positive control group, a widely used method to induce chondrogenic differentiation of MSCs (Figure 4.9A ~ 4.9C). Moreover, the cLbL

coculture system supported superior chondrogenic marker expression of MSCs compared with the direct bilayer coculture system, which was likely attributed to the augmented cell-cell, cell-ECM, and cell-paracrine factor interactions between the cocultured MSCs and chondrocytes in the cLbL coculture (Figure 4.6). Even though the indirectly cocultured MSCs expressed an elevated level of collagen II compared to the non-cocultured MSCs which is consistent with the results of a previous study,[68] *SOX9* expression was not elevated (Figure 4.9A). These data suggest that interactions with chondroinductive soluble paracrine factors secreted by chondrocytes without direct cell-cell/cell-ECM interactions were not sufficient to promote effective chondrogenic differentiation of MSCs.

Interestingly, the coculture groups showed suppressed expression of collagen X, a hypertrophy marker,[169] compared to the pellet positive control group (Figure 4.9A and 4.9B). These data were consistent with results from previous studies, which reported that MSCs cocultured with chondrocytes in direct cell-cell/cell-matrix contact underwent efficient chondrogenic differentiation with significantly suppressed hypertrophy.[7,58,76] Even though MSC pellet cultures, which mimic mesenchymal condensation during developmental chondrogenesis, have been considered an effective method for stimulating chondrogenic differentiation of MSCs, high expression of cartilage hypertrophy phenotype in chondrogenic differentiated MSCs in pellet cultures has been an unsolved problem for application of this method in cartilage tissue engineering.[20-21] The implantation of cells expressing hypertrophic marker causes cellular ossification that leads to cartilage malfunction.[20,170] Therefore, prevention of hypertrophy in chondrogenic differentiated MSCs is particularly important for effective chondrogenesis and cartilage repair. Collectively, the data demonstrate the BNTHP-based cLbL coculture platform facilitated a much higher chondrogenic differentiation efficacy

of MSCs and more suppressed hypertrophic collagen X expression compared to the widely used pellet culture method.

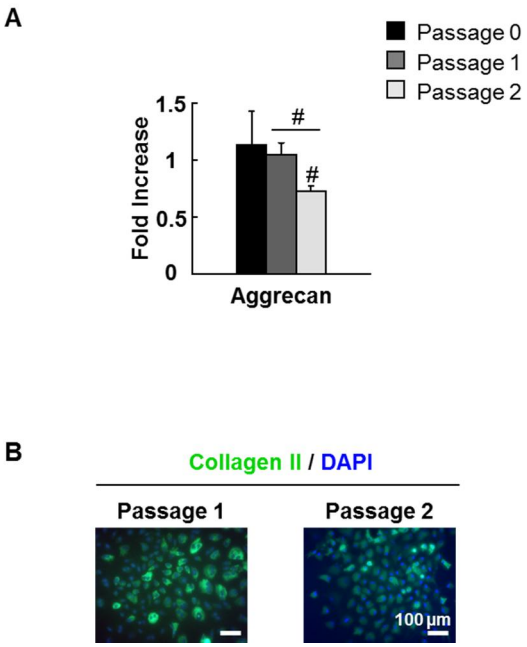

Figure 4.7. Chondrogenic phenotypes of chondrocytes cultured on tissue culture plates at various passage numbers. (A) mRNA expressions of aggrecan relative to freshly isolated chondrocytes (passage 0). $^{\#}p < 0.05$, n=3 per group. (B) Immunocytochemistry for collagen type II.

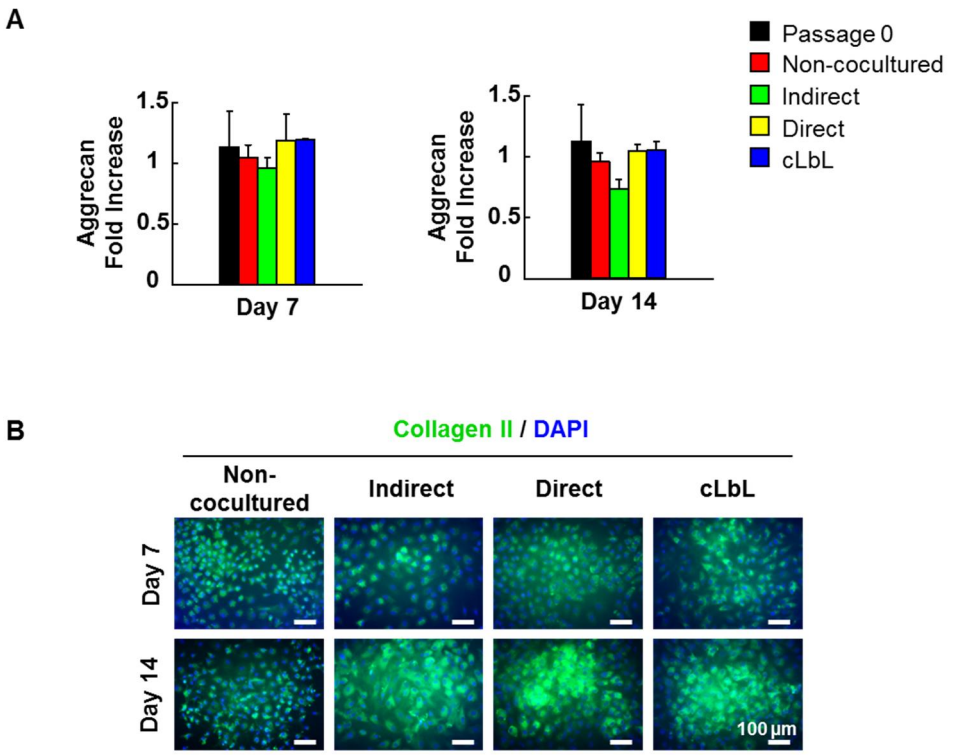

Figure 4.8. Chondrogenic phenotypes of chondrocytes non-cocultured or cocultured with MSCs using various BNTHP-based coculture systems. (A) mRNA expressions of aggrecan relative to freshly isolated chondrocytes (passage 0). n=3 per group. (B) Immunocytochemistry for collagen type II.

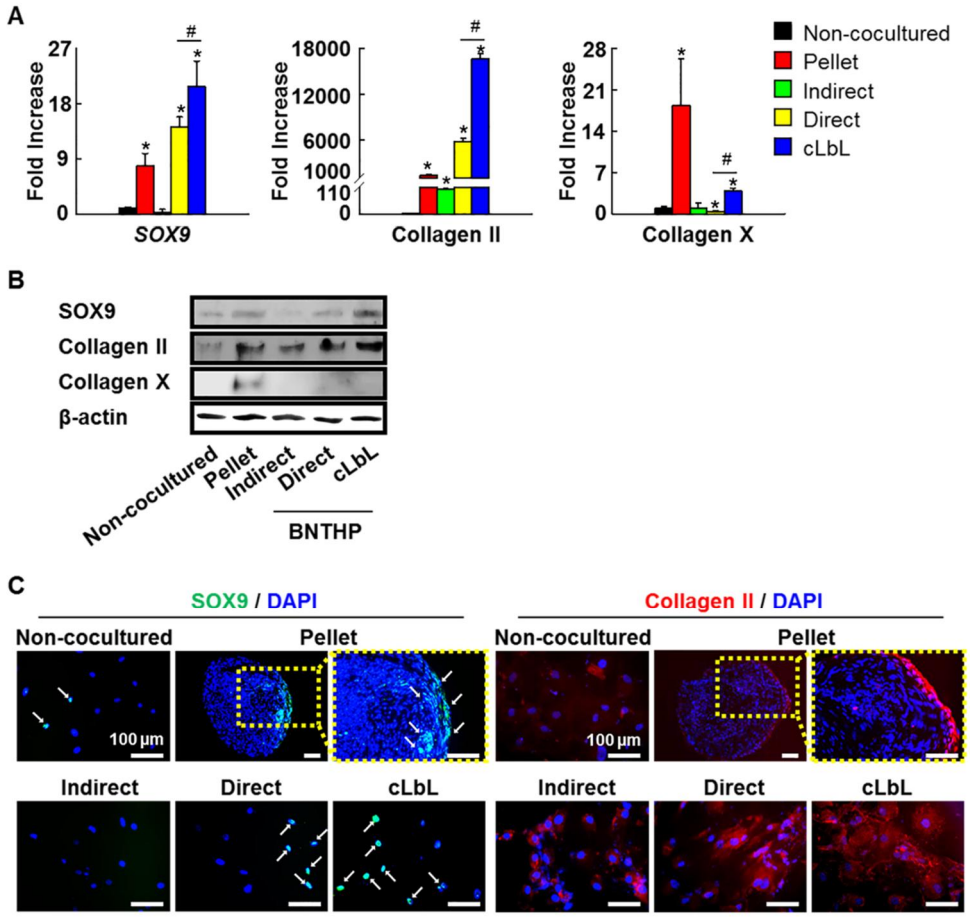

Figure 4.9. Enhanced *in vitro* chondrogenic differentiation of MSCs through BNTHP-based cLbL coculture with chondrocytes for 2 weeks as compared to non-cocultured MSCs on BNTHP membranes (non-cocultured), MSCs in pellet culture (pellet), MSCs cocultured using the BNTHP-based indirect (indirect) and direct (direct) coculture systems. (A) mRNA expressions of a chondrogenic transcription factor (*SOX9*), a chondrogenic ECM (collagen II), and a hypertrophic marker (collagen X) in MSCs cultured under various culture conditions compared to non-cocultured MSCs. $^{*}p < 0.05$ compared to non-cocultured group, $^{\#}p < 0.05$ between two groups, n=3 per group. (B) Western blot analyses of MSCs cultured under various culture conditions for SOX9, collagen II, and collagen X of MSCs. (C)

Immunocytochemistry images of SOX9 and collagen type II in MSCs cultured under various culture conditions. Cell nuclei were counterstained with DAPI. SOX9 expression is indicated with arrows.

4.2.7. Assessment of cartilaginous phenotypes in tissues formed through implantation of the 3D constructs of differentiated cells-laden BNTHP membranes

Following coculture, the *in vitro* differentiated cell-laden BNTHP membranes were subcutaneously implanted into athymic mice for 4 weeks to determine whether the cells with chondrogenic phenotypes and suppressed hypertrophy could form cartilaginous tissues *in vivo*. The BNTHP membranes with robust, nanothin, and highly flexible properties were folded into 3D structures, thus facilitating *in situ* formation of the differentiated cell-BNTHP constructs through quick and simple centrifugation. The biodegradability of BNTHP membranes benefited the membranes as *in vivo* implantable scaffolds. Moreover, this property of the BNTHP membranes eliminated the proteolytic enzyme treatment procedure to harvest the differentiated cells after coculture. The membranes used in the conventional coculture systems are mainly non-biodegradable.[102] Following coculture, the use of proteolytic enzymes to harvest cells from the non-biodegradable membranes may damage the ECM, imposing major drawbacks on cell viability and function.[82-83,102,138-139] The biodegradability of BNTHP membranes overcomes such limitations and allows implantation of the cells together with the membranes, thus avoiding the cell- and ECM-destructive cell harvest procedure. Implantation of cells cultured in pellets was eliminated in the animal studies as the cells expressed a high level of hypertrophic marker (Figure 4.9A and 4.9B), which would be clinically unsuitable for cartilage engineering.[54] Moreover, as BNTHP membranes were not used in the culture, the cells from pellet cultures cannot be implanted.

Four weeks after implantation, the constructs were retrieved. The gross observations of the tissue constructs of the three coculture groups demonstrated off-white tissues with cartilage-like appearances compared to reddish tissues in the

non-coculture group (Figure 4.10A). The relative wet weights of the explanted constructs to the initial implanted constructs were significantly higher in the cLbL group compared to the other groups, followed by that of direct, indirect, and non-coculture group (Figure 4.10B). Hematoxylin & eosin (H&E)-stained cross-sections of the tissue constructs indicated existence and gradual degradation of BNTHP membranes (arrows in Figure 4.10C) in the construct at the 1, 2, and 3-week time point. At the 4-week time point, the constructs exhibited tissue formation with no evidence of the BNTHP membranes, demonstrating high biodegradability of the membranes (Figure 4.10C). Next, immunohistochemical staining of the cross-sections of the constructs for collagen II and aggrecan was performed. The tissues of the cLbL group expressed significantly higher levels of collagen II and aggrecan compared to the other groups (Figure 4.10D). Western blot analyses confirmed that constructs of the cLbL group expressed the highest levels of aggrecan and lowest levels of collagen X (Figure 4.10E). Compared to other groups, constructs in the cLbL group demonstrated the highest chondrogenic phenotypes with suppressed hypertrophy. Coculture of MSCs and chondrocytes has been proposed as a promising method to induce mature chondrogenesis of MSCs with suppressed hypertrophy.[7,58,76] Our coculture system developed enhanced chondrogenic differentiation of MSCs and suppressed hypertrophy compared to other coculture systems. Also, compared to simpler TGF-β3 growth factor only stimulation (*i.e.* non-cocultured MSCs), MSCs cocultured with chondrocytes *via* cLbL coculture platform showed much more efficient *in vivo* chondrogenesis (Figure 4.10D and 4.10E). While BNTHP membranes with no cells showed shape deformation in the subcutaneous pocket within 1 week, cells-laden BNTHP membranes showed 3D unfolded, spherical shape up to 4 weeks (Figure 4.11). Abundant ECM, such as collagen II and X, was observed in the retrieved cells-laden BNTHP membranes with fully degraded BNTHP membrane at 4-week time

point (Figure 4.10D and 4.10E). We postulated that once the cells-laden BNTHP 3D construct was implanted, the laden cells secreted ECM and replaced the BNTHP membranes along with degradation of the membranes, leading to formation of 3D unfolded, compact cartilaginous tissues *in vivo*. Thus, through *in vivo* implantation and chondrogenic phenotype assessment of the 3D constructs, the data collectively emphasized the outstanding performance of the BNTHP-based cLbL coculture platform for generation of cartilage-like tissues from MSCs.

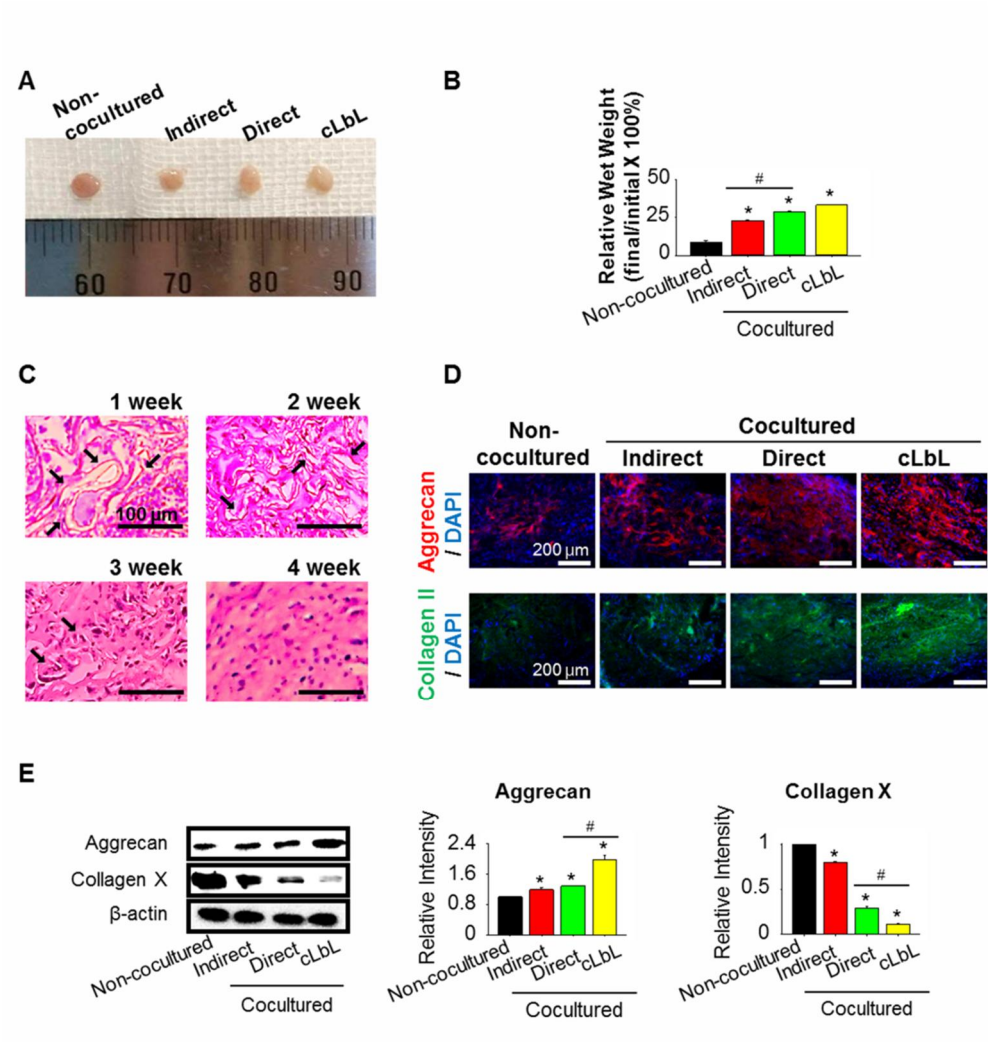

Figure 4.10. Chondrogenic phenotypes assessment of tissues formed by implantation of the 3D constructs of differentiated cells and BNTHP scaffolds into subcutaneous space of athymic mice for 4 weeks. After 2 weeks of chondrogenic differentiation induction of MSCs through various cultures, the differentiated cell-laden BNTHP membranes were centrifuged to form 3D constructs and implanted into mice. (A) Gross images of the constructs explanted at 4 weeks. (B) Wet weights of the constructs relative to the initial wet weight at 4 weeks after implantation of non-cocultured, indirect, direct, and cLbL groups. *$p < 0.05$

compared to non-cocultured group, $^{\#}p < 0.05$ between two groups, n=3 per group. (C) *In vivo* biodegradation of BNTHP, as evaluated by H&E-stained cross-sections of the constructs explanted at 1, 2, 3, and 4 weeks after implantation. While BNTHP (75:25 PLGA polymer, arrows) was observed in the construct at 1, 2, and 3-week time point, BNTHP was not detected at 4-week time point. (D) Immunohistological staining for aggrecan and collagen II of the cross-sectioned constructs 4 weeks after implantation. Nuclei were counterstained with DAPI. (E) Western blot analyses of the constructs for aggrecan and collagen X 4 weeks after implantation. $^{*}p < 0.05$ compared to non-cocultured group, $^{\#}p < 0.05$ between two groups, n=3 per group.

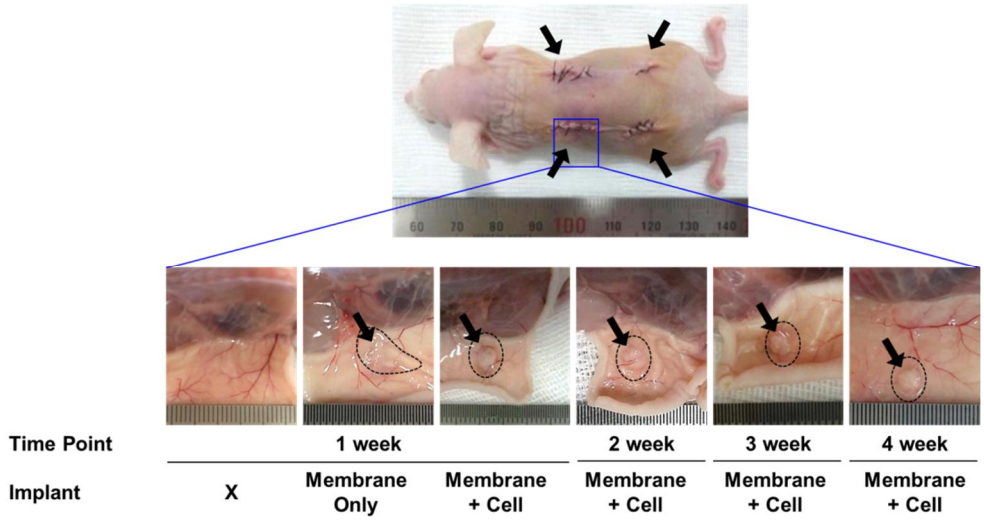

Figure 4.11. Digital images of subcutaneously implanted 3D BNTHP constructs without or with cells (indicated by black dashed lines) at various time points.

Chapter 5.

Development of a reversible cell layering platform in coculture mediated by ionically crosslinked chitosan thin film

5.1. Introduction

Cells in living tissues are in constant communication, engaging in complex cooperation of heterogeneous cells in the face of a dynamically changing environment.[60] In particular, *in vivo* stem cells leave their native microenvironment, so called the stem cell niche, migrate to the target organs, and interact with the target cells in order to differentiate into the corresponding cells.[171-172] Recently, in a hope to recapitulate the complex cell-to-cell interactions occurring in the *in vivo* microenvironments, various cellular assembly approaches have been proposed, including cell sheet engineering,[173] magnetic liposomes,[174] cell-containing gel layers,[175] DNA-cell coating,[176] and nanofilms-cell coating.[177] Previous studies have indicated that coculture of stem cells in direct contact with somatic cells, such as myoblasts,[56] osteoblasts,[57] chondrocytes,[58] and cardiomyocytes,[59] is an effective strategy to promote the stem cell commitment *in vitro*.

Homogenous cell separation following the direct coculture would enable precise phenotypic analysis of the cells and further therapeutic application of the desired cell types following coculture.[77] Even though current cell assembly approaches have shown notable advances in accumulating the cells into intact multilayered coculture system with active cell-cell interactions across the contacting cell layers, none of the methods were able to delayer and separate the layered cells from the mixed cell population constructs following coculture.[173-175,177] Thus, despite the versatile biological advantages of heterogeneous cell coculture in controlling and altering the behavior of the cocultured cells, they possess major limitation for further characterizations and therapeutic applications of the cells as the existing cell assembly approaches only rely on the irreversible layering of the cells. To overcome such a problem of cell separation following coculture, a cell-separating membrane insert-based culture system (Transwell®) has been widely used. However, the physical properties (micro-thick thickness and low

porosity (~2%)) of the membrane impede effective interactions between the cocultured cells separated by the membrane.[178] Thus, it is necessary to develop a heterogeneous cell assembly approach that allows both direct interactions between the cocultured cells and facile cell separation following coculture.

Here, we have developed a cell assembly technique using positively charged chitosan thin film and cells functionalized with negatively charged chondroitin sulfate. Our proof-of-concept study demonstrated the practical application of the reversible cell layering platform to layer/delayer hMSCs and mouse myoblast cell line C2C12 cells (C2C12s) (Figure 5.1). For rapid assembly of cells, confluent hMSCs were modified into the reactive state by mildly reducing the disulfide bonds naturally presented on the surface of cell membranes to free thiol groups.[179-180] Then, we synthesized and grafted MCS onto the hMSCs *via* maleimide-thiol coupling reactions.[181] By adding chitosan polymer-dissolved solution, highly porous chitosan thin film was developed on the hMSC layer *via* ionic crosslinking of cationic groups of the chitosan polymer and anionic groups of MCS-functionalized hMSCs. Thereafter, MCS-functionalized C2C12s were rapidly assembled onto the hMSC layer driven by the electrostatic interactions between negatively charged MCS-functionalized C2C12s and positively charged chitosan thin film. We hypothesized that the highly porous structure of the chitosan thin film formed between the top (C2C12s) and bottom (hMSCs) cell layers would allow active communications between hMSCs and C2C12s *via* direct cell-to-cell contacts, thus promoting myogenic differentiation of hMSCs. Also, the steady formation of chitosan thin film *via* ionic crosslinking between the cocultured cells would not only act as a barrier that prevents mixing of the cocultured cells, but also allow facile delayering of the cells (C2C12s) layered on top of the chitosan thin film with a mild shear stress treatment. Ultimately, the myogenically differentiated hMSCs were collected *via* shear induced separation and intramuscularly delivered into

skeletal muscle injured athymic mice to examine the muscle tissue regeneration efficacy.

The present study highlights the development of a novel cell assembly platform that supports both maximized cell-cell direct interactions and facile separation in coculture of stem cells and target cells. This study demonstrated applications of the developed platform in stem cell differentiation and tissue regeneration.

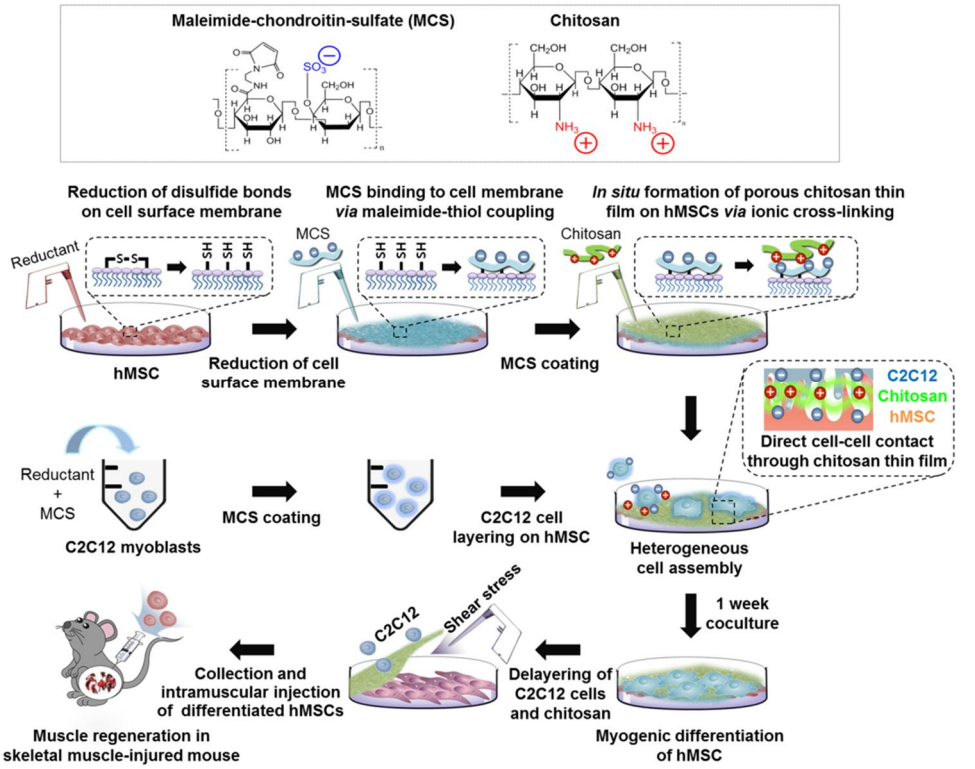

Figure 5.1. Schematic illustration of porous chitosan thin film-aided reversible cell layering and delayering for heterogeneous cell assembly in coculture and its applications in stem cell differentiation and tissue regeneration.

5.2. Results and discussion

5.2.1. Synthesis and engraftment of MCS onto reduced cell surface membrane

We synthesized MCS *via* the EDC-NHS coupling reaction of CS and maleimide functional group and confirmed the MCS synthesis with ^{1}H-NMR (Figure 5.2A). Compared to native CS, a negatively charged natural macromolecule,[182] MCS showed the identical picks with an additional maleimide pick (6.778 ppm). In order to graft MCS onto cell surface membrane, we treated cells with various doses of TCEP, a mild reductant, which reduced natural disulfide on the cell surface into reactive free thiol groups (Figure 5.2B). The data revealed that 1 mM of TCEP was sufficient to expose the efficient amount of thiol groups. To visualize the thiol-maleimide reaction, we reduced red fluorescent PKH26-labeled cells with 1 mM TCEP and treated maleimide-conjugated Alexa fluor-488 fluorescent (Mal-Alexa Fluor 488). Confocal microscopic images indicated that thiol groups were exposed exclusively and evenly on the surface membrane of the reduced cells (Figure 5.2C). To determine the optimal coating concentration of MCS, the reduced cells were treated with various doses of non-fluorescent MCS followed by Mal-Alexa Fluor 488 treatment to observe leftover thiols (Figure 5.2D). Engraftment of the fluorescence onto the cell surface decreased gradually as the concentration of MCS increased, and vanished at the MCS concentration of 10 mM, indicating that the concentration of MCS to graft all thiol groups of cell surface is 10 mM. Surface charges of the MCS-grafted cells indicated higher anionic cell-surface than non-

grafted cells, which was attributed to the highly negative charge of the chondroitin sulfate (Figure 5.2E). Also, the data confirmed that addition of chitosan neutralized the surface charges of the MCS-grafted cells by the electrostatic interactions between MCS and chitosan.

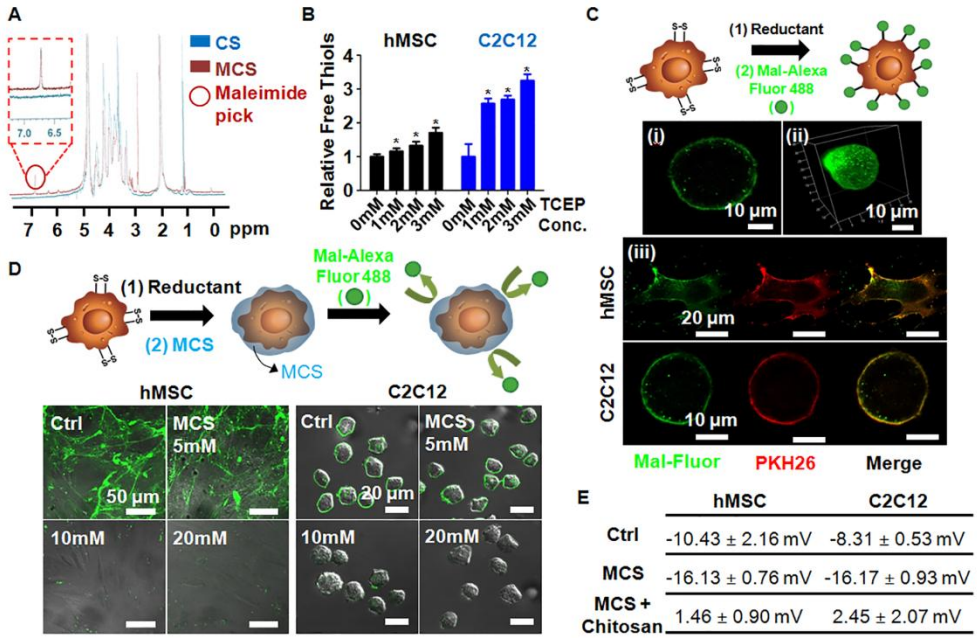

Figure 5.2. MCS grafting onto reduced cell surface membrane of hMSCs and C2C12 cells. (A) ^{1}H-NMR spectra of CS and MCS. Maleimide peaks at 6.663ppm indicate the presence of MCS. (B) Relative amounts of free thiol groups on cells treated with different concentrations of reductant (TCEP). *$p < 0.05$ *vs.* non-treated group, n=5. (C) Confirmation of cell surface membrane reduction. (i) 2D and (ii) z-stacked confocal images of maleimide-Alexa Fluor 488 coated on reduced C2C12 cell. (iii) Confocal images of both maleimide-Alexa Fluor 488 (Green) and PKH26 (Red) double-labeled hMSC and C2C12 cell. (D) Optimization of MCS concentration for cell surface grafting. Following MCS grafting, maleimide-Alexa Fluor 488 was treated to visualize any leftover thiol groups on the cell surface. (E) ζ-potential of untreated cells, MCS-grafted cells and chitosan-MCS-grafted cells. n=3.

5.2.2. Cytotoxicity of the cell surface membrane modification

Cytotoxicity analyses were performed to identify the non-cytotoxic working concentration of TCEP and MCS (Figure 5.3). The cell viability, proliferative activity, and a number of hMSCs and C2C12s, respectively, were thoroughly assessed to identify the ideal cell-friendly working concentration of TCEP. The assays revealed that while treatment of 1 mM TCEP showed no significant effects, a higher dose than 1 mM of TCEP showed adverse effects on cell number and cell proliferation (Figure 5.3A ~ 5.3C). Consecutive treatment of 1 mM TCEP and 10 mM MCS revealed comparable cell viability, proliferative activity, and numbers to the non-treated control group (Figure 5.3D ~ 5.3F). Expressions of apoptotic regulatory genes, caspase-3 and p53, and an anti-apoptotic regulatory gene, *Bcl-2*, 24-hours after treatments were comparable in all groups (Figure 5.3G). The overall data indicated that non-cytotoxic maximal concentrations of TCEP and MCS to engraft MCS onto the cell surface membranes of both hMSCs and C2C12s are 1 mM and 10 mM, respectively. These concentrations were used in the subsequent studies.

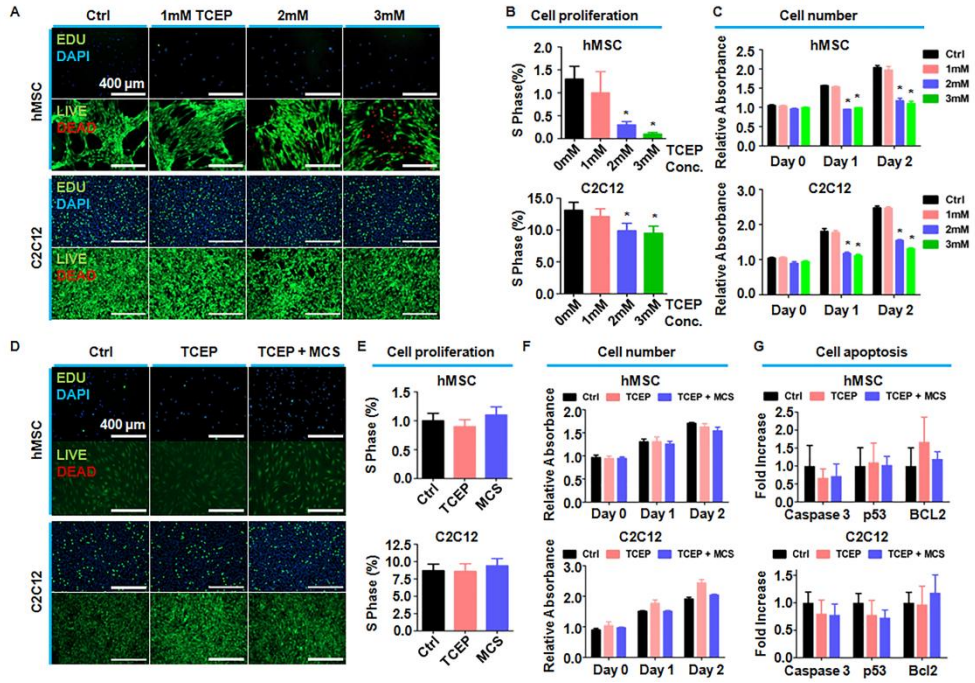

Figure 5.3. Cytotoxicity of the cell surface membrane modification, as evaluated in terms of cell viability, proliferation rate, and apoptotic activity. (A) Images of cell viability and proliferating cells after treatment with various concentrations of reductant (TCEP). Proliferating cells were detected by the EDU assay. Live cells were stained by calcein-AM (green) and dead cell by Ethd-1 (red) using Live/Dead viability assay. Cell proliferation images were obtained by EDU assay kit and analyzed by FACS. (B) The number of proliferating cells was obtained by FACS analysis of EDU-stained cells. (C) The relative number of live cells on tissue culture polystyrene (TCPS) dish at given time and TCEP dose. The data was obtained using the CCK-8 assay. (D, E, F) Images and number of cell viability and proliferating cells of cells treated with 1mM reductant followed by 10 mM MCS. (G) Changes in expressions of apoptosis regulatory genes, apoptotic marker caspase 3, p53 and an anti-apoptotic marker *Bcl-2* of untreated, reduced, and MCS-

grafted hMSCs and C2C12 cells evaluated by qRT-PCR. *$p < 0.05$ *vs.* non-treated group, n=3 in (B)~(C) and (E), n=5 in (G).

5.2.3. Formation of porous chitosan thin film for effective cell assembly into heterogeneous coculture constructs

We investigated the optimal concentration of chitosan to induce *in situ* chitosan thin film formation. For better visualization of the chitosan, chitosan was conjugated with green fluorescence FITC (chitosan-FITC). Formation of well-developed, uniform chitosan layer covering the MCS-grafted hMSCs surfaces was observed at a chitosan concentration of 25 μg/cm^2 (Figure 5.4A). The formed chitosan thin films had an average thickness of 7.63 μm, an average porosity of 21.67% and an average pore size of 6.17 μm (Figure 5.4B). Depositions of MCS and chitosan thin film were evaluated quantitatively with QCM analysis (Figure 5.4C). The significant mass increase following the addition of MCS and chitosan indicated steady deposition of chitosan layer on top of the lipid. For rapid cellular assembly, MCS-grafted C2C12s were layered on top of the chitosan thin film (Figure 5.4D and 5.4E). For better visualization, hMSCs were labeled with red fluorescence DiI, C2C12 with blue fluorescence cell tracker, and FITC was conjugated on chitosan. Without MCS-engraftment, chitosan thin film was not formed with much less layered C2C12s compared to the chitosan thin film-mediated layered C2C12s (Figure 5.4D). The z-stack confocal side images of the coculture construct demonstrated direct contacts between hMSCs and C2C12s across the highly porous, micro-thick chitosan thin film (Figure 5.4E).

We investigated whether such chitosan thin film allows and supports active cell-cell crosstalks between the directly contacting hMSCs and C2C12s with calcein-AM dye transfer assay (Figure 5.4F). Initially, C2C12s on the top-most layer of the coculture construct were dual-labeled with DiI (red, a cell membrane labeling dye) and calcein-AM (green, an intracellular dye). hMSCs at the bottom-most layer were un-labelled. Calcein-AM is a cell-permeable molecule and cleaved

into green fluorescence cell-impermeable calcein within the cells.[99] Calcein can be transferred into adjacent cells only through gap junction channel formed by directly contacting cells.[100] Calcein transfer was observed in coculture of hMSCs and C2C12s with chitosan thin films (Figure 5.4F), verifying that the chitosan thin film both supported active direct cellular communications with the intercellular transfer of cellular components and acted as a barrier between the cell layers, preventing cell fusion.

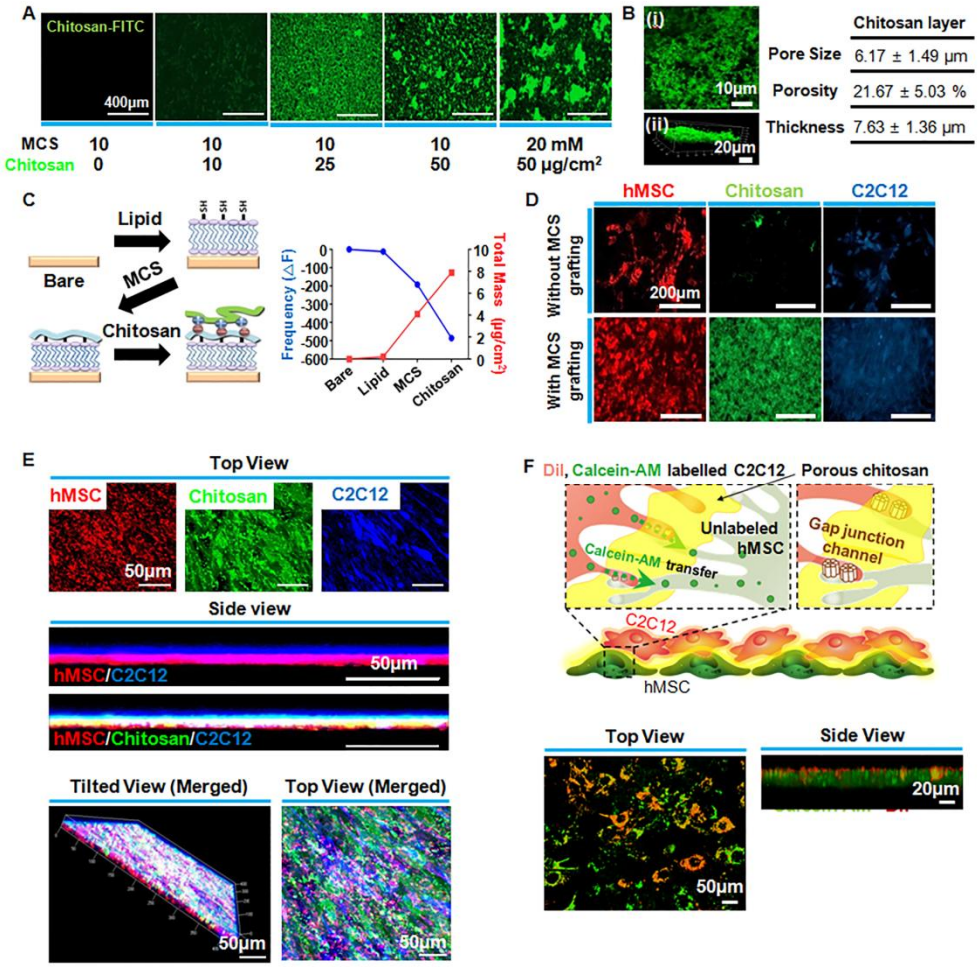

Figure 5.4. *In situ* formation of porous chitosan thin film on cell surface for effective cell assembly into heterogeneous cell coculture constructs, and direct cell-cell interactions through the chitosan film. (A) Optimization of concentrations of chitosan and MCS for chitosan-FITC porous thin film formation on cell surface of hMSCs. (B) Characterization of chitosan-FITC porous thin film formed on cell surface of hMSCs based on (i) top and (ii) z-stack high-resolution confocal images of the film. (C) QCM analysis of MCS and chitosan thin film deposition on lipid that mimics reduced cell lipid bilayer. (D) Images of chitosan-FITC porous thin film formation and cell layering with and without MCS grafting on the cell surface. (E) Z-stack confocal images of 3D heterogeneous cells coculture construct with

chitosan thin layer. (F) Illustrations and confocal images of calcein-AM dye (green) transfer from C2C12 (DiI-labelled, red) to hMSCs (non-labelled) *via* gap junction channel formed between the directly contacting hMSCs and C2C12 cells through the chitosan thin film for 2 days.

5.2.4 Cell delayering of the heterogeneous cell coculture mediated by porous chitosan thin film

To determine the force required to break the ionic crosslinking between hMSCs and chitosan, we conducted an experiment to find the critical shear stress that initiates chitosan thin film detachment from the cell surface of hMSCs under a pressure-driven flow at a steady flow rate (Figure 5.5A). *In situ* microscopic observation indicated that chitosan-FITC thin film remained firmly attached on the cell surface of hMSCs at the flow rate of 140 mL/min and below (Figure 5.5B). In contrast, at a flow rate of 160 mL/min, the chitosan thin film was gradually detached from the hMSCs (Figure 5.5C). Repetitive experiments on chitosan thin film detachment showed that the average critical flow rate required to detach the chitosan thin film was 153.3 mL/min. Based on the CFD calculation, the critical shear stress required to break the ionic crosslinking between chitosan thin film and cell surface of hMSCs, which would delayer the C2C12 cells from hMSCs, was found to be 2.209 dyne/cm^2 (Figure 5.5A). Figure 5.5D demonstrated the reversible cell layering of C2C12s onto hMSCs. While PBS flow effectively delayered C2C12s and chitosan thin film from the surface of hMSCs, hMSCs were robustly attached to the culture plate. MCS was observed to be eliminated along with the detachment of the chitosan thin film (Figure 5.5E). FACS analysis revealed that the purity of the collected hMSCs following delayering of C2C12s after 1 week of coculture was as high as 95.4% (Figure 5.5F), which is comparable to that of commercially available membrane-based coculture system.[78] This data demonstrated the robust function of the chitosan thin film as an effective physical barrier between the cocultured cells and a tool to separate the heterogeneous cells following coculture.

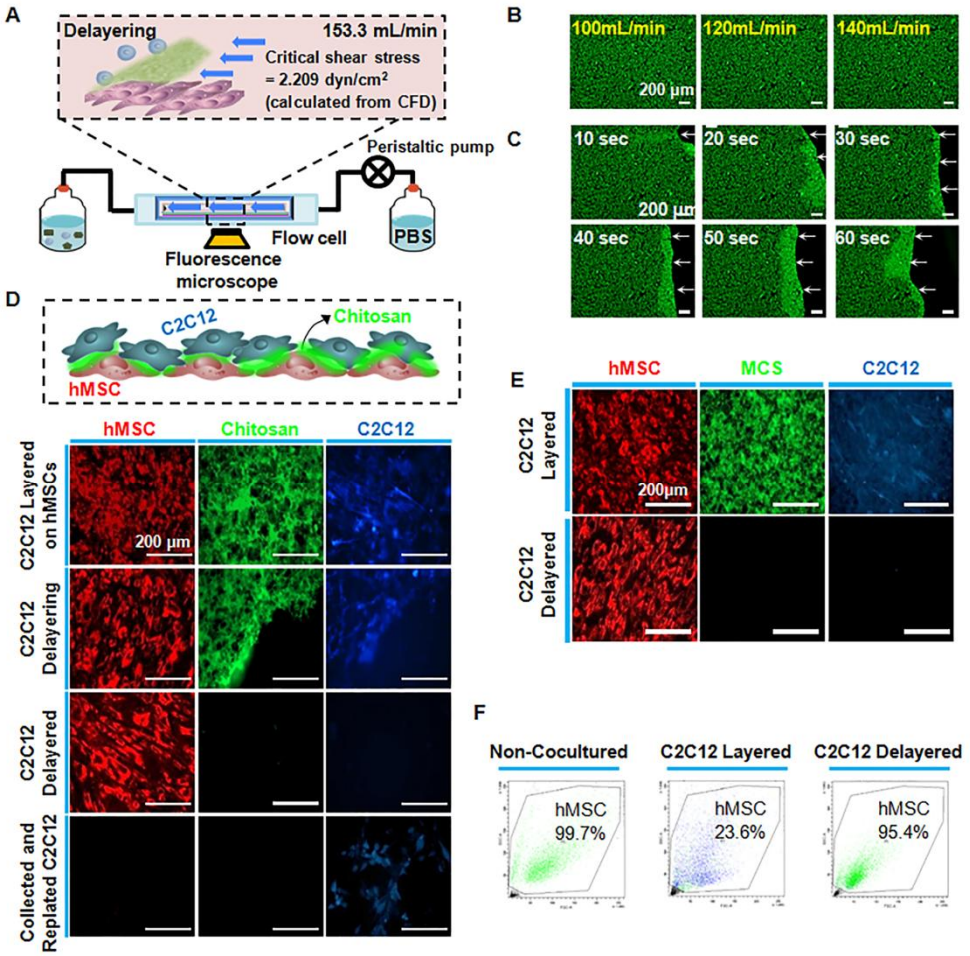

Figure 5.5. Effective cell delayering of heterogeneous cell coculture mediated by porous chitosan thin film. (A) Illustration of cell delayering with fluid shear. (B) Fluorescent images of the chitosan-FITC thin film firmly attached to cell layer under flow with the flow rate of 100 mL/min, 120 mL/min and 140 mL/min. (C) The sequence of the chitosan-FITC thin film detachment from the cell layer at the flow rate of 160 mL/min. (D) Fluorescent images of hMSCs (red) and C2C12 cells (blue) in coculture with chitosan-FITC thin film before, during, and after delayering of chitosan and C2C12 cells. (E) Fluorescence images indicating efficient elimination of FITC-conjugated MCS (green) along with delayering of

C2C12 cells and chitosan thin film. (F) Homogeneity of the collected hMSCs after 1 week of coculture with C2C12 cells evaluated by FACS analysis.

5.2.5. Enhanced myogenic differentiation of hMSCs after cocultured with C2C12 cells based on reversible cell layering platform

Based on a previous study on myogenic differentiation of hMSCs under direct coculture with C2C12s in horse serum supplemented growth medium without any additional exogenous supplements,[183] we examined the myogenic differentiation of hMSCs cocultured with C2C12s in the same medium using chitosan thin film-aided reversible cell layering platform (chitosan or coculture group) for 1 week. As comparative groups, three groups of non-cocultured hMSCs cultured in various medium were compared; hMSCs cultured in 10% fetal bovine serum growth medium (FBS10%-GM, a widely-used conventional medium for hMSCs), cultured in HS5%-GM (HS5%-GM), and cultured in HS5%-GM with myogenic differentiation-inducting supplements (myogenic medium). Also, hMSCs cocultured with C2C12 in HS5%-GM using a conventional membrane-based cocultured system (Transwell®) was set as comparative groups to comprehensively assess the efficacy of myogenic differentiation of hMSCs. The chitosan group showed higher myogenic mRNA expressions of regulatory factors (*MYF5*, *MRF4*, *MyoD*, myogenin), cytoplasm protein (dystrophin), and contractile proteins (*MYH1*, *sTnT*) compared to the other groups (Figure 5.6A). Conforming with previous studies, the differentiation efficacy of hMSCs through coculture with differentiated cells using Transwell® was very low, mainly due to the low-porous (~2%) and micro-thick (10 μm) membrane that hampers efficient interaction between the cocultured cells.[178] Our data also confirmed chitosan thin film itself did not promote the myogenic differentiation of hMSCs. (Figure 5.6B). Myogenic protein expressions of hMSCs, such as myogenic regulatory factors (myogenin, MRF4, Pax-7) and contractile protein (sTnI), were much greater in the chitosan group

compared to the other groups (Figure 5.6C and 5.6D). Formation of multinucleated cells, a myogenic-specific morphological change,[184] was observed in the myogenic medium and chitosan groups, with a greater number of multinucleated cells in the chitosan group (Figure 5.6E). Meanwhile, hMSCs after 1 week coculture in the chitosan group also expressed elevated levels of paracrine factors that are favorable for skeletal muscle repair, *i.e.* pro-survival (pentraxin 3, uPA, and MCP-1), tissue remodeling (IGFBP-2 and IGFBP-3), and angiogenesis-related factors (thrombospondin-1 and VEGF) (Figure 5.7).[185-186] This result is consistent with previous studies that reported that myogenic-differentiated cells expressed tissue repair-favorable paracrine factors, such as MCP-1, IGFBP-2, IGFBP-3, and VEGF.[187-190]

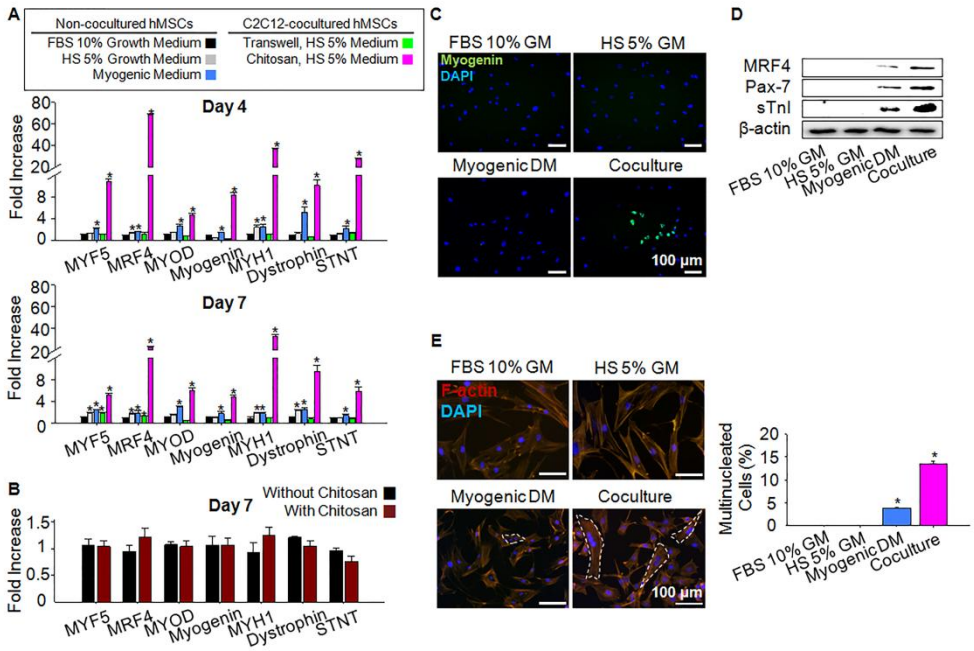

Figure 5.6. Enhanced myogenic differentiation of hMSCs through the porous chitosan thin film-aided heterogeneous coculture with C2C12 cells for 1 week. (A) mRNA expression of myogenic factors in hMSCs. *$p < 0.05$ *vs.* non-cocultured hMSCs in 10% FBS growth medium, n=3. (B) Myogenic mRNA expression of non-cocultured hMSCs without or with chitosan thin film in 10% FBS growth medium, n=3. (C) Immunocytochemistry images of myogenin in hMSCs. Cell nuclei were counterstained with DAPI. (D) Western blot analysis of hMSCs for myogenic proteins. (E) Fluorescence images and quantification of multinucleated hMSCs (indicated in white dashed lines) after monoculture or coculture for 1 week under various culture conditions. The actin filaments were stained with phalloidin (red), and the cell nuclei were counterstained with DAPI. *$p < 0.05$ *vs.* non-cocultured hMSCs in FBS 10% growth medium, n = 200 cells.

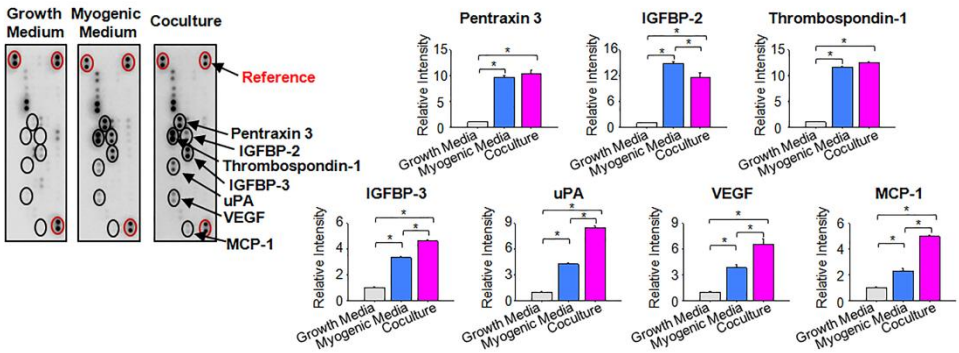

Figure 5.7. Elevated profiles of skeletal muscle repair-favorable paracrine factors secreted by hMSCs after 1-week coculture with C2C12 cells compared to those of hMSCs monocultured in 10% FBS growth medium or myogenic differentiation medium. The left panel is the representative images for the dot blot analysis. The right panel graphs are the quantification of the dot blot analysis. n=4.

5.2.6. Application of the reversible cell layering platform in stem cell-based tissue regeneration

We further examined the skeletal muscle regeneration efficacy of the differentiated hMSCs by intramuscular injection of hMSCs differentiated *via* coculture (coculture), myogenic medium (myogenic medium), and growth medium (growth medium) into cardiotoxin-induced TA muscle-injured mice. Untreated cardiotoxin-induced TA muscle-injured mice injected with phosphate-buffered saline solution (PBS) and non-injured mice (normal) served as comparative groups. Histological analysis based on H&E staining 10 days after cell implantation revealed that myofibre density and cross-sectional area (CSA) of the chitosan group were significantly higher and larger compared to the other groups (Figure 5.8A and 5.8B). Higher phosphorylation of Akt and mTOR cellular signaling pathway in the chitosan group demonstrated more active muscle regeneration compared to the other groups (Figure 5.8C).[191] Immunohistochemical staining for human nuclear antigen (HNA) and myogenic structural proteins (desmin, laminin, troponin I) confirmed incorporation of the implanted cells into the muscle and successful muscle fiber formation in the chitosan group compared to the other groups (Figure 5.8D). Thus, in accordance with a previous study, higher myogenic marker expressions of the implanted cells prior to implantation vastly elevated efficacy of the cells in muscle regeneration.[26]

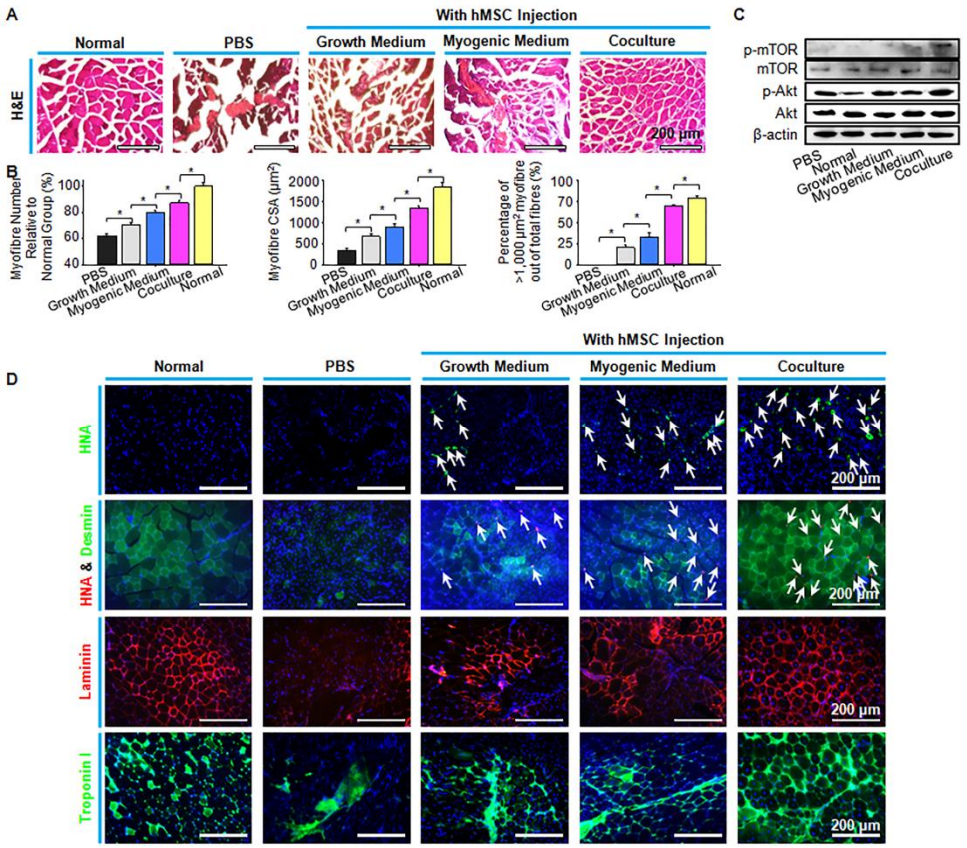

Figure 5.8. Cell implantation-mediated skeletal muscle regeneration in athymic mice with a skeletal muscle injury. (A) Representative images of the H&E-stained TA muscles. (B) Quantifications of myofibre number, CSA, and large myofibres of the H&E stained TA muscles. n = 6 images per group. *$p < 0.05$. (C) Western blot analysis for intracellular signaling molecules involved in skeletal muscle hypertrophy. (D) Immunostaining for HNA and myogenic protein markers in the TA muscles. White arrows indicated HNA-positive cells, *i.e.* implanted cells.

Chapter 6.

Conclusions

This dissertation presents the development of membrane-based coculture platforms for effective stem cell therapy.

Chapter 3 demonstrates the development of NTHP membranes for the generation of transfer-printable, stem cell-derived, multilayered cardiac sheets. The feasibility of NTHP membranes as effective substrates for coculture was confirmed by the demonstration of the biocompatibility of the membrane, direct cell-cell contact between MSC-H9C2, fast protein diffusion across the membrane, and enhanced cardiac differentiation of MSCs following coculture. The precise control of the pore architecture of NTHP membranes at the nanoscale level enabled a systematic search for the most efficient pore size for stem cell coculture. The tunable pore dimension was a key parameter in regulating cell-to-cell communication, ranging from diffusion of soluble paracrine factors to direct gap junction-mediated cell-to-cell contacts, and preventing cellular cross-migrations between the cocultured cell populations. In addition, thermoresponsive NTHP membranes enabled the facile engineering of multilayered cell sheets by the transfer-printing technique.

Chapter 4 demonstrates the development of cLbL coculture platform using BNTHP membranes for the generation of readily implantable 3D constructs of chondrogenic differentiated cells and BNTHP membranes. The BNTHP-based cLbL coculture platform demonstrated amplified interactions between MSCs and chondrocytes in three-dimensional manner compared to BNTHP-based direct bilayer coculture. BNTHP-based cLbL coculture platform showed notably enhanced chondrogenesis with suppressed hypertrophy of MSCs. Moreover, the highly flexible and biodegradable features of BNTHP membranes enabled the generation of readily implantable 3D constructs of chondrogenic differentiated cells and BNTHP scaffolds through a simple centrifugation procedure. Such properties of the BNTHP-based cLbL coculture platform enabled avoidance of

enzymatic harvesting of the cultured cells which often impairs the cells and, in turn, functional tissue formation of the harvested cells.

Chapter 5 demonstrates a reversible cell layering platform mediated by a chitosan thin film for heterogeneous cell assembly of hMSCs and C2C12s. *In situ* formation of a highly porous chitosan thin film was induced by ionic crosslinking between chitosan and functionalized cell surface membranes without causing cellular toxicity. The well-defined porous architecture of chitosan thin film allowed dynamic direct cell-cell communications between the cells, while preventing mixture of the cells. Administration of mild shear stress initiated chitosan film detachment, leading to an effective delayering of C2C12s from hMSCs. The system was highly efficient in myogenic differentiation of hMSCs, likely due to active direct cell-cell communications between the cocultured cells. The differentiation efficiency was much superior compared to those of previously reported systems. hMSCs differentiated through this system showed much higher efficacy in muscle tissue regeneration in animal models than naïve hMSCs and hMSCs differentiated with myogenesis-inducting artificial supplements.

The novel development of customized and tunable coculture platforms presented in these chapters will serve as efficient coculture systems that can regulate the cell-to-cell interactions between the cocultured cells. Also, these platforms might prove useful for engineering various types of functional tissues by coculturing stem cells and the desired type of differentiated cells. Since these platforms can potentially be used to differentiate patient-derived stem cells, it opens up the possibility for patient-specific, personalized drug testing and toxicological studies. The developed platforms may serve as a promising modality for effective stem cell therapy.

References

1. Strauer, B. E.; Kornowski, R. Stem cell therapy in perspective. *Circulation* **2003,** *107*, 929-934.

2. Brunt, K. R.; Weisel, R. D.; Li, R.-K. Stem cells and regenerative medicine—future perspectives. *Can. J. Physiol. Pharmacol.* **2012,** *90*, 327-335.

3. Wu, S. M.; Hochedlinger, K. Harnessing the potential of induced pluripotent stem cells for regenerative medicine. *Nat. Cell Biol.* **2011,** *13*, 497-505.

4. Herberts, C. A.; Kwa, M. S.; Hermsen, H. P. Risk factors in the development of stem cell therapy. *J. Transl. Med.* **2011,** *9*, 29-42.

5. Perin, E. C.; Geng, Y.-J.; Willerson, J. T. Adult stem cell therapy in perspective. *Circulation* **2003,** *107*, 935-938.

6. Pessina, A.; Gribaldo, L. The key role of adult stem cells: therapeutic perspectives. *Curr. Med. Res. Opin.* **2006,** *22*, 2287-2300.

7. Bian, L.; Zhai, D. Y.; Mauck, R. L.; Burdick, J. A. Coculture of human mesenchymal stem cells and articular chondrocytes reduces hypertrophy and enhances functional properties of engineered cartilage. *Tissue Eng., Part A* **2011,** *17*, 1137-1145.

8. Giovannini, S.; Diaz-Romero, J.; Aigner, T.; Heini, P.; Mainil-Varlet, P.; Nesic, D. Micromass coculture of human articular chondrocytes and human bone marrow mesenchymal stem cells to investigate stable neocartilage tissue formation *in vitro*. *Eur. Cell. Mater.* **2010,** *20*, 245-259.

9. Barry, F. P.; Murphy, J. M. Mesenchymal stem cells: clinical applications and biological characterization. *Int. J. Biochem. Cell Biol.* **2004,** *36*, 568-584.

10. DiMarino, A. M.; Caplan, A. I.; Bonfield, T. L. Mesenchymal stem cells in tissue repair. *Front. Immunol.* **2013,** *4*, 201-209.

11. Djouad, F.; Bouffi, C.; Ghannam, S.; Noël, D.; Jorgensen, C. Mesenchymal stem cells: innovative therapeutic tools for rheumatic diseases. *Nat. Rev. Rheumatol.* **2009,** *5*, 392-399.

12. Sharma, R. R.; Pollock, K.; Hubel, A.; McKenna, D. Mesenchymal stem or stromal cells: a review of clinical applications and manufacturing practices. *Transfusion* **2014,** *54*, 1418-1437.

13. Michel, J.-B. Anoikis in the cardiovascular system. *Arterioscler. Thromb. Vasc. Biol.* **2003,** *23*, 2146-2154.

14. Taddei, M.; Giannoni, E.; Fiaschi, T.; Chiarugi, P. Anoikis: an emerging hallmark in health and diseases. *J. Pathol.* **2012,** *226*, 380-393.

15. Mooney, D. J.; Vandenburgh, H. Cell delivery mechanisms for tissue repair. *Cell stem cell* **2008,** *2*, 205-213.

16. Roell, W.; Lewalter, T.; Sasse, P.; Tallini, Y. N.; Choi, B.-R.; Breitbach, M.; Doran, R.; Becher, U. M.; Hwang, S.-M.; Bostani, T. Engraftment of connexin 43-expressing cells prevents post-infarct arrhythmia. *Nature* **2007,** *450*, 819-824.

17. Beeres, S. L.; Zeppenfeld, K.; Bax, J. J.; Dibbets-Schneider, P.; Stokkel, M. P.; Fibbe, W. E.; van der Wall, E. E.; Atsma, D. E.; Schalij, M. J. Electrophysiological and arrhythmogenic effects of intramyocardial bone marrow cell injection in patients with chronic ischemic heart disease. *Heart rhythm* **2007,** *4*, 257-265.

18. Chen, H.-S. V.; Kim, C.; Mercola, M. Electrophysiological challenges of cell-based myocardial repair. *Circulation* **2009,** *120*, 2496-2508.

19. Chang, M. G.; Tung, L.; Sekar, R. B.; Chang, C. Y.; Cysyk, J.; Dong, P.; Marbán, E.; Abraham, M. R. Proarrhythmic potential of mesenchymal stem cell transplantation revealed in an *in vitro* coculture model. *Circulation* **2006,** *113*, 1832-1841.

20. Pelttari, K.; Winter, A.; Steck, E.; Goetzke, K.; Hennig, T.; Ochs, B. G.; Aigner, T.; Richter, W. Premature induction of hypertrophy during *in vitro* chondrogenesis of human mesenchymal stem cells correlates with calcification and vascular invasion after ectopic transplantation in SCID mice. *Arthritis Rheum.* **2006,** *54*, 3254-3266.

21. Mueller, M. B.; Tuan, R. S. Functional characterization of hypertrophy in chondrogenesis of human mesenchymal stem cells. *Arthritis Rheum.* **2008,** *58*, 1377-1388.

22. Song, H.; Hwang, H. J.; Chang, W.; Song, B.-W.; Cha, M.-J.; Kim, I.-K.; Lim, S.; Choi, E. J.; Ham, O.; Lee, C. Y. Cardiomyocytes from phorbol myristate acetate-activated mesenchymal stem cells restore electromechanical function in infarcted rat hearts. *Proc. Natl. Acad. Sci.* **2011,** *108*, 296-301.

23. Hahn, J.-Y.; Cho, H.-J.; Kang, H.-J.; Kim, T.-S.; Kim, M.-H.; Chung, J.-H.; Bae, J.-W.; Oh, B.-H.; Park, Y.-B.; Kim, H.-S. Pre-treatment of mesenchymal stem cells with a combination of growth factors enhances gap junction formation, cytoprotective effect on cardiomyocytes, and therapeutic efficacy for myocardial infarction. *J. Am. Coll. Cardiol.* **2008,** *51*, 933-943.

24. Han, J.; Kim, B.; Shin, J.-Y.; Ryu, S.; Noh, M.; Woo, J.; Park, J.-S.; Lee, Y.; Lee, N.; Hyeon, T. Iron oxide nanoparticle-mediated development of cellular gap junction crosstalk to improve mesenchymal stem cells' therapeutic efficacy for myocardial infarction. *ACS Nano* **2015,** *9*, 2805-2819.

25. Choi, K.-H.; Choi, B. H.; Park, S. R.; Kim, B. J.; Min, B.-H. The chondrogenic differentiation of mesenchymal stem cells on an extracellular matrix scaffold derived from porcine chondrocytes. *Biomaterials* **2010,** *31*, 5355-5365.

26. Muguruma, Y.; Reyes, M.; Nakamura, Y.; Sato, T.; Matsuzawa, H.; Miyatake, H.; Akatsuka, A.; Itoh, J.; Yahata, T.; Ando, K. *In vivo* and *in vitro*

differentiation of myocytes from human bone marrow–derived multipotent progenitor cells. *Exp. Hematol.* **2003,** *31*, 1323-1330.

27. Shi, Y.; Hu, G.; Su, J.; Li, W.; Chen, Q.; Shou, P.; Xu, C.; Chen, X.; Huang, Y.; Zhu, Z. Mesenchymal stem cells: a new strategy for immunosuppression and tissue repair. *Cell Res.* **2010,** *20*, 510-518.

28. Karp, J. M.; Teo, G. S. L. Mesenchymal stem cell homing: the devil is in the details. *Cell stem cell* **2009,** *4*, 206-216.

29. Newman, R. E.; Yoo, D.; LeRoux, M. A.; Danilkovitch-Miagkova, A. Treatment of inflammatory diseases with mesenchymal stem cells. *Inflamm. Allergy Drug Targets* **2009,** *8*, 110-123.

30. Shapiro, F.; Koide, S.; Glimcher, M. Cell origin and differentiation in the repair of full-thickness defects of articular cartilage. *J. Bone Joint Surg. Am.* **1993,** *75*, 532-553.

31. Bruder, S. P.; Fink, D. J.; Caplan, A. I. Mesenchymal stem cells in bone development, bone repair, and skeletal regenaration therapy. *J. Cell. Biochem.* **1994,** *56*, 283-294.

32. Schmid, T. M.; Linsenmayer, T. F. Developmental acquisition of type X collagen in the embryonic chick tibiotarsus. *Dev. Biol.* **1985,** *107*, 373-381.

33. Damien, C. J.; Parsons, J. R. Bone graft and bone graft substitutes: a review of current technology and applications. *J. Appl. Biomater.* **1991,** *2*, 187-208.

34. Franzen, A.; Heinegard, D.; Solursh, M. Evidence for sequential appearance of cartilage matrix proteins in developing mouse limbs and in cultures of mouse mesenchymal cells. *Differentiation* **1987,** *36*, 199-210.

35. Xue, J. X.; Gong, Y. Y.; Zhou, G. D.; Liu, W.; Cao, Y.; Zhang, W. J. Chondrogenic differentiation of bone marrow-derived mesenchymal stem cells induced by acellular cartilage sheets. *Biomaterials* **2012,** *33*, 5832-5840.

36. Vincent, T.; McLean, C.; Full, L.; Peston, D.; Saklatvala, J. FGF-2 is bound to perlecan in the pericellular matrix of articular cartilage, where it acts as a chondrocyte mechanotransducer. *Osteoarthr. Cartilage* **2007,** *15*, 752-763.

37. Tuli, R.; Tuli, S.; Nandi, S.; Huang, X.; Manner, P. A.; Hozack, W. J.; Danielson, K. G.; Hall, D. J.; Tuan, R. S. Transforming growth factor-β-mediated chondrogenesis of human mesenchymal progenitor cells involves N-cadherin and mitogen-activated protein kinase and Wnt signaling cross-talk. *J. Biol. Chem.* **2003,** *278*, 41227-41236.

38. Schmitt, B.; Ringe, J.; Häupl, T.; Notter, M.; Manz, R.; Burmester, G. R.; Sittinger, M.; Kaps, C. BMP-2 initiates chondrogenic lineage development of adult human mesenchymal stem cells in high-density culture. *Differentiation* **2003,** *71*, 567-577.

39. Longobardi, L.; O'Rear, L.; Aakula, S.; Johnstone, B.; Shimer, K.; Chytil, A.; Horton, W. A.; Moses, H. L.; Spagnoli, A. Effect of IGF-1 in the chondrogenesis of bone marrow mesenchymal stem cells in the presence or absence of TGF-beta signaling. *J. Bone Miner. Res.* **2006,** *21*, 626-636.

40. Handorf, A. M.; Li, W.-J. Fibroblast growth factor-2 primes human mesenchymal stem cells for enhanced chondrogenesis. *Plos One* **2011,** *6*, e22887-e22897.

41. Tomita, S.; Li, R.-K.; Weisel, R. D.; Mickle, D. A.; Kim, E.-J.; Sakai, T.; Jia, Z.-Q. Autologous transplantation of bone marrow cells improves damaged heart function. *Circulation* **1999,** *100*, 247-256.

42. Wang, J.-S.; Shum-Tim, D.; Galipeau, J.; Chedrawy, E.; Eliopoulos, N.; Chiu, R. C.-J. Marrow stromal cells for cellular cardiomyoplasty: feasibility and potential clinical advantages. *J. Thorac. Cardiovasc. Surg.* **2000,** *120*, 999-1006.

43. Saito, T.; Kuang, J.-Q.; Lin, C. C.; Chiu, R. C.-J. Transcoronary implantation of bone marrow stromal cells ameliorates cardiac function after myocardial infarction. *J. Thorac. Cardiovasc. Surg.* **2003,** *126*, 114-122.

44. Charge, S. B.; Rudnicki, M. A. Cellular and molecular regulation of muscle regeneration. *Physiol. Rev.* **2004,** *84*, 209-238.

45. Doherty, K. R.; Cave, A.; Davis, D. B.; Delmonte, A. J.; Posey, A.; Earley, J. U.; Hadhazy, M.; McNally, E. M. Normal myoblast fusion requires myoferlin. *Development* **2005,** *132*, 5565-5575.

46. Sorimachi, H.; Ishiura, S.; Suzuki, K. Structure and physiological function of calpains. *Biochem. J.* **1997,** *328*, 721-732.

47. Engler, A. J.; Sen, S.; Sweeney, H. L.; Discher, D. E. Matrix elasticity directs stem cell lineage specification. *Cell* **2006,** *126*, 677-689.

48. Engler, A. J.; Griffin, M. A.; Sen, S.; Bönnemann, C. G.; Sweeney, H. L.; Discher, D. E. Myotubes differentiate optimally on substrates with tissue-like stiffness. *J. Cell Biol.* **2004,** *166*, 877-887.

49. Herzog, E. L.; Chai, L.; Krause, D. S. Plasticity of marrow-derived stem cells. *Blood* **2003,** *102*, 3483-3493.

50. Lee, S. H.; Shin, H. Matrices and scaffolds for delivery of bioactive molecules in bone and cartilage tissue engineering. *Adv. Drug Del. Rev.* **2007,** *59*, 339-359.

51. Park, H.; Temenoff, J. S.; Tabata, Y.; Caplan, A. I.; Mikos, A. G. Injectable biodegradable hydrogel composites for rabbit marrow mesenchymal stem cell and growth factor delivery for cartilage tissue engineering. *Biomaterials* **2007,** *28*, 3217-3227.

52. Ryu, S.; Lee, C.; Park, J.; Lee, J. S.; Kang, S.; Seo, Y. D.; Jang, J.; Kim, B. S. Three-dimensional scaffolds of carbonized polyacrylonitrile for bone tissue regeneration. *Angew. Chem. Int. Ed.* **2014,** *53*, 9213-9217.

53. Hwang, N. S.; Varghese, S.; Elisseeff, J. Controlled differentiation of stem cells. *Adv. Drug Del. Rev.* **2008,** *60*, 199-214.

54. Richardson, S. M.; Hoyland, J. A.; Mobasheri, R.; Csaki, C.; Shakibaei, M.; Mobasheri, A. Mesenchymal stem cells in regenerative medicine: opportunities and challenges for articular cartilage and intervertebral disc tissue engineering. *J. Cell. Physiol.* **2010,** *222*, 23-32.

55. Paschos, N. K.; Brown, W. E.; Eswaramoorthy, R.; Hu, J. C.; Athanasiou, K. A. Advances in tissue engineering through stem cell-based co-culture. *J. Tissue Eng. Regener. Med.* **2015,** *9*, 488-503.

56. Beier, J. P.; Bitto, F. F.; Lange, C.; Klumpp, D.; Arkudas, A.; Bleiziffer, O.; Boos, A. M.; Horch, R. E.; Kneser, U. Myogenic differentiation of mesenchymal stem cells co-cultured with primary myoblasts. *Cell Biol. Int.* **2011,** *35*, 397-406.

57. Csaki, C.; Matis, U.; Mobasheri, A.; Shakibaei, M. Coculture of canine mesenchymal stem cells with primary bone-derived osteoblasts promotes osteogenic differentiation. *Histochem. Cell Biol.* **2009,** *131*, 251-266.

58. Acharya, C.; Adesida, A.; Zajac, P.; Mumme, M.; Riesle, J.; Martin, I.; Barbero, A. Enhanced chondrocyte proliferation and mesenchymal stromal cells chondrogenesis in coculture pellets mediate improved cartilage formation. *J. Cell. Physiol.* **2012,** *227*, 88-97.

59. Fukuhara, S.; Tomita, S.; Yamashiro, S.; Morisaki, T.; Yutani, C.; Kitamura, S.; Nakatani, T. Direct cell-cell interaction of cardiomyocytes is key for bone marrow stromal cells to go into cardiac lineage *in vitro*. *J. Thorac. Cardiovasc. Surg.* **2003,** *125*, 1470-1479.

60. Battiston, K. G.; Cheung, J. W.; Jain, D.; Santerre, J. P. Biomaterials in co-culture systems: towards optimizing tissue integration and cell signaling within scaffolds. *Biomaterials* **2014,** *35*, 4465-4476.

61. Anthony, D. F.; Shiels, P. G. Exploiting paracrine mechanisms of tissue regeneration to repair damaged organs. *Transplant. Res.* **2013,** *2*, 10-17.

62. Gnecchi, M.; Zhang, Z.; Ni, A.; Dzau, V. J. Paracrine mechanisms in adult stem cell signaling and therapy. *Circ. Res.* **2008,** *103*, 1204-1219.

63. Fagotto, F.; Gumbiner, B. M. Cell contact-dependent signaling. *Dev. Biol.* **1996,** *180*, 445-454.

64. Morrison, S. J.; Spradling, A. C. Stem cells and niches: mechanisms that promote stem cell maintenance throughout life. *Cell* **2008,** *132*, 598-611.

65. Kim, S.-H.; Turnbull, J.; Guimond, S. Extracellular matrix and cell signalling: the dynamic cooperation of integrin, proteoglycan and growth factor receptor. *J. Endocrinol.* **2011,** *209*, 139-151.

66. Juliano, R. L.; Haskill, S. Signal transduction from the extracellular matrix. *J. Cell Biol.* **1993,** *120*, 577-585.

67. Birmingham, E.; Niebur, G.; McHugh, P. Osteogenic differentiation of mesenchymal stem cells is regulated by osteocyte and osteoblast cells in a simplified bone niche. *Eur. Cells Mater.* **2012,** *23*, 13-27.

68. Hwang, N. S.; Im, S. G.; Wu, P. B.; Bichara, D. A.; Zhao, X.; Randolph, M. A.; Langer, R.; Anderson, D. G. Chondrogenic priming adipose-mesenchymal stem cells for cartilage tissue regeneration. *Pharm. Res.* **2011,** *28*, 1395-1405.

69. Rustom, A.; Saffrich, R.; Markovic, I.; Walther, P.; Gerdes, H.-H. Nanotubular highways for intercellular organelle transport. *Science* **2004,** *303*, 1007-1010.

70. Niu, X.; Gupta, K.; Yang, J. T.; Shamblott, M. J.; Levchenko, A. Physical transfer of membrane and cytoplasmic components as a general mechanism of cell-cell communication. *J. Cell Sci.* **2009,** *122*, 600-610.

71. Guilak, F.; Cohen, D. M.; Estes, B. T.; Gimble, J. M.; Liedtke, W.; Chen, C. S. Control of stem cell fate by physical interactions with the extracellular matrix. *Cell stem cell* **2009,** *5*, 17-26.

72. Lawrence, T. S.; Beers, W. H.; Gilula, N. B. Transmission of hormonal stimulation by cell-to-cell communication. *Nature* **1978,** *272*, 501-506.

73. Scheven, B. A.; Visser, J. W.; Nijweide, P. J. *In vitro* osteoclast generation from different bone marrow fractions, including a highly enriched haematopoietic stem cell population. *Nature* **1986,** *321*, 79-81.

74. Traphagen, S. B.; Titushkin, I.; Sun, S.; Wary, K. K.; Cho, M. Endothelial invasive response in a co-culture model with physically-induced osteodifferentiation. *J. Tissue Eng. Regener. Med.* **2013,** *7*, 621-630.

75. Ou, D. B.; He, Y.; Chen, R.; Teng, J. W.; Wang, H. T.; Zeng, D.; Liu, X. T.; Ding, L.; Huang, J. Y.; Zheng, Q. S. Three-dimensional co-culture facilitates the differentiation of embryonic stem cells into mature cardiomyocytes. *J. Cell. Biochem.* **2011,** *112*, 3555-3562.

76. Chen, W. H.; Lai, M. T.; Wu, A. T.; Wu, C. C.; Gelovani, J. G.; Lin, C. T.; Hung, S. C.; Chiu, W. T.; Deng, W. P. *In vitro* stage-specific chondrogenesis of mesenchymal stem cells committed to chondrocytes. *Arthritis Rheum.* **2009,** *60*, 450-459.

77. Yoon, Y.-S.; Park, J.-S.; Tkebuchava, T.; Luedeman, C.; Losordo, D. W. Unexpected severe calcification after transplantation of bone marrow cells in acute myocardial infarction. *Circulation* **2004,** *109*, 3154-3157.

78. Kim, S.; Ahn, S. E.; Lee, J. H.; Lim, D. S.; Kim, K. S.; Chung, H. M.; Lee, S. H. A novel culture technique for human embryonic stem cells using porous membranes. *Stem Cells* **2007,** *25*, 2601-2609.

79. Jang, Y.; Lee, H.; Char, K.; Nam, J. M. Transparent, nanoporous, and transferable membrane-based cell-cell paracrine signaling assay. *Adv. Mater.* **2015,** *27*, 1893-1899.

80. Agrawal, A. A.; Nehilla, B. J.; Reisig, K. V.; Gaborski, T. R.; Fang, D. Z.; Striemer, C. C.; Fauchet, P. M.; McGrath, J. L. Porous nanocrystalline silicon membranes as highly permeable and molecularly thin substrates for cell culture. *Biomaterials* **2010,** *31*, 5408-5417.

81. Pandiyan, P.; Zheng, L.; Ishihara, S.; Reed, J.; Lenardo, M. J. CD4+ CD25+ Foxp3+ regulatory T cells induce cytokine deprivation–mediated apoptosis of effector CD4+ T cells. *Nat. Immunol.* **2007,** *8*, 1353-1362.

82. Sekine, H.; Shimizu, T.; Dobashi, I.; Matsuura, K.; Hagiwara, N.; Takahashi, M.; Kobayashi, E.; Yamato, M.; Okano, T. Cardiac cell sheet transplantation improves damaged heart function *via* superior cell survival in comparison with dissociated cell injection. *Tissue Eng., Part A* **2011,** *17*, 2973-2980.

83. Ohashi, K.; Yokoyama, T.; Yamato, M.; Kuge, H.; Kanehiro, H.; Tsutsumi, M.; Amanuma, T.; Iwata, H.; Yang, J.; Okano, T. Engineering functional two-and three-dimensional liver systems *in vivo* using hepatic tissue sheets. *Nat. Med.* **2007,** *13*, 880-885.

84. Matsuda, N.; Shimizu, T.; Yamato, M.; Okano, T. Tissue engineering based on cell sheet technology. *Adv. Mater.* **2007,** *19*, 3089-3099.

85. Ku, S. H.; Ryu, J.; Hong, S. K.; Lee, H.; Park, C. B. General functionalization route for cell adhesion on non-wetting surfaces. *Biomaterials* **2010,** *31*, 2535-2541.

86. Zhang, R. M.; Wang, J. W.; Wang, M. J.; He, Y. D. Fabrication of honeycomb polyvinyl butyral film under humidity provided by super saturated salt solutions. *J. Appl. Polym. Sci.* **2012,** *124*, 495-500.

87. Bouyer, D.; Vachoud, L.; Chakrabandhu, Y.; Pochat-Bohatier, C. Influence of mass transfer on gelation time using VIPS-gelation process for chitin dissolved in LiCl/NMP solvent—modelling and experimental study. *Chem. Eng. J.* **2010,** *157*, 605-619.

88. Li, H.; Wu, J. M. T.; Huang, X.; Yin, Z. Y.; Liu, J. Q.; Zhang, H. A universal, rapid method for clean transfer of nanostructures onto various substrates. *ACS Nano* **2014,** *8*, 6563-6570.

89. Manickam, S. S.; Gelb, J.; McCutcheon, J. R. Pore structure characterization of asymmetric membranes: non-destructive characterization of porosity and tortuosity. *J. Membr. Sci.* **2014,** *454*, 549-554.

90. Sirc, J.; Hobzova, R.; Kostina, N.; Munzarova, M.; Juklickova, M.; Lhotka, M.; Kubinova, S.; Zajicova, A.; Michalek, J. Morphological characterization of nanofibers: methods and application in practice. *J. Nanomater.* **2012,** *2012*, 212-225.

91. Ahola, S.; Turon, X.; Osterberg, M.; Laine, J.; Rojas, O. J. Enzymatic hydrolysis of native cellulose nanofibrils and other cellulose model films: effect of surface structure. *Langmuir* **2008,** *24*, 11592-11599.

92. Zhu, Y.; Mao, Z. W.; Shi, H. Y.; Gao, C. Y. In-depth study on aminolysis of poly(epsilon-caprolactone): back to the fundamentals. *Sci. China Chem.* **2012,** *55*, 2419-2427.

93. Hou, Y.; Chen, J.; Sun, P. J.; Gan, Z. Z.; Zhang, G. Z. In situ investigations on enzymatic degradation of poly(epsilon-caprolactone). *Polymer* **2007,** *48*, 6348-6353.

94. Jang, Y.; Akgun, B.; Kim, H.; Satija, S.; Char, K. Controlled release from model blend multilayer films containing mixtures of strong and weak polyelectrolytes. *Macromolecules* **2012,** *45*, 3542-3549.

95. Jang, Y.; Seo, J.; Akgun, B.; Satija, S.; Char, K. Molecular weight dependence on the disintegration of spin-assisted weak polyelectrolyte multilayer films. *Macromolecules* **2013,** *46*, 4580-4588.

96. Hwang, W.; Xin, G.; Cho, M.; Cho, S. M.; Chae, H. Electrospray deposition of polymer thin films for organic light-emitting diodes. *Nanoscale Res. Lett.* **2012,** *7*, 52-58.

97. Kim, Y. N.; Shin, H. G.; Song, J. K.; Cho, D. H.; Lee, H. S.; Jung, Y. G. Thermal degradation behavior of indium tin oxide thin films deposited by radio frequency magnetron sputtering. *J. Mater. Res.* **2005,** *20*, 1574-1579.

98. Gao, L.; McBeath, R.; Chen, C. S. Stem cell shape regulates a chondrogenic *versus* myogenic fate through Rac1 and N-Cadherin. *Stem Cells* **2010,** *28*, 564-572.

99. Haraguchi, Y.; Shimizu, T.; Yamato, M.; Kikuchi, A.; Okano, T. Electrical coupling of cardiomyocyte sheets occurs rapidly *via* functional gap junction formation. *Biomaterials* **2006,** *27*, 4765-4774.

100. Lampe, P. D. Analyzing phorbol ester effects on gap junctional communication: a dramatic inhibition of assembly. *J. Cell Biol.* **1994,** *127*, 1895-1905.

101. de Windt, T. S.; Saris, D. B.; Slaper-Cortenbach, I. C.; van Rijen, M. H.; Gawlitta, D.; Creemers, L. B.; de Weger, R. A.; Dhert, W. J.; Vonk, L. A. Direct cell–cell contact with chondrocytes is a key mechanism in multipotent mesenchymal stromal cell-mediated chondrogenesis. *Tissue Eng., Part A* **2015,** *21*, 2536-2547.

102. Zhang, Z.; Kuijer, R.; Bulstra, S. K.; Grijpma, D. W.; Feijen, J. The *in vivo* and *in vitro* degradation behavior of poly(trimethylene carbonate). *Biomaterials* **2006,** *27*, 1741-1748.

103. Gong, Y. Y.; Xue, J. X.; Zhang, W. J.; Zhou, G. D.; Liu, W.; Cao, Y. A sandwich model for engineering cartilage with acellular cartilage sheets and chondrocytes. *Biomaterials* **2011,** *32*, 2265-2273.

104. Hyun, J. S.; Tran, M. C.; Wong, V. W.; Chung, M. T.; Lo, D. D.; Montoro, D. T.; Wan, D. C.; Longaker, M. T. Enhancing stem cell survival *in vivo* for tissue repair. *Biotechnol. Adv.* **2013,** *31*, 736-743.

105. Kay Sinclair, S. S.; Burg, K. J. Effect of osteoclast co-culture on the differentiation of human mesenchymal stem cells grown on bone graft granules. *J. Biomater. Sci. Polym. Ed.* **2011,** *22*, 789-808.

106. Yen, B. L.; Chien, C.-C.; Chen, Y.-C.; Chen, J.-T.; Huang, J.-S.; Lee, F.-K.; Huang, H.-I. Placenta-derived multipotent cells differentiate into neuronal and glial cells *in vitro*. *Tissue Eng., Part A* **2008,** *14*, 9-17.

107. Kiger, A. A.; White-Cooper, H.; Fuller, M. T. Somatic support cells restrict germline stem cell self-renewal and promote differentiation. *Nature* **2000,** *407*, 750-754.

108. Haraguchi, Y.; Shimizu, T.; Sasagawa, T.; Sekine, H.; Sakaguchi, K.; Kikuchi, T.; Sekine, W.; Sekiya, S.; Yamato, M.; Umezu, M. Fabrication of functional three-dimensional tissues by stacking cell sheets *in vitro*. *Nat. Protoc.* **2012,** *7*, 850-858.

109. Sekiya, N.; Matsumiya, G.; Miyagawa, S.; Saito, A.; Shimizu, T.; Okano, T.; Kawaguchi, N.; Matsuura, N.; Sawa, Y. Layered implantation of myoblast sheets attenuates adverse cardiac remodeling of the infarcted heart. *J. Thorac. Cardiovasc. Surg.* **2009,** *138*, 985-993.

110. Iwata, T.; Yamato, M.; Tsuchioka, H.; Takagi, R.; Mukobata, S.; Washio, K.; Okano, T.; Ishikawa, I. Periodontal regeneration with multi-layered periodontal ligament-derived cell sheets in a canine model. *Biomaterials* **2009,** *30*, 2716-2723.

111. Annamalai, P. K.; Pochat-Bohatier, C.; Bouyer, D.; Li, C. L.; Deratani, A.; Wang, D. M. Kinetics of mass transfer during vapour-induced phase separation (VIPS) process and its influence on poly-(vinylidene fluoride) (PVDF) membrane structure and surface morphology. *Desalin. Water. Treat.* **2011,** *34*, 204-210.

112. Li, M.; Katsouras, I.; Piliego, C.; Glasser, G.; Lieberwirth, I.; Blom, P. W. M.; de Leeuw, D. M. Controlling the microstructure of poly(vinylidene-fluoride) (PVDF) thin films for microelectronics. *J. Mater. Chem. C* **2013,** *1*, 7695-7702.

113. Venault, A.; Chang, Y.; Wang, D.-M.; Bouyer, D. A review on polymeric membranes and hydrogels prepared by vapor-induced phase separation process. *Polym. Rev.* **2013,** *53*, 568-626.

114. Yamato, M.; Okano, T. Cell sheet engineering. *Mater. Today* **2004,** *7*, 42-47.

115. Cole, M. A.; Voelcker, N. H.; Thissen, H.; Griesser, H. J. Stimuli-responsive interfaces and systems for the control of protein–surface and cell–surface interactions. *Biomaterials* **2009,** *30*, 1827-1850.

116. Kushida, A.; Yamato, M.; Konno, C.; Kikuchi, A.; Sakurai, Y.; Okano, T. Decrease in culture temperature releases monolayer endothelial cell sheets together with deposited fibronectin matrix from temperature-responsive culture surfaces. *J. Biomed. Mater. Res.* **1999,** *45*, 355-362.

117. Akiyama, Y.; Kikuchi, A.; Yamato, M.; Okano, T. Ultrathin poly (N-isopropylacrylamide) grafted layer on polystyrene surfaces for cell adhesion/detachment control. *Langmuir* **2004,** *20*, 5506-5511.

118. Masuda, S.; Shimizu, T.; Yamato, M.; Okano, T. Cell sheet engineering for heart tissue repair. *Adv. Drug Del. Rev.* **2008,** *60*, 277-285.

119. Im, S. G.; Gleason, K. K. Solvent-free modification of surfaces with polymers: the case for initiated and oxidative chemical vapor deposition (CVD). *AICHE J.* **2011,** *57*, 276-285.

120. Kim, M.-J.; Lee, B.; Yang, K.; Park, J.; Jeon, S.; Um, S. H.; Kim, D.-I.; Im, S. G.; Cho, S.-W. BMP-2 peptide-functionalized nanopatterned substrates for enhanced osteogenic differentiation of human mesenchymal stem cells. *Biomaterials* **2013,** *34*, 7236-7246.

121. Saltzman, W. M.; Langer, R. Transport rates of proteins in porous materials with known microgeometry. *Biophys. J.* **1989,** *55*, 163-171.

122. Guo, Y.; O'Donohue, S. J.; Langley, K. H.; Karasz, F. E. Polymer diffusion in porous media of fumed silica studied by forced rayleigh scattering. *Phys. Rev. A* **1992,** *46*, 3335-3342.

123. Makino, S.; Fukuda, K.; Miyoshi, S.; Konishi, F.; Kodama, H.; Pan, J.; Sano, M.; Takahashi, T.; Hori, S.; Abe, H. Cardiomyocytes can be generated from marrow stromal cells *in vitro*. *J. Clin. Invest.* **1999,** *103*, 697-705.

124. Hwang, S.-T.; Kang, S.-W.; Lee, S.-J.; Lee, T.-H.; Suh, W.; Shim, S. H.; Lee, D.-R.; Taite, L. J.; Kim, K.-S.; Lee, S.-H. The expansion of human ES and iPS cells on porous membranes and proliferating human adipose-derived feeder cells. *Biomaterials* **2010,** *31*, 8012-8021.

125. Murasawa, S.; Kawamoto, A.; Horii, M.; Nakamori, S.; Asahara, T. Niche-dependent translineage commitment of endothelial progenitor cells, not cell fusion in general, into myocardial lineage cells. *Arterioscler. Thromb. Vasc. Biol.* **2005,** *25*, 1388-1394.

126. Plotnikov, E.; Khryapenkova, T.; Vasileva, A.; Marey, M.; Galkina, S.; Isaev, N.; Sheval, E.; Polyakov, V.; Sukhikh, G.; Zorov, D. Cell-to-cell cross-talk between mesenchymal stem cells and cardiomyocytes in co-culture. *J. Cell. Mol. Med.* **2008,** *12*, 1622-1631.

127. Mohanty, S.; Bose, S.; Jain, K. G.; Bhargava, B.; Airan, B. TGFβ1 contributes to cardiomyogenic-like differentiation of human bone marrow mesenchymal stem cells. *Int. J. Cardiol.* **2013,** *163*, 93-99.

128. He, X.-q.; Chen, M.-s.; Li, S.-H.; Liu, S.-m.; Zhong, Y.; Kinkaid, H. Y. M.; Lu, W.-Y.; Weisel, R. D.; Li, R.-K. Co-culture with cardiomyocytes enhanced the myogenic conversion of mesenchymal stromal cells in a dose-dependent manner. *Mol. Cell. Biochem.* **2010,** *339*, 89-98.

129. Connell, J. P.; Augustini, E.; Moise, K. J.; Johnson, A.; Jacot, J. G. Formation of functional gap junctions in amniotic fluid-derived stem cells induced by transmembrane co-culture with neonatal rat cardiomyocytes. *J. Cell. Mol. Med.* **2013,** *17*, 774-781.

130. Antonitsis, P.; Ioannidou-Papagiannaki, E.; Kaidoglou, A.; Papakonstantinou, C. *In vitro* cardiomyogenic differentiation of adult human bone marrow mesenchymal stem cells. The role of 5-azacytidine. *Interact. Cardiovasc. Thorac. Surg.* **2007,** *6*, 593-597.

131. Hescheler, J.; Meyer, R.; Plant, S.; Krautwurst, D.; Rosenthal, W.; Schultz, G. Morphological, biochemical, and electrophysiological characterization of a clonal cell (H9C2) line from rat heart. *Circ. Res.* **1991,** *69*, 1476-1486.

132. Gryshchenko, A. Changes in expression of the ion channels in mammalian cardiomyocytes in early embryogenesis. *Neurophysiology* **1998,** *30*, 185-189.

133. Yang, L.; Cheng, F.; Liu, T.; Lu, J. R.; Song, K.; Jiang, L.; Wu, S.; Guo, W. Comparison of mesenchymal stem cells released from poly(N-isopropylacrylamide) copolymer film and by trypsinization. *Biomed. Mater.* **2012,** *7*, 35003-35015.

134. Huang, C. C.; Tsai, H. W.; Lee, W. Y.; Lin, W. W.; Chen, D. Y.; Hung, Y. W.; Chen, J. W.; Hwang, S. M.; Chang, Y.; Sung, H. W. A translational approach in using cell sheet fragments of autologous bone marrow-derived mesenchymal stem cells for cellular cardiomyoplasty in a porcine model. *Biomaterials* **2013,** *34*, 4582-4591.

135. Shimizu, T.; Yamato, M.; Isoi, Y.; Akutsu, T.; Setomaru, T.; Abe, K.; Kikuchi, A.; Umezu, M.; Okano, T. Fabrication of pulsatile cardiac tissue grafts

using a novel 3-dimensional cell sheet manipulation technique and temperature-responsive cell culture surfaces. *Circ. Res.* **2002,** *90*, 40-48.

136. Miyahara, Y.; Nagaya, N.; Kataoka, M.; Yanagawa, B.; Tanaka, K.; Hao, H.; Ishino, K.; Ishida, H.; Shimizu, T.; Kangawa, K. Monolayered mesenchymal stem cells repair scarred myocardium after myocardial infarction. *Nat. Med.* **2006,** *12*, 459-465.

137. Tsuchiya, K.; Chen, G.; Ushida, T.; Matsuno, T.; Tateishi, T. The effect of coculture of chondrocytes with mesenchymal stem cells on their cartilaginous phenotype *in vitro*. *Mater. Sci. Eng., C* **2004,** *24*, 391-396.

138. Qi, Y.; Du, Y.; Li, W.; Dai, X.; Zhao, T.; Yan, W. Cartilage repair using mesenchymal stem cell (MSC) sheet and MSCs-loaded bilayer PLGA scaffold in a rabbit model. *Knee Surg. Sports Traumatol. Arthrosc.* **2014,** *22*, 1424-1433.

139. Kaneshiro, N.; Sato, M.; Ishihara, M.; Mitani, G.; Sakai, H.; Mochida, J. Bioengineered chondrocyte sheets may be potentially useful for the treatment of partial thickness defects of articular cartilage. *Biochem. Biophys. Res. Commun.* **2006,** *349*, 723-731.

140. Allen, K. D.; Golightly, Y. M. Epidemiology of osteoarthritis: state of the evidence. *Curr. Opin. Rheumatol.* **2015,** *27*, 276-283.

141. Coburn, J. M.; Gibson, M.; Monagle, S.; Patterson, Z.; Elisseeff, J. H. Bioinspired nanofibers support chondrogenesis for articular cartilage repair. *Proc. Natl. Acad. Sci. U. S. A.* **2012,** *109*, 10012-10017.

142. Pittenger, M. F.; Mackay, A. M.; Beck, S. C.; Jaiswal, R. K.; Douglas, R.; Mosca, J. D.; Moorman, M. A.; Simonetti, D. W.; Craig, S.; Marshak, D. R. Multilineage potential of adult human mesenchymal stem cells. *Science* **1999,** *284*, 143-147.

143. Li, W.-J.; Tuli, R.; Okafor, C.; Derfoul, A.; Danielson, K. G.; Hall, D. J.; Tuan, R. S. A three-dimensional nanofibrous scaffold for cartilage tissue engineering using human mesenchymal stem cells. *Biomaterials* **2005,** *26*, 599-609.

144. Gentile, P.; Chiono, V.; Carmagnola, I.; Hatton, P. V. An overview of poly(lactic-*co*-glycolic) acid (PLGA)-based biomaterials for bone tissue engineering. *Int. J. Mol. Sci.* **2014,** *15*, 3640-3659.

145. Wu, L.; Prins, H.-J.; Helder, M. N.; van Blitterswijk, C. A.; Karperien, M. Trophic effects of mesenchymal stem cells in chondrocyte co-cultures are independent of culture conditions and cell sources. *Tissue Eng., Part A* **2012,** *18*, 1542-1551.

146. Meretoja, V. V.; Dahlin, R. L.; Wright, S.; Kasper, F. K.; Mikos, A. G. The effect of hypoxia on the chondrogenic differentiation of co-cultured articular chondrocytes and mesenchymal stem cells in scaffolds. *Biomaterials* **2013,** *34*, 4266-4273.

147. Meretoja, V. V.; Dahlin, R. L.; Wright, S.; Kasper, F. K.; Mikos, A. G. Articular chondrocyte redifferentiation in 3D co-cultures with mesenchymal stem cells. *Tissue Eng., Part C Methods* **2014,** *20*, 514-523.

148. Dahlin, R. L.; Ni, M.; Meretoja, V. V.; Kasper, F. K.; Mikos, A. G. TGF-β3-induced chondrogenesis in co-cultures of chondrocytes and mesenchymal stem cells on biodegradable scaffolds. *Biomaterials* **2014,** *35*, 123-132.

149. Meretoja, V. V.; Dahlin, R. L.; Kasper, F. K.; Mikos, A. G. Enhanced chondrogenesis in co-cultures with articular chondrocytes and mesenchymal stem cells. *Biomaterials* **2012,** *33*, 6362-6369.

150. Wu, L.; Leijten, J. C.; Georgi, N.; Post, J. N.; van Blitterswijk, C. A.; Karperien, M. Trophic effects of mesenchymal stem cells increase chondrocyte proliferation and matrix formation. *Tissue Eng., Part A* **2011,** *17*, 1425-1436.

151. Levorson, E. J.; Santoro, M.; Kasper, F. K.; Mikos, A. G. Direct and indirect co-culture of chondrocytes and mesenchymal stem cells for the generation of polymer/extracellular matrix hybrid constructs. *Acta Biomater.* **2014,** *10*, 1824-1835.

152. Middleton, J. C.; Tipton, A. J. Synthetic biodegradable polymers as orthopedic devices. *Biomaterials* **2000,** *21*, 2335-2346.

153. Makadia, H. K.; Siegel, S. J. Poly Lactic-co-Glycolic Acid (PLGA) as Biodegradable Controlled Drug Delivery Carrier. *Polymers (Basel)* **2011,** *3*, 1377-1397.

154. Fuchs, K.; Bauer, T.; Thomann, R.; Wang, C.; Friedrich, C.; Mulhaupt, R. Nanostructure formation *via* association of tectons in amorphous polymer matrices. *Macromolecules* **1999,** *32*, 8404-8412.

155. Lu, L.; Garcia, C. A.; Mikos, A. G. *In vitro* degradation of thin poly(DL-lactic-*co*-glycolic acid) films. *J. Biomed. Mater. Res.* **1999,** *46*, 236-244.

156. Lu, L.; Peter, S. J.; Lyman, M. D.; Lai, H. L.; Leite, S. M.; Tamada, J. A.; Uyama, S.; Vacanti, J. P.; Langer, R.; Mikos, A. G. *In vitro* and *in vivo* degradation of porous poly(DL-lactic-*co*-glycolic acid) foams. *Biomaterials* **2000,** *21*, 1837-1845.

157. Stallock, J.; Molyneaux, K.; Schaible, K.; Knudson, C. M.; Wylie, C. The pro-apoptotic gene Bax is required for the death of ectopic primordial germ cells during their migration in the mouse embryo. *Development* **2003,** *130*, 6589-6597.

158. Li, W.; Ma, N.; Ong, L. L.; Nesselmann, C.; Klopsch, C.; Ladilov, Y.; Furlani, D.; Piechaczek, C.; Moebius, J. M.; Lützow, K. Bcl-2 engineered MSCs inhibited apoptosis and improved heart function. *Stem Cells* **2007,** *25*, 2118-2127.

159. Zhu, W.; Chen, J.; Cong, X.; Hu, S.; Chen, X. Hypoxia and serum deprivation-induced apoptosis in mesenchymal stem cells. *Stem Cells* **2006,** *24*, 416-425.

160. Hirsch, M. S.; Lunsford, L. E.; Trinkaus-Randall, V.; Svoboda, K. K. Chondrocyte survival and differentiation *in situ* are integrin mediated. *Dev. Dyn.* **1997,** *210*, 249-263.

161. Johnson, K.; Zhu, S.; Tremblay, M. S.; Payette, J. N.; Wang, J.; Bouchez, L. C.; Meeusen, S.; Althage, A.; Cho, C. Y.; Wu, X. A stem cell–based approach to cartilage repair. *Science* **2012,** *336*, 717-721.

162. Cai, T.-Y.; Zhu, W.; Chen, X.-S.; Zhou, S.-Y.; Jia, L.-S.; Sun, Y.-Q. Fibroblast growth factor-2 induces mesenchymal stem cells to differentiate into tenocytes through the MAPK pathway. *Mol. Med. Rep.* **2013,** *8*, 1323-1328.

163. Yoon, H. H.; Bhang, S. H.; Kim, T.; Yu, T.; Hyeon, T.; Kim, B. S. Dual roles of graphene oxide in chondrogenic differentiation of adult stem cells: cell-adhesion substrate and growth factor-delivery carrier. *Adv. Funct. Mater.* **2014,** *24*, 6455-6464.

164. Sáez, J. C.; Berthoud, V. M.; Branes, M. C.; Martinez, A. D.; Beyer, E. C. Plasma membrane channels formed by connexins: their regulation and functions. *Physiol. Rev.* **2003,** *83*, 1359-1400.

165. Zhang, L.; He, A.; Yin, Z.; Yu, Z.; Luo, X.; Liu, W.; Zhang, W.; Cao, Y.; Liu, Y.; Zhou, G. Regeneration of human-ear-shaped cartilage by co-culturing human microtia chondrocytes with BMSCs. *Biomaterials* **2014,** *35*, 4878-4887.

166. Mauck, R.; Byers, B.; Yuan, X.; Tuan, R. Regulation of cartilaginous ECM gene transcription by chondrocytes and MSCs in 3D culture in response to dynamic loading. *Biomech. Model. Mechan.* **2007,** *6*, 113-125.

167. Seror, J.; Merkher, Y.; Kampf, N.; Collinson, L.; Day, A. J.; Maroudas, A.; Klein, J. Articular cartilage proteoglycans as boundary lubricants: structure and frictional interaction of surface-attached hyaluronan and hyaluronan–aggrecan complexes. *Biomacromolecules* **2011,** *12*, 3432-3443.

168. Bi, W.; Deng, J. M.; Zhang, Z.; Behringer, R. R.; de Crombrugghe, B. SOX 9 is required for cartilage formation. *Nat. Genet.* **1999,** *22*, 85-89.

169. Zheng, Q.; Zhou, G.; Morello, R.; Chen, Y.; Garcia-Rojas, X.; Lee, B. Type X collagen gene regulation by Runx2 contributes directly to its hypertrophic chondrocyte–specific expression *in vivo*. *J. Cell Biol.* **2003,** *162*, 833-842.

170. Craft, A. M.; Rockel, J. S.; Nartiss, Y.; Kandel, R. A.; Alman, B. A.; Keller, G. M. Generation of articular chondrocytes from human pluripotent stem cells. *Nat. Biotechnol.* **2015,** *33*, 638-645.

171. Fong, E. L.; Chan, C. K.; Goodman, S. B. Stem cell homing in musculoskeletal injury. *Biomaterials* **2011,** *32*, 395-409.

172. Lund, A. W.; Yener, B.; Stegemann, J. P.; Plopper, G. E. The natural and engineered 3D microenvironment as a regulatory cue during stem cell fate determination. *Tissue Eng., Part B, Rev.* **2009,** *15*, 371-380.

173. Yang, J.; Yamato, M.; Sekine, H.; Sekiya, S.; Tsuda, Y.; Ohashi, K.; Shimizu, T.; Okano, T. Tissue engineering using laminar cellular assemblies. *Adv. Mater.* **2009,** *21*, 3404-3409.

174. Ito, A.; Takizawa, Y.; Honda, H.; Hata, K.-i.; Kagami, H.; Ueda, M.; Kobayashi, T. Tissue engineering using magnetite nanoparticles and magnetic force: heterotypic layers of cocultured hepatocytes and endothelial cells. *Tissue Eng.* **2004,** *10*, 833-840.

175. Grossin, L.; Cortial, D.; Saulnier, B.; Félix, O.; Chassepot, A.; Decher, G.; Netter, P.; Schaaf, P.; Gillet, P.; Mainard, D. Step-by-step build-up of biologically active cell-containing stratified films aimed at tissue engineering. *Adv. Mater.* **2009,** *21*, 650-655.

176. Gartner, Z. J.; Bertozzi, C. R. Programmed assembly of 3-dimensional microtissues with defined cellular connectivity. *Proc. Natl. Acad. Sci.* **2009,** *106*, 4606-4610.

177. Nishiguchi, A.; Yoshida, H.; Matsusaki, M.; Akashi, M. Rapid construction of three-dimensional multilayered tissues with endothelial tube networks by the cell-accumulation technique. *Adv. Mater.* **2011,** *23*, 3506-3510.

178. Ryu, S.; Yoo, J.; Jang, Y.; Han, J.; Yu, S. J.; Park, J.; Jung, S. Y.; Ahn, K. H.; Im, S. G.; Char, K. Nanothin coculture membranes with tunable pore architecture and thermoresponsive functionality for transfer-printable stem cell-derived cardiac sheets. *ACS Nano* **2015,** *9*, 10186-10202.

179. Saito, G.; Swanson, J. A.; Lee, K.-D. Drug delivery strategy utilizing conjugation *via* reversible disulfide linkages: role and site of cellular reducing activities. *Adv. Drug Del. Rev.* **2003,** *55*, 199-215.

180. Metcalfe, C.; Cresswell, P.; Ciaccia, L.; Thomas, B.; Barclay, A. N. Labile disulfide bonds are common at the leucocyte cell surface. *Open Biol.* **2011,** *1*, 110010-110010.

181. Wall, S. T.; Saha, K.; Ashton, R. S.; Kam, K. R.; Schaffer, D. V.; Healy, K. E. Multivalency of sonic hedgehog conjugated to linear polymer chains modulates protein potency. *Bioconj. Chem.* **2008,** *19*, 806-812.

182. Rodrigues, M. N.; Oliveira, M. B.; Costa, R. R.; Mano, J. F. Chitosan/chondroitin sulfate membranes produced by polyelectrolyte complexation for cartilage engineering. *Biomacromolecules* **2016,** *17*, 2178-2188.

183. Lee, J.-H.; Kemp, D. M. Human adipose-derived stem cells display myogenic potential and perturbed function in hypoxic conditions. *Biochem. Biophys. Res. Commun.* **2006,** *341*, 882-888.

184. Dezawa, M.; Ishikawa, H.; Itokazu, Y.; Yoshihara, T.; Hoshino, M.; Takeda, S.-i.; Ide, C.; Nabeshima, Y.-i. Bone marrow stromal cells generate muscle cells and repair muscle degeneration. *Science* **2005,** *309*, 314-317.

185. Deng, Y.; Yang, Z.; Terry, T.; Pan, S.; Woodside, D. G.; Wang, J.; Ruan, K.; Willerson, J. T.; Dixon, R. A.; Liu, Q. Prostacyclin-producing human mesenchymal

cells target H19 lncRNA to augment endogenous progenitor function in hindlimb ischaemia. *Nat. Commun.* **2016,** *7*, 1-12.

186. Lluís, F.; Roma, J.; Suelves, M.; Parra, M.; Aniorte, G.; Gallardo, E.; Illa, I.; Rodríguez, L.; Hughes, S. M.; Carmeliet, P. Urokinase-dependent plasminogen activation is required for efficient skeletal muscle regeneration *in vivo*. *Blood* **2001,** *97*, 1703-1711.

187. Peterson, J. M.; Pizza, F. X. Cytokines derived from cultured skeletal muscle cells after mechanical strain promote neutrophil chemotaxis *in vitro*. *J. Appl. Physiol.* **2009,** *106*, 130-137.

188. Chan, X. a. C.; McDermott, J. C.; Siu, K. M. Identification of secreted proteins during skeletal muscle development. *J. Proteome Res.* **2007,** *6*, 698-710.

189. Bryan, B. A.; Walshe, T. E.; Mitchell, D. C.; Havumaki, J. S.; Saint-Geniez, M.; Maharaj, A. S.; Maldonado, A. E.; D'Amore, P. A. Coordinated vascular endothelial growth factor expression and signaling during skeletal myogenic differentiation. *Mol. Biol. Cell* **2008,** *19*, 994-1006.

190. Foulstone, E. J.; Savage, P. B.; Crown, A. L.; Holly, J. M.; Stewart, C. E. Role of insulin-like growth factor binding protein-3 (IGFBP-3) in the differentiation of primary human adult skeletal myoblasts. *J. Cell. Physiol.* **2003,** *195*, 70-79.

191. Cai, X.; Zhu, C.; Xu, Y.; Jing, Y.; Yuan, Y.; Wang, L.; Wang, S.; Zhu, X.; Gao, P.; Zhang, Y. Alpha-ketoglutarate promotes skeletal muscle hypertrophy and protein synthesis through Akt/mTOR signaling pathways. *Sci. Rep.* **2016,** *6*, 26802-26802.

요약 (국문초록)

다양한 퇴행성 질환과 장기 손상을 치료하기 위한 줄기세포 치료법에 대한 수요가 증가하고 있다. 체내 이식 전, 줄기세포를 미리 분화시킨 뒤 이식하는 것이 줄기세포 치료의 결과를 향상시킨다는 것으로 보고되어 왔다. 생체 내에서 줄기세포는 주위의 삼차원 미세환경과의 상호작용을 통해 세포 거동 및 기능이 조절된다. 그 동안 줄기세포와 원하는 세포 유형의 공배양은 줄기세포 분화를 유도하는데 효과적인 방법으로 보고되어 왔는데, 다공성 막 기반 공배양 시스템은 막을 통한 세포-세포간 상호작용 및 공배양 후 두 세포 종 간의 용이한 분리를 지원하기에 공배양 플랫폼으로 널리 사용되어왔다. 막 기반 공배양 시스템에서 사용되는 막의 특성은 줄기세포 분화를 유도하는데 중요한 역할을 한다. 막은 공배양 된 타종의 세포 혼합을 막는 물리적 장벽 역할을 하는 동시에, 세포 간의 효과적인 상호작용을 허용해야 한다. 불행하게도, 현재 널리 사용되고 있는 막 기반 공배양 시스템은 이러한 요건을 충분히 충족시키지 못한다. 널리 사용되고 있는 막은 두께가 수 마이크로 단위로 두껍고 현저히 낮은 기공도를 가져 공배양된 세포 사이의 상호작용을 제한하여 낮은 줄기세포 분화율을 보인다. 또한, 공배양 후 세포를 채취하는 과정에서 단백질 분해 효소 처리를 수반하게 되어 세포 생존력과 세포외 기질을 손상시킨다.

따라서 이 논문은 효과적인 줄기세포 치료를 위한 막 기반 공배양 플랫폼의 개발을 제시한다. 이 연구의 주요 목표는 다음과 같이 요약된다. 1) 효과적인 줄기세포 분화를 촉진하면서 세포 채취 과정에서 단백질 분화 효소 사용을 피하기 위해 온도 반응성 기능을 가진 나노 두께 및 다공성의 공배양 막 제조. 2) 생체 내 삼차원 세포-세포간 상호작용을 보다 잘 모사하기 위해 생분해성, 나노 두께 및 다공성 막을 개발 및

사용하여 세포 층별 배열을 통한 삼차원 세포 공배양 구조 형성. 또한, 공배양 후 분화된 줄기세포를 간편하게 삼차원 세포-막 구조물로 변환하여 이식 가능성 재현. 3) 키토산 박막을 이용해 줄기세포와 분화된 세포를 다층 공배양 시스템으로 쌓고 분리 가능한 가역적 공배양 플랫폼 시연 및 분화된 줄기세포를 이식하여 조직 재생 효과 검증.

첫째, 우리는 기존의 공배양 막 보다 약 20 배 더 얇고 25 배 이상 기공도가 높은 (nanothin highly porous, NTHP)막을 개발했다. 나노 수준에서 조절되는 NTHP 막의 기공 크기는 공배양 된 세포들 간의 직접적인 접촉을 통한 간극연접 형성에 중요한 요소로 밝혀졌다. 기공 크기가 조절된 NTHP 막을 사용한 공배양 시스템에서 줄기세포는 기존의 공배양 시스템에서 보다 향상된 분화율을 보였으며, 이는 NTHP 막을 통해 공배양된 세포간 효율적인 생체 활성 분자의 확산 및 효과적인 세포간 물리적 접촉에 의한 것으로 보였다. 또한, NTHP 막의 온도 반응성 기능을 통해 이동-부착 가능하며, 세포외 기질이 보존되어 세포 생존율이 높은 심근 분화된 세포층을 효율적으로 생성했다.

둘째, 우리는 생분해성, 나노 두께 및 높은 다공성의 (biodegradable nanothin and highly porous, BNTHP) 막을 사용하여 세포를 층별로 (cellular layer-by-layer, cLbL) 공배양하는 플랫폼을 개발했다. cLbL 공배양 플랫폼은 생체 내 삼차원 미세 환경을 보다 정확히 모사하고, 나노 크기에서 발생하는 다층 세포간 상호작용을 통해 이중층 배양 시스템보다 높은 줄기세포 분화 효율을 보였다. 또한, BNTHP 막은 생분해성, 생체 적합성 및 유연성이 뛰어난 특성을 가지기 때문에, 보다 용이하게 막에 부착된 세포를 삼차원 세포 구조물로 전환 및 이식이 가능하여 세포에 유해한 효소적 수확 방법을 피할 수 있었다.

마지막으로 우리는 공배양된 세포 층 사이에 키토산 박막을 생성하여 가역적으로 세포를 적층하는 플랫폼을 개발했다. 음이온성 말레이미드-콘드로이틴-황산염을 C2C12 근육아세포와 줄기세포 표면 막에 결합하여 세포 독성 없이 세포의 표면 전하를 변형시켰다. 이와 같이 세포막이 변형된 줄기세포 위에 양이온성 키토산 및 C2C12 세포를 순차적으로 첨가하였을 때, 세포 층 사이에 이온 교차결합으로 다공성 키토산 박막이 형성된 이중층 공배양 세포 구조물을 형성할 수 있었다. 세포 층 사이의 키토산 박막은 공배양 세포간 직접적인 상호작용을 지원할 수 있음과 동시에, 미세한 전단응력 처리로 공배양된 세포 층을 쉽게 탈착시킬 수 있었다. 개발 된 플랫폼을 통해 공배양된 줄기세포는 C2C12 세포와 직접 접촉 이뤄 분화가 촉진 되었고, 이렇게 근육분화된 줄기세포를 근육 손상 모델에 이식하여 뛰어난 근육 재생능을 확인하였다.

주요어 : 공배양 • 분화 • 막 • 중간엽 줄기세포 • 줄기세포 치료

학번 : 2012-23294